STUDY OF UNCERTAINTIES OF PREDICTING SPACE SHUTTLE THERMAL ENVIRONMENT

FINAL REPORT

CR-123821

MCDONNELL DOUGLAS ASTRONAUTICS COMPANY - EAST

MCDONNELL DOUGLAS CORPORATION

COPY NO. 3

STUDY OF UNCERTAINTIES OF PREDICTING SPACE SHUTTLE THERMAL ENVIRONMENT

30 JUNE 1972

MDC E0639

FINAL REPORT

By A. L. FEHRMAN and R. V. MASEK

Submitted Under Contract No. NAS8-26699

Prepared for: National Aeronautics and Space Administration
George C. Marshall Space Flight Center
Alabama 35812

MCDONNELL DOUGLAS ASTRONAUTICS COMPANY - EAST
Saint Louis, Missouri 63166 (314) 232-0232

MCDONNELL DOUGLAS CORPORATION

FOREWORD

This report summarizes all work conducted by McDonnell Douglas Astronautics Company-East (MDAC-E) in St. Louis, Missouri for the Aero-Astronautics Laboratory of the Marshall Space Flight Center (MSFC) under contract NAS 8-26699, "Study of Uncertainties of Predicting Space Shuttle Thermal Environment". The Contracting Officer Representative for this study was Mr. Homer Wilson and the Study Manager was Mr. Robert Masek. Significant contributions to this study were provided by Mr. Alan Forney of the NASA MSFC, Dr. Thomas Kane and Mr. Lambert Ebbesmeyer of MDAC-E. The transition correlations presented in Figures 48 through 50 were generated as a part of independent research and development (IRAD) at MDAC-E and are reported herein for information only.

The International System of Units is used as the primary system for all results reported herein. The results have also been reported in the British Engineering System of Units which was used as the primary system for all calculations made during the course of this study.

TABLE OF CONTENTS

LIST OF PAGES

Title Page

ii and iii

1 through 133

I. INTRODUCTION AND SUMMARY

This study was conducted to develop quantitative estimates of the uncertainty in predicting aerodynamic heating rates for a fully reusable Space Shuttle system, and the impact of these uncertainties on Thermal Protection System (TPS) weight. Widely differing temperature predictions for the Shuttle on the part of the several Phase A and Phase B contractors showed that a study of this type was required, especially when the effect of vehicle weight increases on totally reuseable system cost (e.g., $28,000 per pound for the orbiter based on MDC Phase B cost studies) is considered.

The study approach consisted of statistical evaluations of the scatter of heating data on Shuttle configurations about state-of-the-art (e.g., Phase B) heating prediction methods to define the uncertainty in these heating predictions. The uncertainties were then applied as heating rate increments to the nominal predicted heating rate to define the uncertainty in TPS weight. Separate evaluations were made for the booster and orbiter,for trajectories which included boost through reentry and touchdown.

For purposes of analysis, the vehicle configuration is divided into areas in which a given prediction method is expected to apply (e.g., lower surface centerline, shielded regions, interference regions), and separate uncertainty factors and corresponding uncertainty in TPS weight derived for each area.

Various prediction methods were investigated for application to local areas on the Shuttle configuration. These included the prediction methods recommended by the Aerodynamic Heating Panel, and alternate state-of-the-art methods. These included: (1) direct correlation of the wind tunnel data for a specific configuration in terms of h/h_{ref}, i.e., normalization of heating data to Fay-Riddell theory, (2) experimental determination of three-dimensional cross flow correction factors for candidate theories using data on a specified configuration.

"Best fits" were made to available wind tunnel data to define the nominal heating. The data are assumed to be normally distributed about the "best fit" method and multiplication factors corresponding to 1, 2,and 3 standard deviations of the data about the fit determined.

Heat transfer analyses were subsequently made for a completely reusable Shuttle system consisting of an aluminum heat sink booster and orbiter with reusable surface insulation (RSI) for thermal protection. These analyses showed that the largest contribution to the uncertainty in TPS weight for the orbiter

occurred on lower surface areas due to the combined effect of heating and boundary layer transition uncertainties. The critical regions on the booster occurred on lower surface regions and upper nose region, but the major region which consisted of LOX and LH_2 tanks were sized by structural requirements. Also, it was found that the major contribution to weight uncertainty were uncertainties in wing heating because of the large area involved. The booster, on the other hand, was much less sensitive to uncertainties in boundary layer transition.

Although the heat sink booster skin thickness was found to be more sensitive to heating uncertainties than the RSI concept, a large portion of the booster is cryogenic tankage and these sections of the vehicle are sized by structural rather than thermodynamic requirements. Therefore, the weight fraction affected by the heating uncertainties is smaller than estimates based on heat sink requirements alone.

II THE AEROTHERMODYNAMIC PHENOMENA

For purposes of this study, the Shuttle mission and configuration concepts were assumed to be the fully reusable system developed in Phase B. Figure 1 shows in pictorial form the important mission phases. The corresponding trajectory variables are contained in Figures 2 and 3. During liftoff and boost the orbiter is mated to the top of the booster. While in this configuration, prior to staging at approximately 2.135 km/sec (7000 ft/sec), critical booster heating is encountered on the forward portion of the top of the booster fuselage due to bow shock intersections and channeled flow between the two vehicles. The flow is turbulent and(since radiation cooling of the surfaces is difficult due to the shading by the other vehicle) temperatures may approach the total temperature of air.

During the separation maneuver,the aft upper fuselage encounters plume impingement heating from the orbiter engines. The booster is powered down and the attitude pitched to $\pi/3$ radians (60 degrees) angle of attack and booster reentry begun. Booster reentry is accomplished at this fixed angle of attack throughout the hypersonic flight regime during which lower surface heating is critical. Due to the presence of wings and canards, heating because of shock impingement produces local hot spots on the side of the fuselage. Local heating increase may also occur on the wings due to nose/wing shock interactions.

After vehicle separation, the orbiter engines deliver the vehicle to the planned orbit, the experiments or other orbital mission is accomplished,and the vehicle prepared for reentry. Except for abort or once around missions, the boost phase heating to the orbiter is dissipated and the initial TPS temperatures determined by the orbit, vehicle inclination,and thermal control provisions. Thus, the orbiter TPS is sized primarily by reentry with the possible exception of certain regions on the upper surface which may become critical during boost.

A sketch of the MDC mated configuration is included in Figure 4. The NAR/GD Phase B configuration is similar. However, the orbiter nose is forward of the booster and the booster has a low delta wing with high canard instead of the high wing with low canard shown in Figure 4. As shown in Figure 5, the flow field produced in this mated configuration is quite complex, with interfering flow and unpredictable heating patterns, even at zero angle of attack.

Examples of the flow field during reentry for the unmated configurations are shown in Figure 6. Because of the high booster angle of attack during reentry,the flow is similar to a cylinder in crossflow on the lower surface and

FIGURE 1

FULLY REUSABLE SPACE SHUTTLE

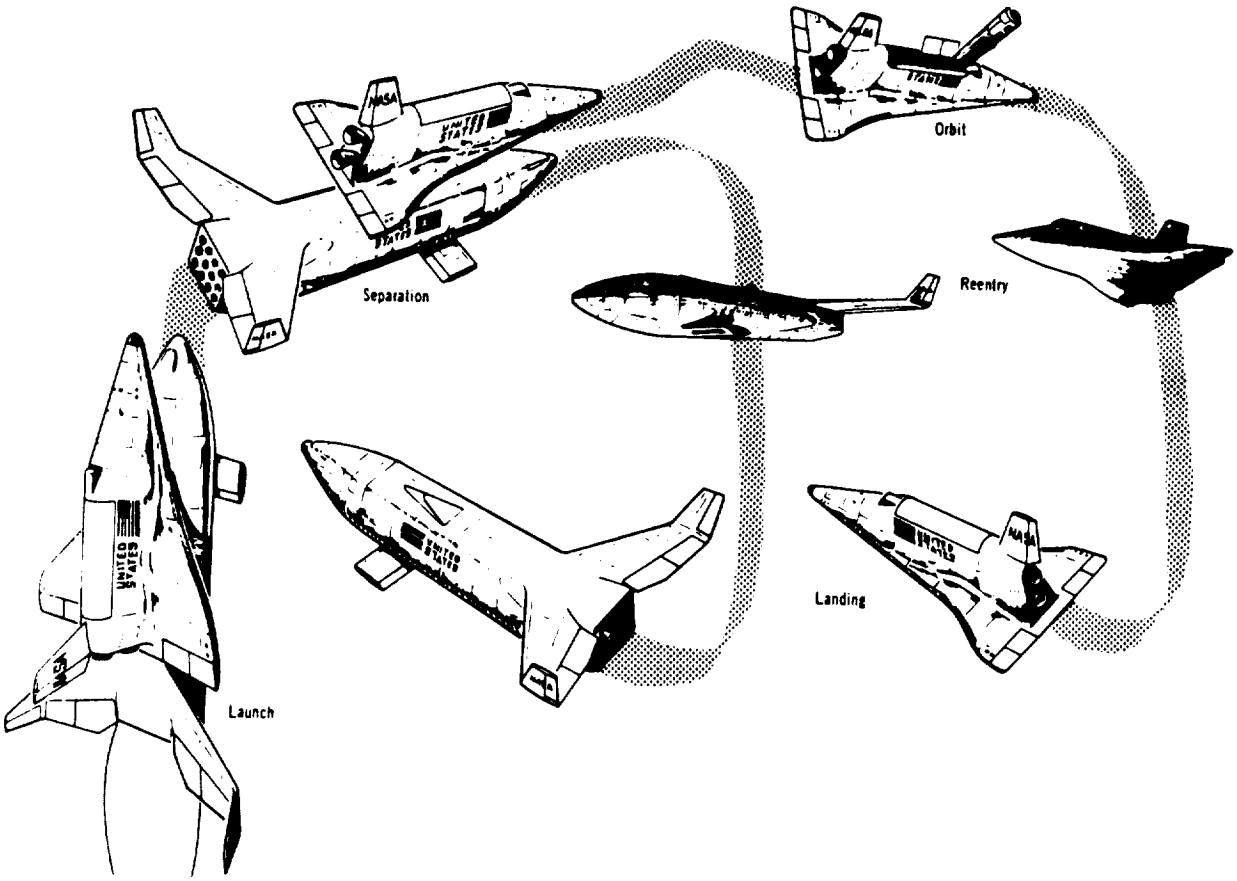

FIGURE 2

HEAT SINK BOOSTER TRAJECTORY

TIME (SECONDS)	ALTITUDE (METERS)	ALTITUDE (FEET)	VELOCITY (m/SEC)	VELOCITY (FT/SEC)	ANGLE OF ATTACK (RADIANS)	ANGLE OF ATTACK (DEGREES)	MACH NO.	UNIT Re ($Re/_m \times 10^{-6}$)	UNIT Re ($Re/FT \times 10^{-6}$)
30.0	1871.2	6139	125.1	410	0	0	0.37	6.95	2.12
60.0	7906.5	25940	299.2	981	0	0	0.95	9.97	3.04
90.0	18263.6	59920	561.7	1843	0	0	1.95	5.22	1.59
120.0	32552.6	106800	1039.7	3411	0	0	3.37	0.840	0.256
150.0	49317.1	161802	1723.9	5656	0	0	5.22	0.120	0.0366
180.0	66374.5	217764	2344.8	7693	0.098	5.6	7.75	0.023	0.0070
210.0	77863.0	255456	2288.7	7509	0.880	50.6	8.18	0.005	0.0015
240.0	81534.0	267500	2267.3	7439	1.05	60.0	8.32	0.003	0.00085
270.0	77416.8	253992	2278.0	7474	1.05	60.0	8.11	0.005	0.0016
300.0	65549.7	215058	2301.7	7551	1.05	60.0	7.57	0.025	0.0076
330.0	47079.4	154460	2174.2	7133	1.05	60.0	6.60	0.200	0.061
360.0	30407.0	99760	1408.4	4621	0.513	29.4	4.62	1.61	0.491
390.0	23528.9	77195	834.7	2738	0.407	23.3	2.02	2.98	0.910
420.0	19380.5	63584	508.0	1667	0.234	13.4	1.75	3.84	1.17

FIGURE 3

TYPICAL MDAC ORBITER ENTRY TRAJECTORY

TIME	ALTITUDE		VELOCITY		ANGLE OF ATTACK		MACH NO.	REYNOLDS NUMBER	
(SECONDS)	(METERS)	(FEET)	(m/SEC)	(FT/SEC)	(RADIANS)	(DEGREES)		($Re/m \times 10^{-6}$)	($Re/FT \times 10^{-6}$)
0	121920.0	400000	7821.5	25661	.551	31.6	19.53	.00000641	.00000195
100	110420.2	362271	7834.3	25703	↓	↓	24.01	.00004287	.00001307
200	98697.6	323811	7846.2	25742	↓	↓	27.22	.0003573	.00010892
300	87025.3	285516	7847.1	25745	.551	31.6	29.12	.003530	.0010760
400	76559.7	251180	7778.5	25520	.581	33.3	27.86	.020612	.0062824
523	71365.3	234138	7419.1	24341	.593	34.0	25.34	.038451	.011720
623	69378.3	227619	7053.4	23141	↓	↓	23.66	.046430	.014152
723	67102.3	220152	6609.0	21683	↓	↓	21.75	.056732	.017292
823	64211.9	210669	6068.3	19909	↓	↓	19.51	.071654	.021840
923	62577.9	205308	5472.7	17955	↓	↓	17.37	.078166	.023825
1023	60037.7	196974	4871.0	15981	↓	↓	15.26	.092402	.028164
1123	57145.1	187484	4206.5	13801	↓	↓	13.05	.111503	.033986
1223	54067.9	177385	3533.2	11592	↓	↓	10.84	.134285	.04093
1323	50177.7	164625	2840.7	9320	.593	34.0	8.68	.171654	.05232
1423	45880.6	150527	2156.8	7076	.558	32.0	6.65	.23540	.07175
1523	40298.5	132213	1548.7	5081	.471	27.0	4.93	.387172	.11801
1578	37034.7	121505	1247.9	4094	.401	23.0	3.98	.499016	.1521
1678	30772.0	100958	841.9	2762	.314	18.0	2.06	.9288	.2831
1778	23558.9	77293	531.3	1743	.227	13.0	1.79	1.6932	.5161
1878	17708.0	58097	314.6	1032	.175	10.0	1.07	.2830	.0863
1978	12955.2	42504	235.0	771	.140	8.0	0.80	.4416	.1346
2058	10762.5	35310	196.9	646	.140	8.0	0.66	.5157	.1572

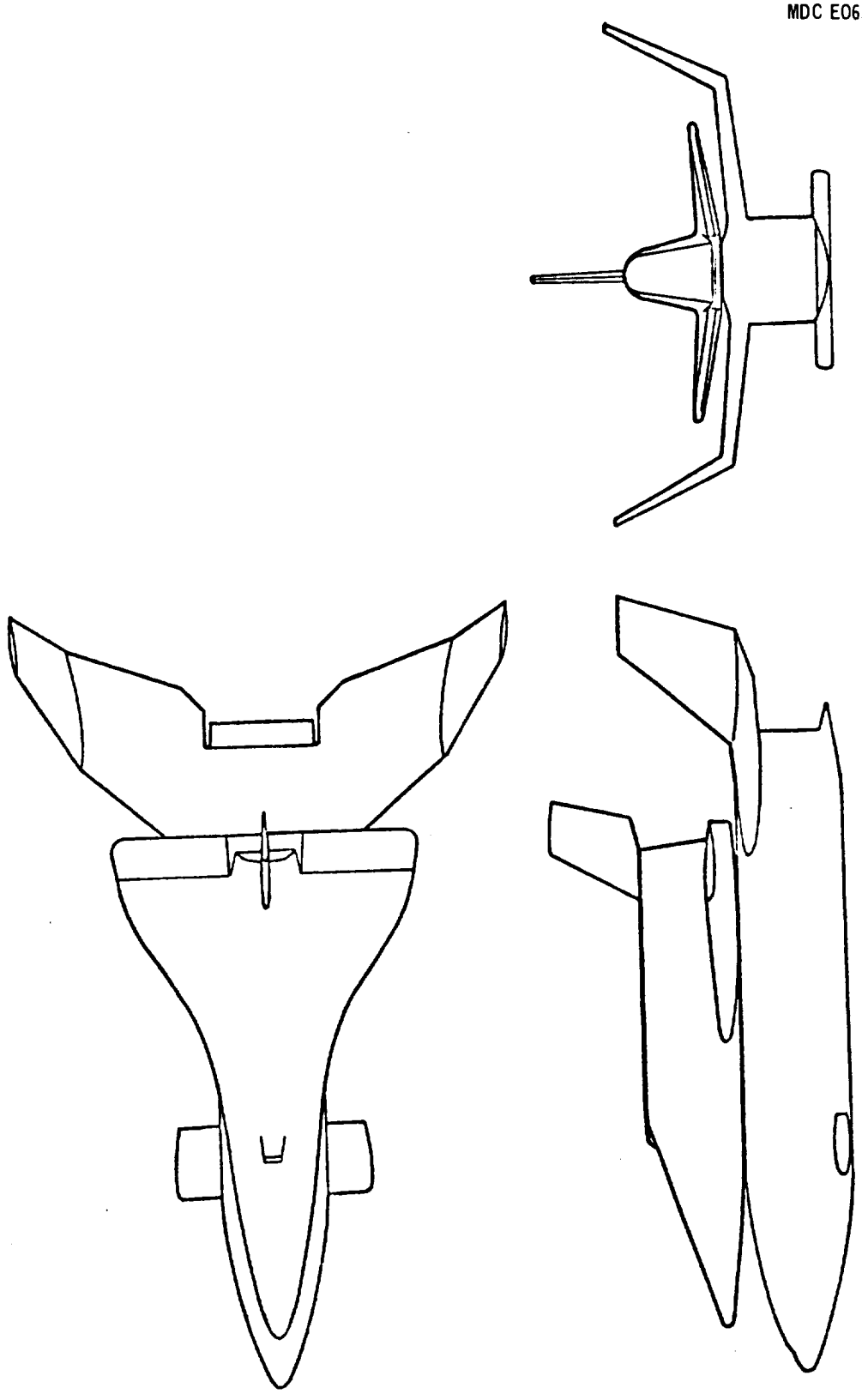

FIGURE 4
SPACE SHUTTLE MATED CONFIGURATION

FIGURE 5

MATED CONFIGURATION FLOW FIELD

SHOCK SYSTEM

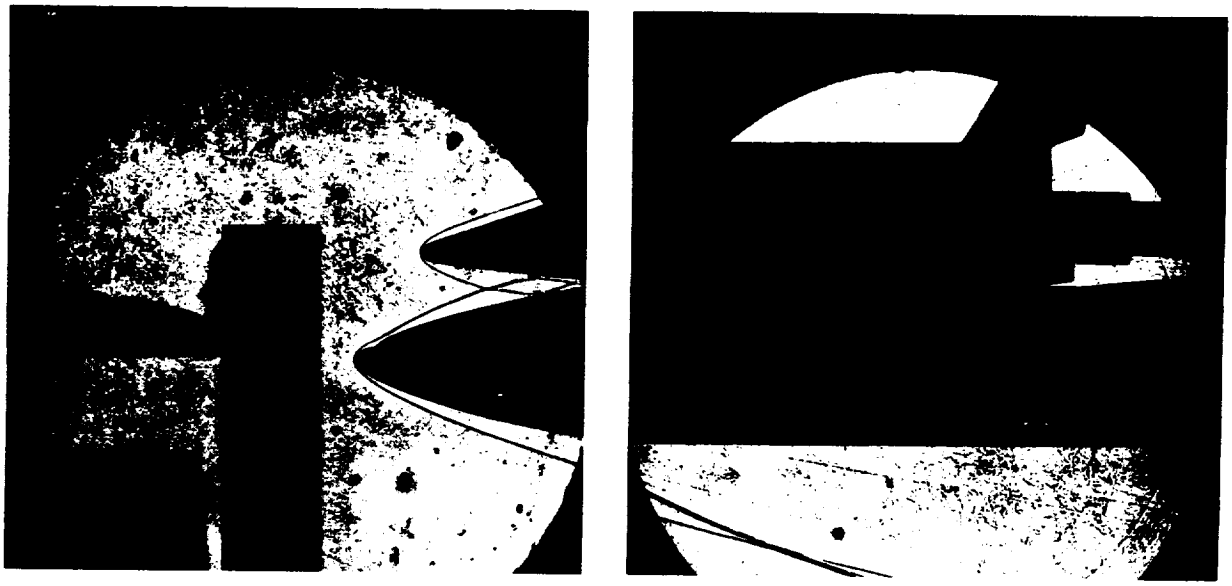

HEATING PATTERN

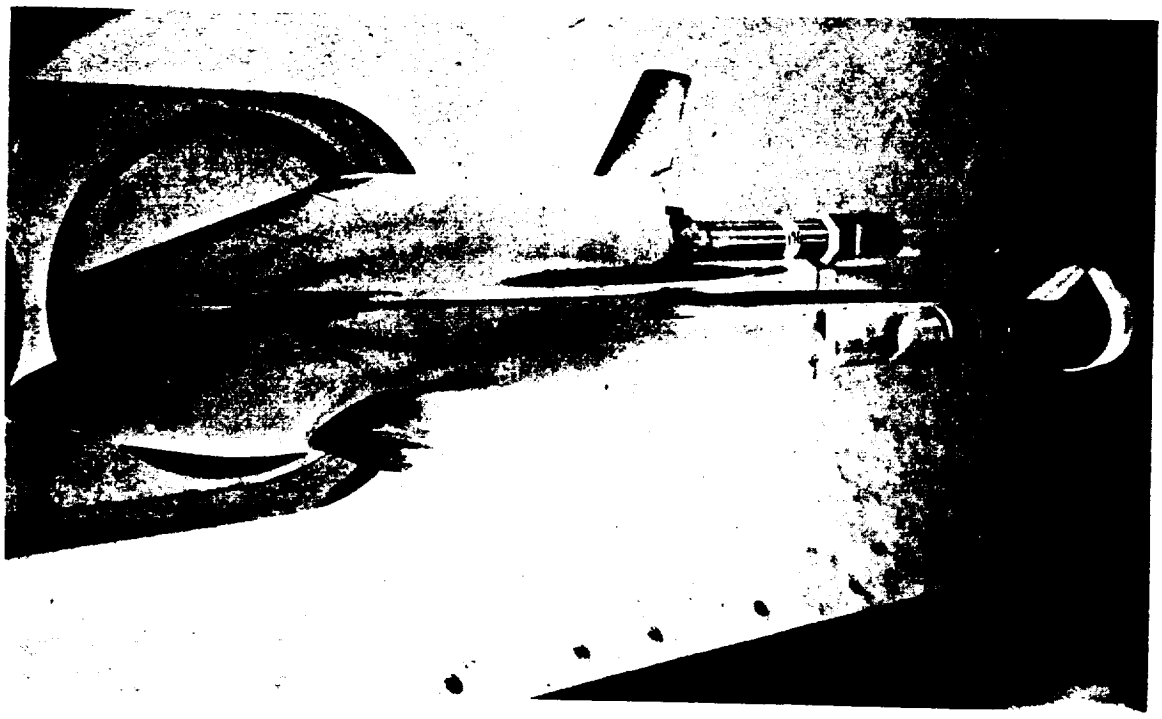

FIGURE 6

FLOW PATTERNS DURING REENTRY

ORBITER

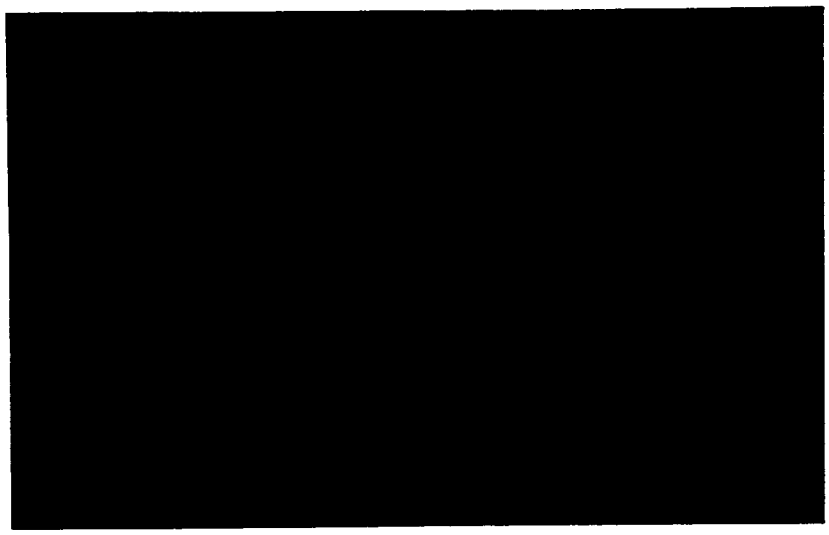

BOOSTER

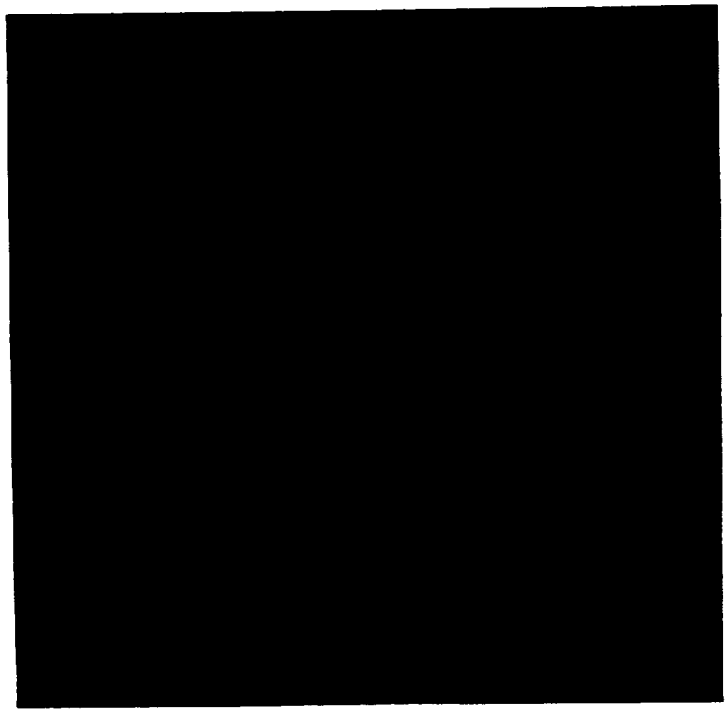

the flow over the major portion of the upper surface is separated. Locally high heating at the canard and below the wing still occurs. The flow is laminar during early reentry with transition to turbulent flow occurring slightly before peak heating is encountered. Thus, the heating (to lower surface areas, at least) is turbulent in boost, and transitional and turbulent during reentry.

The orbiter angle of attack is lower than that of the booster for the high cross range 2040 km (1100 nmi) mission. Portions of the upper surface area are in a region of separated flow, but (depending on the geometric details) reattachment and vortex impingement may be present. Critical heating occurs on the lower surface and the flow is likely to be turbulent during peak heating.

Because of the distinct differences in the heating phenomena for booster and orbiter (which differ, as well, on lower surfaces area, shielded areas, and regions of shock/flowfield interference) and the lack of complete flowfield solutions for such configurations, heating predictions must rely on data correlations. These data correlations will probably take a different form for the various configurations and locations and will have different levels of uncertainty.

III DATA COLLECTION AND EVALUATION

The basic approach selected for this study consisted of a "hard" look at the ground test data generated by the Phase A and Phase B contractors. To assist in this evaluation,data available through SADSAC and contractor reports were cataloged and screened, reduced where necessary, and analyzed and correlated.

As part of this task the tests were cataloged and summarized by configuration, facility,and test condition. The number of tests run in each tunnel for each configuration are listed in Figure 7. This chart shows that the bulk of the data were obtained in the Langley Variable Density Tunnel and that only a few configurations were tested in more than 3 facilities. It should be noted that all data were not available for analysis and correlation in this study,since a number of tests were run too late to be incorporated. In Figures 8 and 9 the Mach/Reynolds number simulations provided for booster and orbiter are shown. Only a few booster runs were made below Mach 7, a probable staging velocity for the heat sink booster. It should be noted, however, that higher staging velocities were under strong consideration in Phase B. The Mach simulations were even poorer for the orbiter, with no data taken above Mach 16 where peak heating is likely to occur. Although Figure 9 was developed for the MDC orbiter, similar conclusions are inferred for the configurations of other contractors.

Data analysis was made more burdensome by the form of the data provided by SADSAC, particularly when the paint technique was used to define the heat transfer. The heat transfer coefficients were derived for arbitrarily assumed recovery temperatures and nondimensionalized to reference sphere heating. The relationship between the q and h thus varied for the various test conditions and when compared with theory. The reported h had to be adjusted to the corresponding theoretical recovery temperature or rather large discrepancies would result. Figure 10 shows the relationship between q and h as a function of wall temperature and assumed recovery temperature ratio.

The SADSAC isotherm data (Figure 11) did not include grids to help define the location of the isotherms,and a time consuming scaling of the figure was required. Although a corresponding grid figure was provided, stretching of the paper during reproduction did not allow direct overlay.

FIGURE 7

SUMMARY OF HEAT TRANSFER TESTS ON SHUTTLE CONFIGURATIONS

VEHICLE	MODEL	FACILITY								
		LaRC				CAL		AEDC		ARC
		VDT	CFHT	HRNT	UPWT	20"	HST	B	F	3.5'
BOOSTER	MDAC B1	23*	16							
	B2	22	11							
	B3	8					23	14		
	256-20 SS		17		32	20				
	GD/C B-8B	17	26							28
	B-9J	9	25		11					18
	B-15B	67								
	B-15B-2	15						17		
	B-9U	36								
	B-9-V			34						
	B-18E3					20				
	LaRC Clipped Delta		3							
ORBITER	MDAC 01	22	21							
	02	32	47							
	03	6								
	050/B	35					26	40	17	
	Int Tank Orb					8				
	NAR 130C	45	21							31
	134B	36	21		16					33
	161B	23						23		
	VC70-0110D	25	3							
	GRUM ROS-NB2		24							
	H-3T		43							
	LMSC LS-200-5	29								
	With Ext. Cone/Cyl Tank	92								
		3	29							
	LaRC 9.90							17	16	

* NUMBER OF TEST RUNS

FIGURE 7 (CONTINUED)

SUMMARY OF HEAT TRANSFER TESTS
ON SHUTTLE CONFIGURATIONS

VEHICLE	MODEL	FACILITY								
		LaRC				CAL		AEDC		ARC
		VDT	CFHT	HRNT	UPWT	20"	HST	B	F	3.5'
MATED	MDAC 01/B1	10*	7							
	01/B2	10	2							
	011B3						11	25		
	02/B1	11								
	02/B2	7								
	03/B1	4	6							
	03/B2	4	4							
	050/B/B3						22	25		
	NAR 130C/B-8B	9								
	130C/B-9J	1			20					
	134B/B-8B	4								
	134B/B-9J	1			37					
	161B/B-15B-2								11	
	161C/B-9U	7								
	GAC/ H-3T/1202 TBC		20							
	LMSC LS-200-2**	4								

* NUMBER OF TEST RUNS

** 1-1/2 STAGE

FIGURE 8

COMPARISON OF GROUND TEST AND FLIGHT CONDITIONS
GD/C BOOSTER CONFIGURATIONS

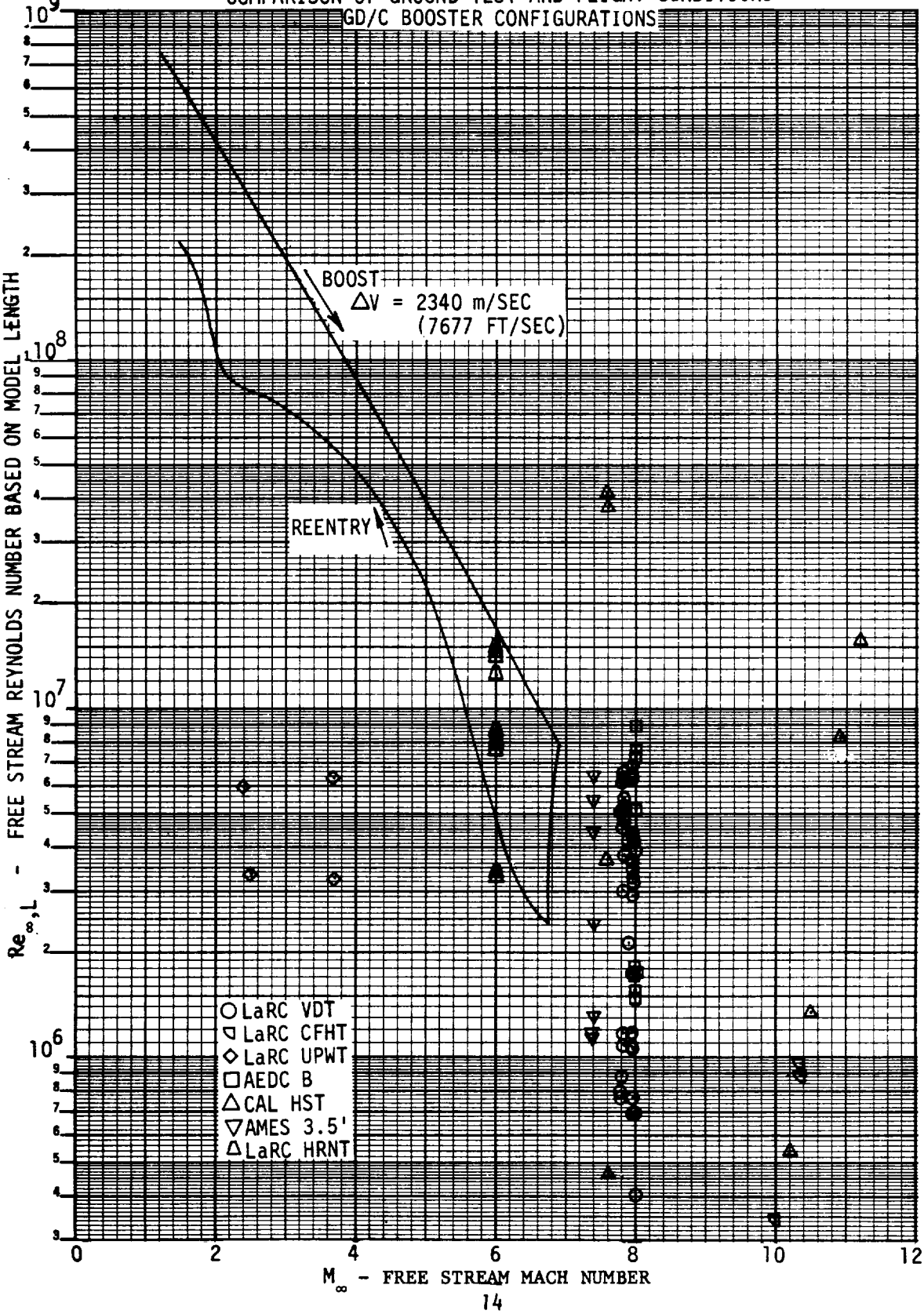

FIGURE 9

COMPARISON OF GROUND TEST AND FLIGHT CONDITIONS

MDAC ORBITERS

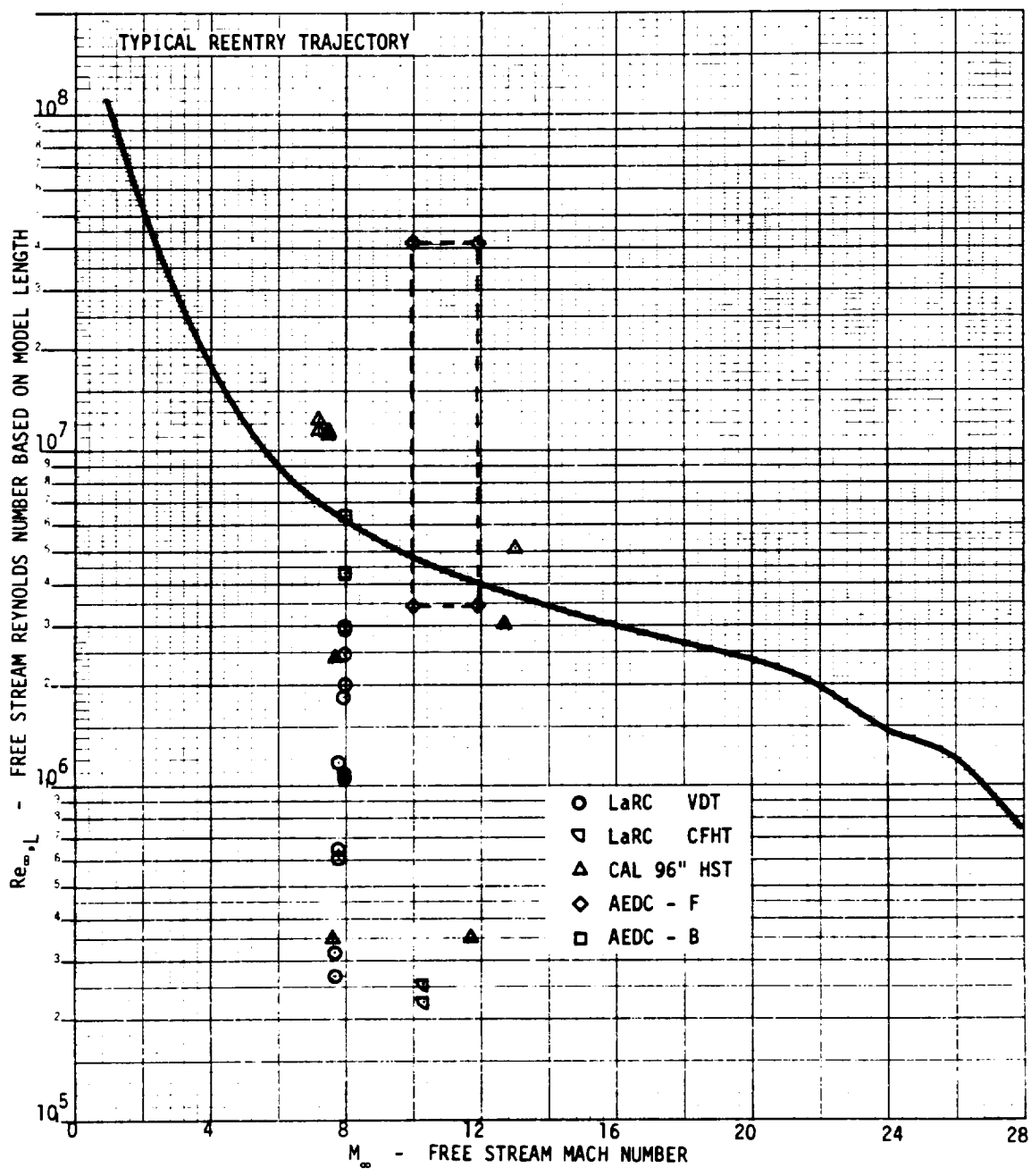

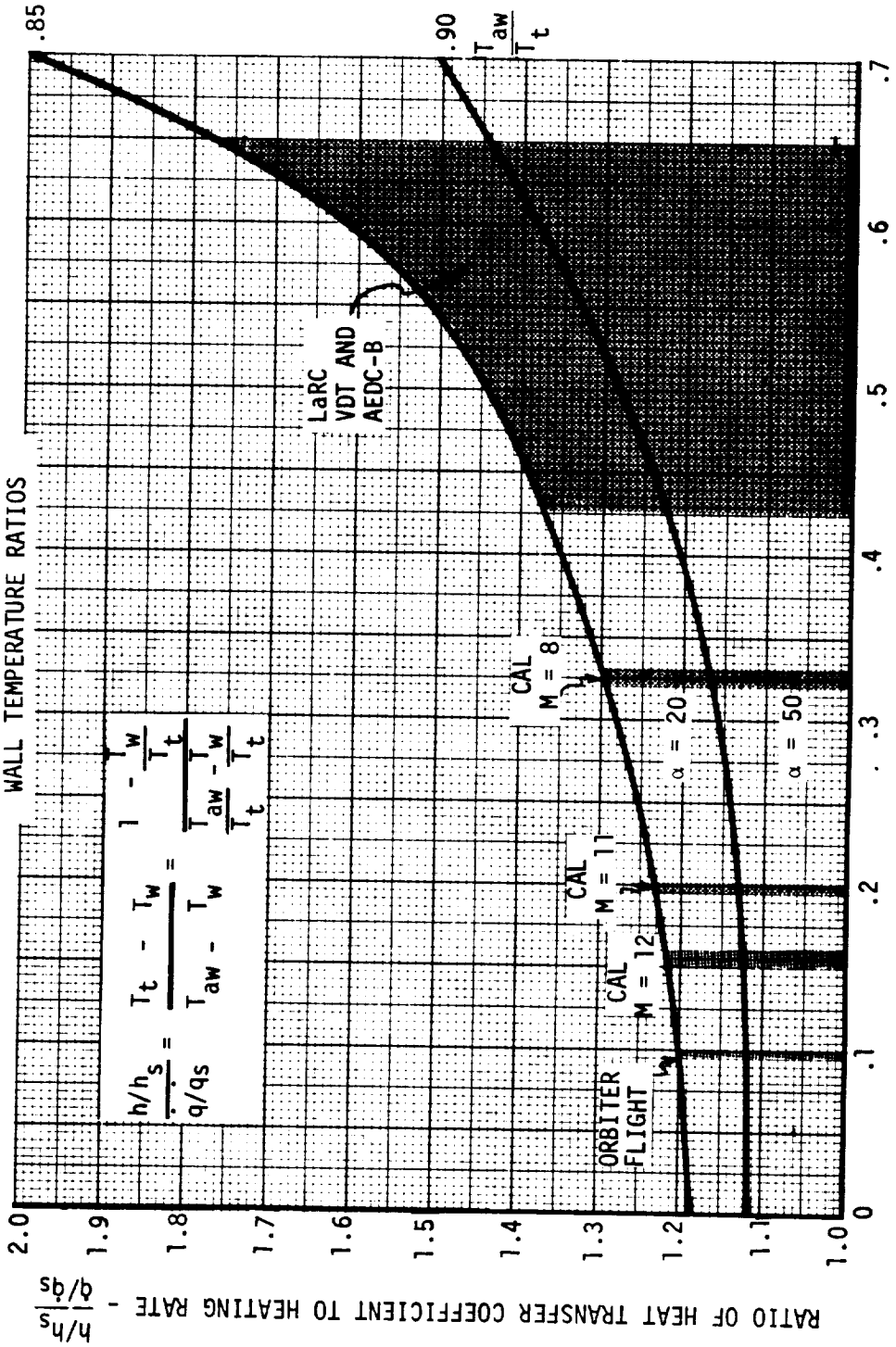
WALL TEMPERATURE RATIOS
RATIO OF WALL TO TOTAL TEMPERATURE - T_w/T_t
RATIO OF HEAT TRANSFER COEFFICIENT TO HEATING RATE - $\frac{h/h_s}{\dot{q}/\dot{q}_s}$
$\frac{h/h_s}{\dot{q}/\dot{q}_s} = \frac{T_t - T_w}{T_{aw} - T_w} = \frac{1 - \frac{T_w}{T_t}}{\frac{T_{aw}}{T_t} - \frac{T_w}{T_t}}$
LaRC VDT AND AEDC-B
CAL M = 8
CAL M = 11
CAL M = 12
ORBITER FLIGHT
α = 20
α = 50
$\frac{T_{aw}}{T_t}$
2.0
1.9
1.8
1.7
1.6
1.5
1.4
1.3
1.2
1.1
1.0
.85
.90
0
.1
.2
.3
.4
.5
.6
.7

FIGURE 10

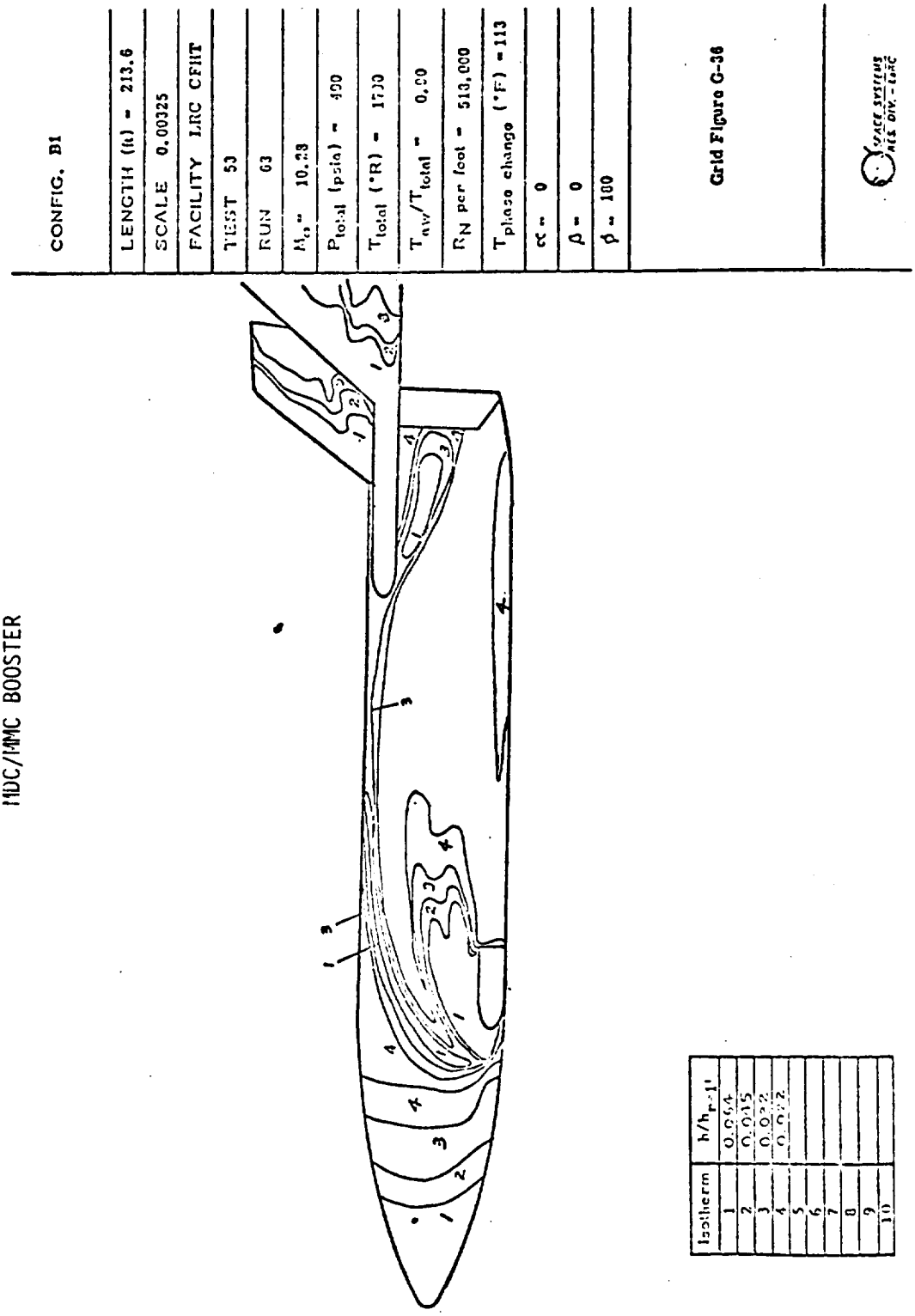

FIGURE 11

TYPICAL SADSAC PAINT DATA

MDC/MMC BOOSTER

IV DATA CORRELATIONS

The bulk of the data analysis and correlation effort was spent evaluating the GD/C and MDC (Martin) booster and NAR and MDC orbiter configurations. The correlations were of two general types: curve fits to reported h/h_{ref} data and development of factors to relate the measurements to an appropriate theory. The theories evaluated included the Eckert Reference Enthalpy; $\rho\mu$,and Beckwith and Gallagher for laminar flow;and Spalding-Chi, $\rho\mu$,and Beckwith and Gallagher for turbulent flow conditions. Local flow properties were based on equivalent sharp cone flow except for the booster at zero degrees angle of attack for which expansion from normal shock entropy was assumed. All theoretical calculations were performed with the MINIVER computer program developed by MDC and described in Reference 1.

1. Booster

A. Windward Surfaces

To assist in defining the local flow field properties on the windward surface of the GD/C booster, shock wave angles were measured from Schlieren photographs. Figure 12 shows the windward shock wave angle with respect to the free stream at the aft end of the GD/C cylindrical booster as a function of angle of attack. The shock angle is compared with that obtained from Delta Wing Test (Reference 2) and with analytical predictions for the delta, cone, and wedge. At an angle of attack of $\pi/3$ radians (60 degrees) the figure show the difference between the shock wave and the GD/C booster surface angle to be less than $\pi/180$ radians (1 degree), but is approximately $2\pi/45$ radians (8 degrees) for the AFFDL delta wing. Although small, these differences have a significant effect on the boundary layer edge temperature and velocity.

Heat transfer data obtained on the forward lower surface centerline of the GD/C booster were correlated with theoretical heating rates given by the Eckert strip, $\rho\mu$ strip, and Beckwith and Gallagher swept cylinder theories. For local flow deflection angles less than $\pi/3$ radians (60 degrees) the Eckert and $\rho\mu$ theories were computed using the conical shock flow field assumption contained in the MINIVER program, and for local angles equal to, or greater than, $\pi/3$ radians (60 degrees) shock wave angles were specified. Cross flow corrections, h_{DATA}/h_{THEORY}, were computed and least square curve fits obtained. The standard deviations of h_{DATA}/h_{THEORY} about the curve fits were computed for each theory. The curve fits, their equations, and standard deviations for an angle of attack equal to $\pi/9$ radians (20 degrees) are shown in Figures 13 through 15. A comparison of these results shows that the better fits are obtained with the Eckert, and Beckwith and Gallagher theories. These curves show that none of the theories is able to model the heating, since they do not account for the three dimensional character of the flow. A comparison of the standard deviations throughout the entire angle of attack range tested, $\pi/9$ to $\pi/3$ radians (20 to 60 degrees), showed that the Beckwith and Gallagher theory yields the lowest values. However, when the standard deviations are compared on a percentage basis, there is little difference in the quality of the data fits for the three theories.

FIGURE 12

SHOCK WAVE ANGLE COMPARISON

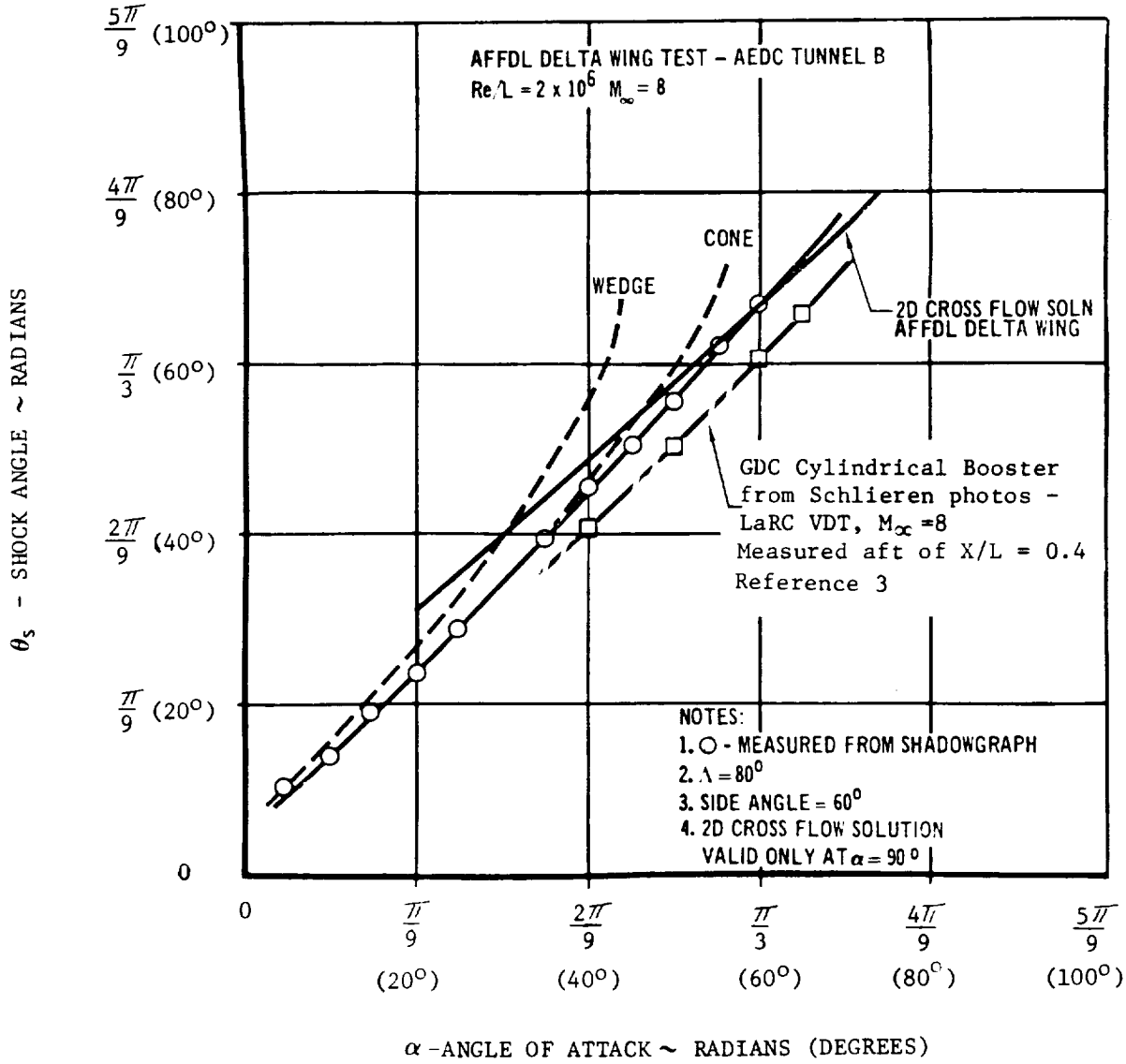

FIGURE 13

GD/C DELTA WING BOOSTER LOWER SURFACE CENTERLINE
RATIO OF HEAT TRANSFER COEFFICIENT DATA
TO ECKERT LAMINAR STRIP THEORY

ANGLE OF ATTACK: $\alpha = \pi/9$ RADIANS (20°)

SYMBOL	M_∞	$Re_\infty/L \times 10^{-6}$ [1/m]	[1/FT]	REFERENCE
□	10.4	3.46	1.055	4
○	8.0	19.25	5.87	5

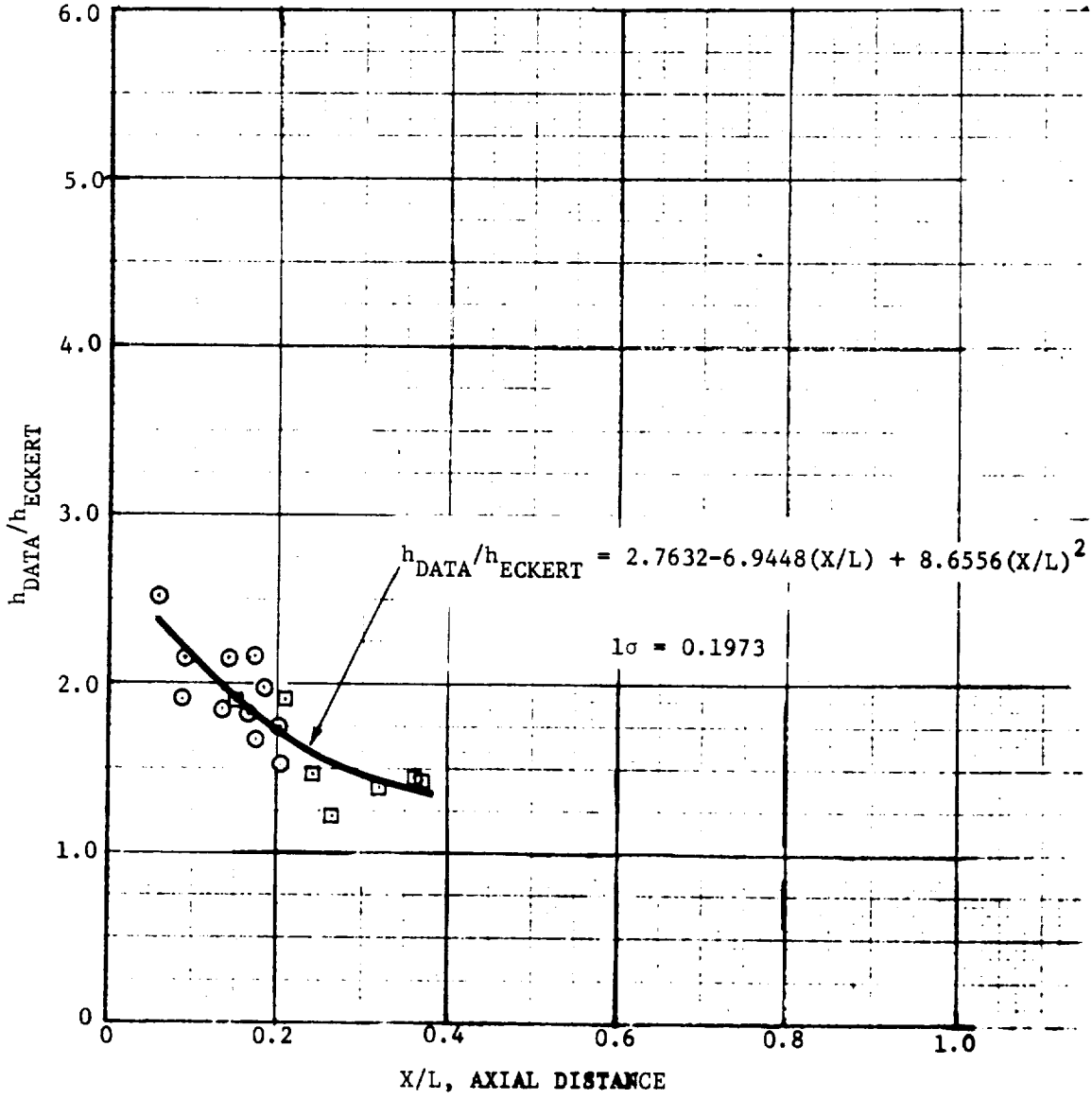

FIGURE 14

GD/C DELTA WING BOOSTER LOWER SURFACE CENTERLINE
RATIO OF HEAT TRANSFER COEFFICIENT DATA
TO $\rho\mu$ LAMINAR STRIP THEORY

ANGLE OF ATTACK: $\alpha = \pi/9$ RADIANS (20°)

SYMBOL	M_∞	$Re_\infty/L \times 10^{-6}$ [1/m]	[1/FT]	REFERENCE
□	10.4	3.46	1.055	4
○	8.0	19.25	5.87	5

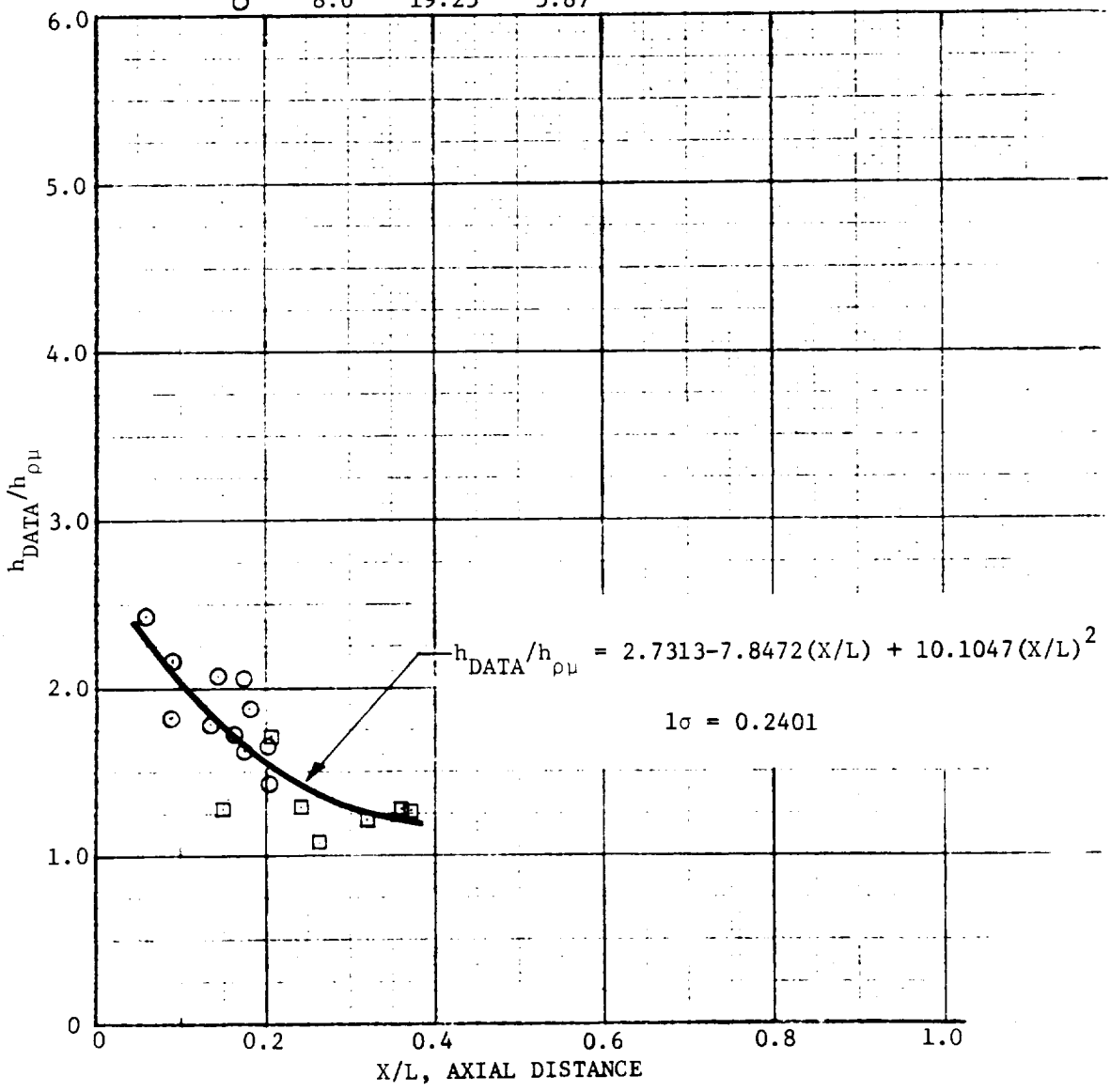

FIGURE 15

GD/C DELTA WING BOOSTER LOWER SURFACE CENTERLINE
RATIO OF HEAT TRANSFER COEFFICIENT DATA
TO BECKWITH & GALLAGHER LAMINAR SWEPT CYLINDER THEORY
ANGLE OF ATTACK: $\alpha = \pi/9$ RADIANS (20°)

SYMBOL	M_∞	$Re_\infty/L \times 10^{-6}$ [1/m]	$Re_\infty/L \times 10^{-6}$ [1/FT]	REFERENCE
□	10.4	3.46	1.055	4
○	8.0	19.25	5.87	5

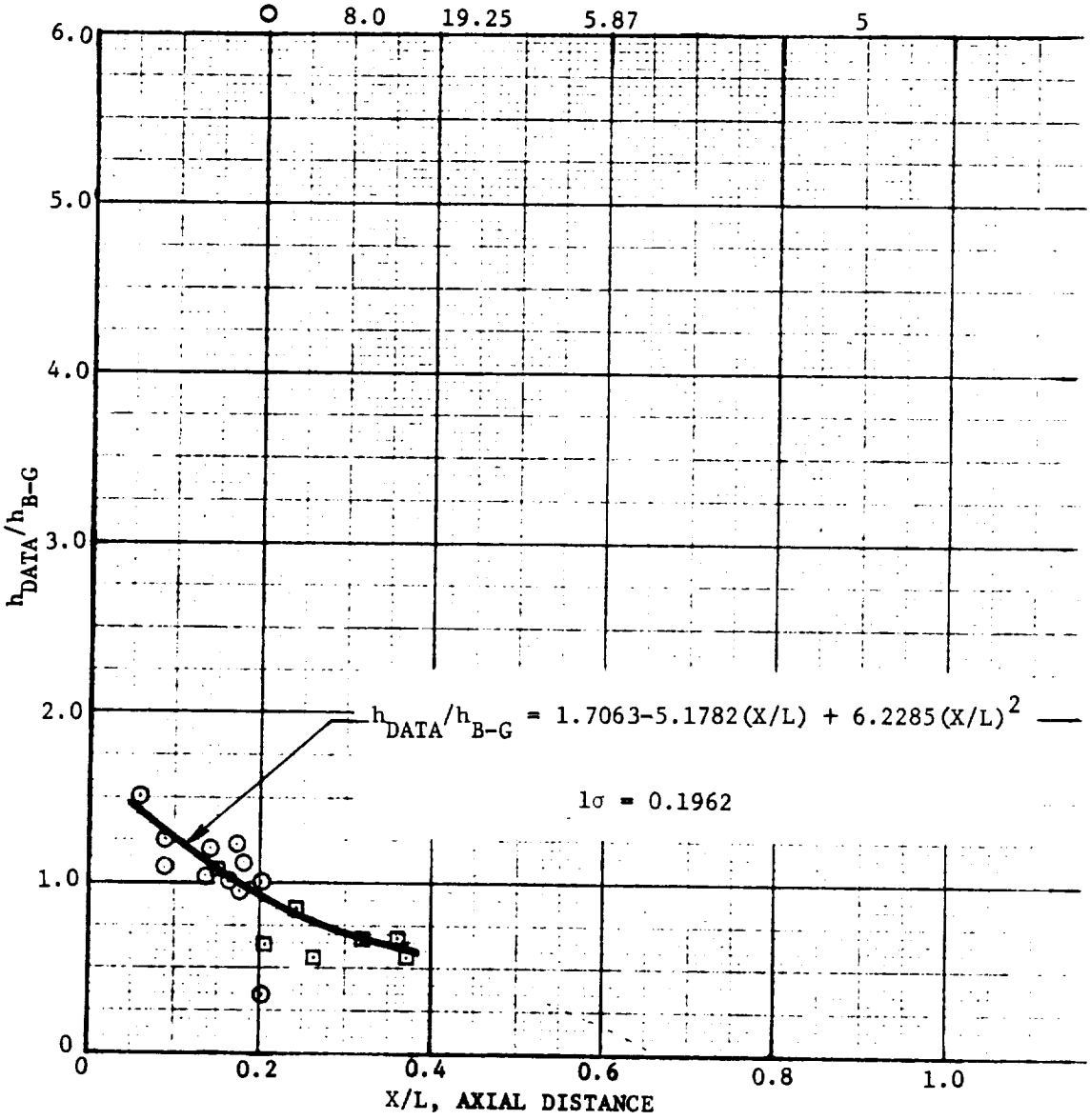

The AEDC Tunnel B data on the GD/C B-15B-2 booster were compared directly with theory. A comparison of the zero angle of attack data with laminar Eckert, $\rho\mu$ strip,and Beckwith and Gallagher swept cylinder results is shown in Figure 16. Although there is good agreement with all three theories on the extreme forward portion of the vehicle, little agreement exists aft of X/L = 0.4. Therefore, the design curve based on direct correlation in terms of h/h_{ref} was used for the nominal case.

A comparison of transitional and turbulent data with turbulent Spalding-Chi, $\rho\mu$,and Beckwith and Gallagher swept cylinder results,as well as with the laminar theories, was also made for the data taken at high angles of attack. Typical results for an angle of attack equal to $\pi/3$ radians (60 degrees) are shown in Figure 17. The Beckwith and Gallagher results show good agreement with the turbulent data,but the three dimensional character of the flow prevented the laminar theories from matching the test results. Therefore, the laminar design curves shown in this figure are based on direct correlation of the data. The ratio of data to theory, h_{DATA}/h_{THEORY}, for the turbulent Beckwith and Gallagher results at $\pi/3$ radian (60 degree) angle of attack is shown in Figure 18. This correlation was used for the nominal turbulent, $\pi/3$ radians (60 degree) angle of attack case.

Peripheral heating data for both the straight and delta wing booster configurations at X/L = 0.25 and angle of attack equal to $\pi/6$ radians (30 degrees) are shown in Figure 19. These data were obtained from the NASA Langley Continuous Flow Hypersonic and Variable Density Tunnels and the NASA Ames 3.5 foot tunnel. The data for these various configurations have been combined because the geometric similarity in the forward portion would be expected to produce equivalent peripheral distributions. This figure also shows a least squares curve fit to the data in the form $\ln (h/h_{ref}) = f(\phi, \phi^2, \phi^3)$ with the angle ϕ measured from the lower surface centerline. In general, the Mach 7.95 paint data are higher than either the Mach 10 paint and gage data or the Mach 7.4 gage data. Since no reasonable explanation of these differences could be determined, all of the data were used in the correlation.

General trends of heat transfer data on the wing lower surface of the GD/C B-15B-2 booster were investigated by CalComp plotting from a data tape obtained from the AEDC Tunnel B facility. Machine plots of the wing lower surface heat transfer coefficient, as a function of percent span, were made for eight chordwise locations over the angle-of-attack range tested. From these plots it was determined

FIGURE 16

GD/C (B-15B-2) BOOSTER LOWER SURFACE CENTERLINE HEATING DISTRIBUTION

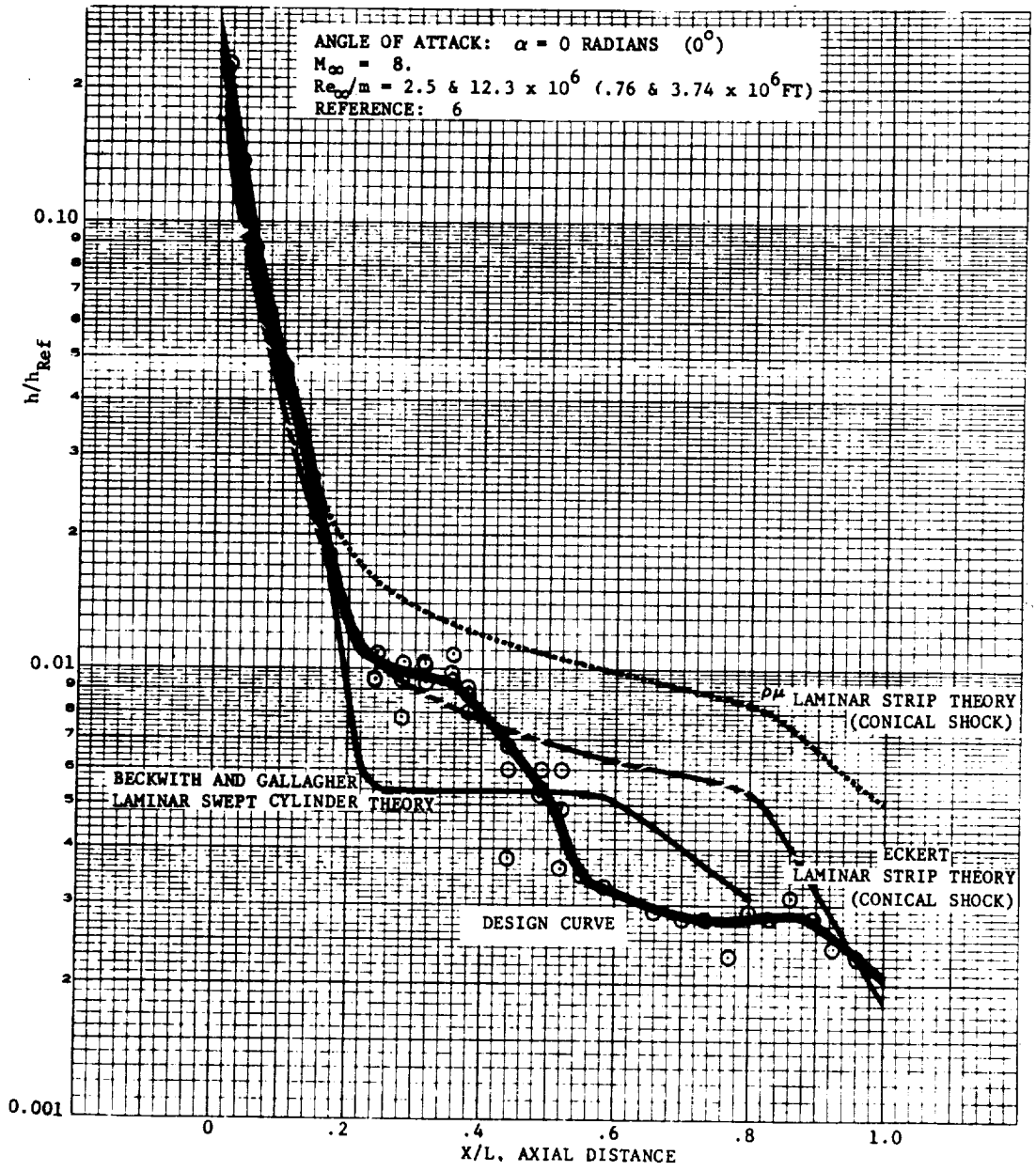

FIGURE 17

GD/C B-15B-2 BOOSTER LOWER SURFACE CENTERLINE HEATING DISTRIBUTION

ANGLE OF ATTACK = $\frac{\pi}{3}$ RADIANS (60°)

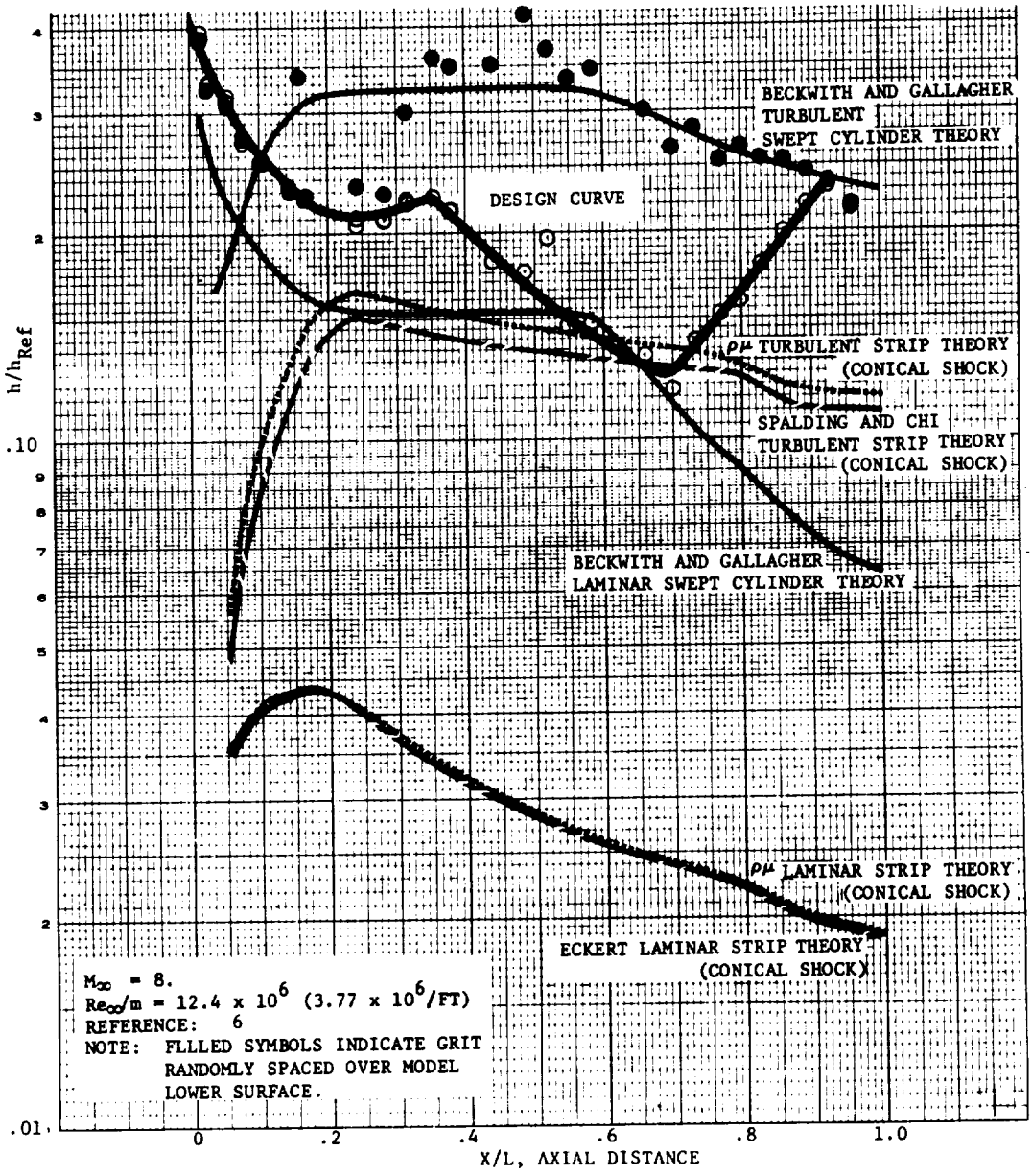

FIGURE 18

RATIO OF LOWER SURFACE CENTERLINE HEAT TRANSFER COEFFICIENT DATA TO TURBULENT BECKWITH AND GALLAGHER SWEPT CYLINDER VALUE

$M_\infty = 8.0$

ANGLE OF ATTACK: $\alpha = \pi/3$ RADIANS (60°)

$Re_\infty/m = 12.3 \times 10^6$ (3.75×10^6/FT)

NOTE: GRIT RANDOMLY SPACED ON LOWER SURFACE

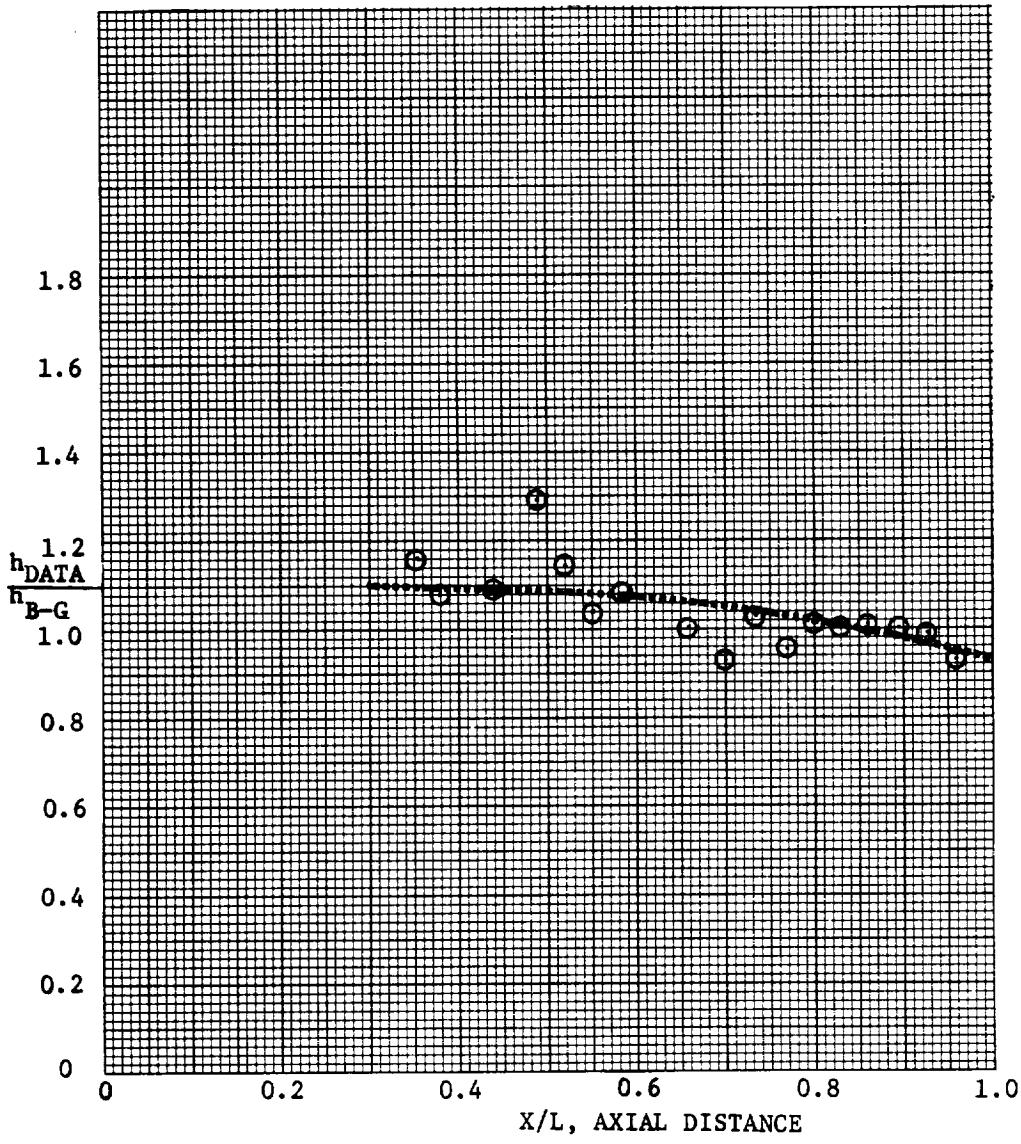

FIGURE 19
PERIPHERAL HEATING DISTRIBUTION
ANGLE OF ATTACK = $\frac{\pi}{6}$ RADIANS (30°)
X/L = 0.25

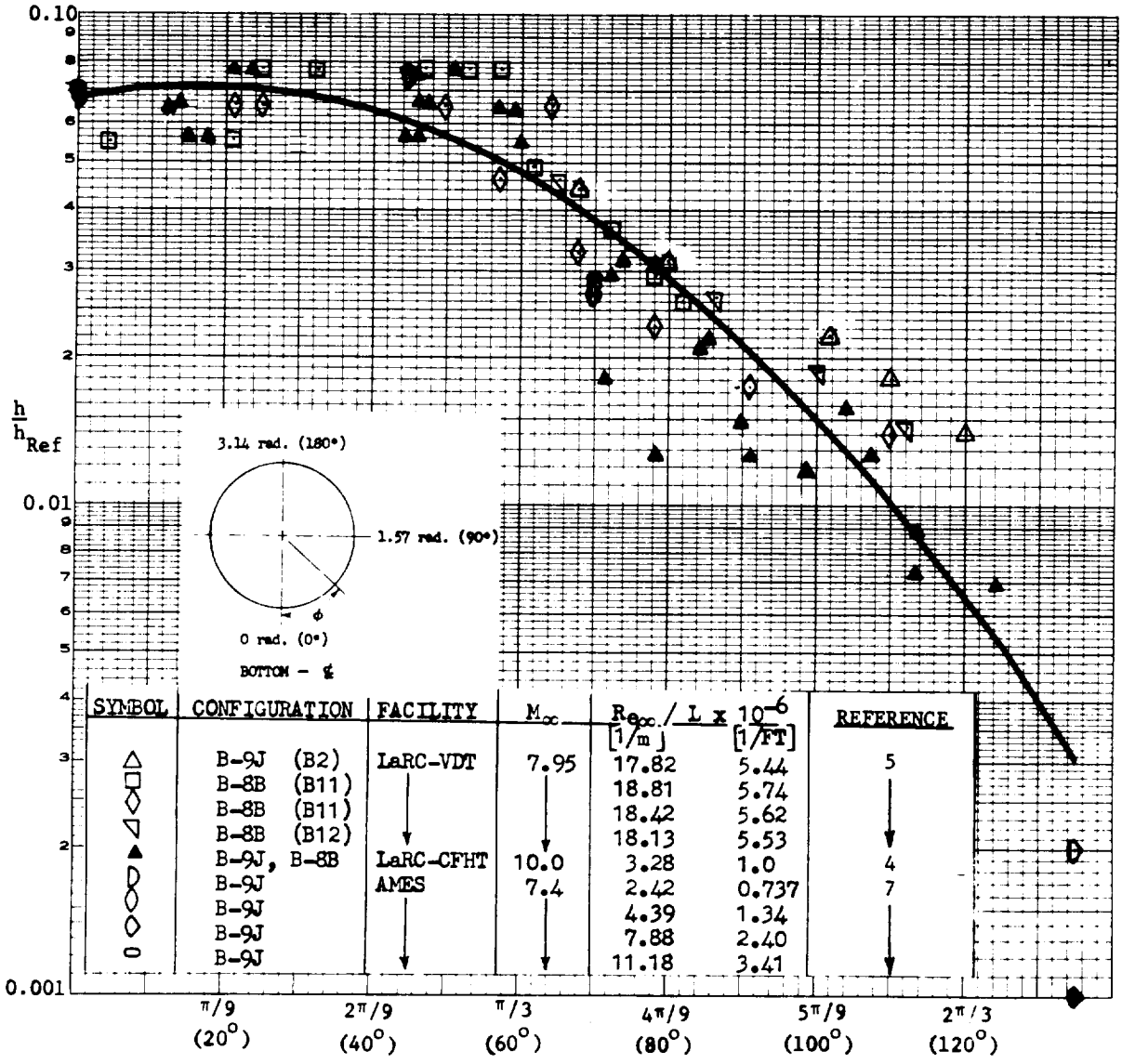

SYMBOL	CONFIGURATION	FACILITY	M_∞	Re_∞ / L x 10^{-6} [1/m]	[1/FT]	REFERENCE
△	B-9J (B2)	LaRC-VDT	7.95	17.82	5.44	5
□	B-8B (B11)	↓	↓	18.81	5.74	↓
◇	B-8B (B11)	↓	↓	18.42	5.62	↓
◁	B-8B (B12)	↓	↓	18.13	5.53	↓
▲	B-9J, B-8B	LaRC-CFHT	10.0	3.28	1.0	4
▷	B-9J	AMES	7.4	2.42	0.737	7
◇	B-9J	↓	↓	4.39	1.34	↓
◇	B-9J	↓	↓	7.88	2.40	↓
○	B-9J	↓	↓	11.18	3.41	↓

that as the angle of attack increases to $\pi/3$ radians (60 degrees) the heat transfer coefficients tend to become relatively independent of chordwise and spanwise location except in the vicinity of the leading edge.

Data-theory comparisons were made in the chordwise direction at the 50 percent span location on the lower surface. Eckert laminar, and Spalding and Chi turbulent strip theory, calculations were made using both oblique and conical shock flow field assumptions. These calculations were carried out over the total surface distance at this spanwise location. Also, in conjunction with the Eckert, and Spalding and Chi calculations, a Prandtl-Meyer expansion was carried out from the 50 percent chord location to the trailing edge of the wing. There was little difference in the results regardless of method, but the oblique shock calculation showed slightly better agreement with data at the lower angles of attack. On the basis of the theoretical calculations it was concluded that the flow was laminar for angles of attack of 0 and $\pi/18$ radians (0 and 10 degrees), turbulent at $\pi/9$ radians (40 degrees) when grit was applied to the lower surface and laminar without the grit. The $5\pi/18$ radian (50 degree) data appeared to be transitional and the $\pi/3$ radian (60 degree) data were turbulent (with or without grit on the lower surface). The data and their respective curve fits used for the nominal case are shown at the 50 percent span location for zero and $\pi/3$ radian (60 degree) angles of attack in Figures 20 and 21.

B. Leeward Surfaces

Upper surface centerline data for the GD/C B-15B-2 booster at zero angle of attack, obtained in AEDC Tunnel B, are shown in Figure 22. The curve fit shown in the figure was used in conjunction with mated interference results as the nominal case.

Upper surface centerline data on the GD/C B-15B-2 at $\pi/3$ radian (60 degree) angle of attack are shown in Figure 23. A portion of these data were obtained during a test with grit on the lower surface to induce turbulent flow. As indicated by the data, the grit did not affect the upper surface centerline flow. These data vary around the Eckert laminar strip theory computed for zero angle of attack. The systematic variations in the data indicate that this is not data scatter and is probably due to vortex impingement on the upper surface centerline. Because the Eckert laminar theory went through the mean of the data, it was used in the estimates of the thermal protection system weight.

Wing upper surface heat transfer data at the 50-percent span location is shown plotted against angle of attack in Figure 24. At the lower angles of attack the data decrease moving aft along the chord, while at the higher angles of attack

FIGURE 20

GD/C B-15B-2 BOOSTER WING LOWER SURFACE HEATING DISTRIBUTION

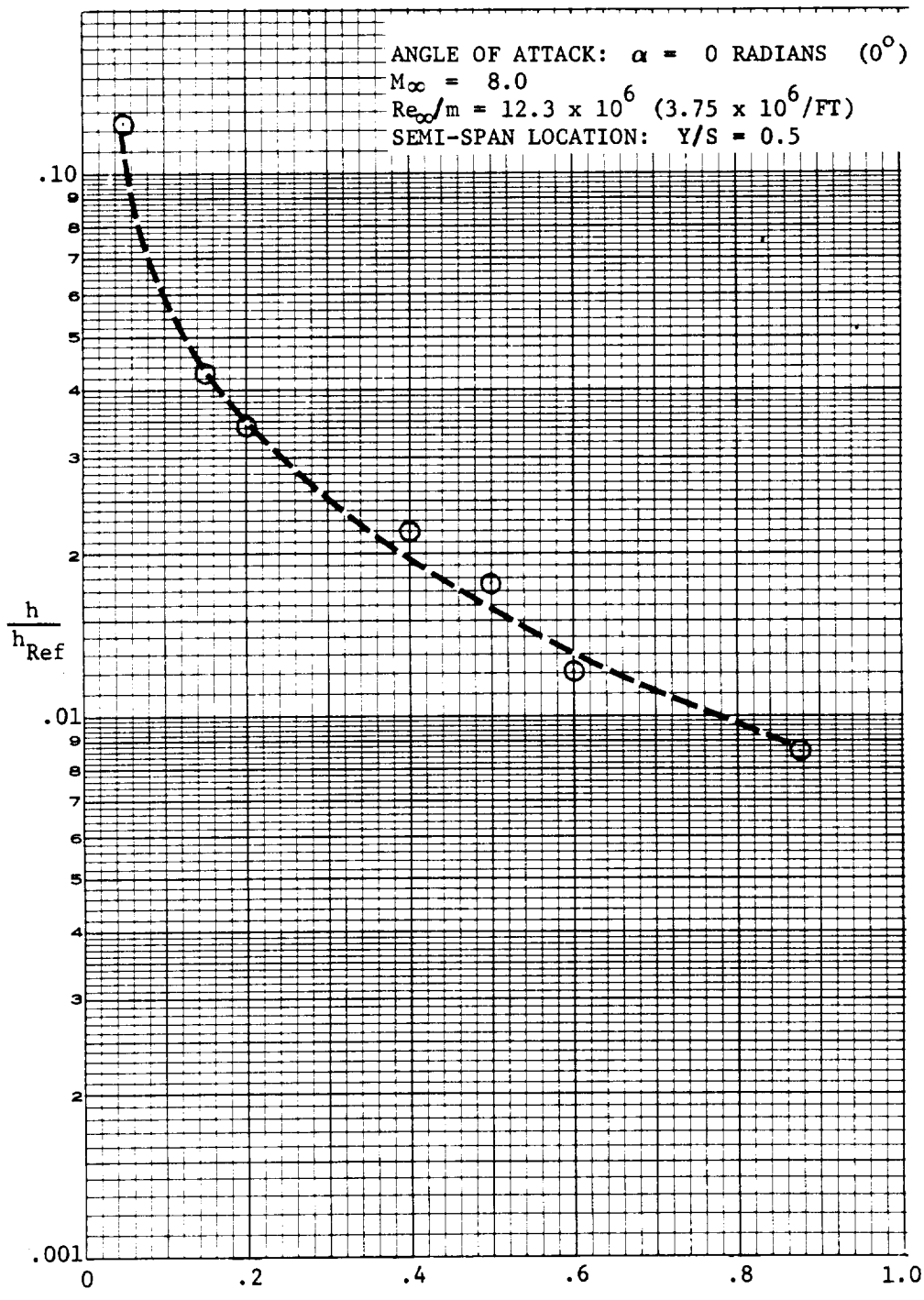

FIGURE 21

GD/C B-15B-2 BOOSTER WING LOWER SURFACE HEATING DISTRIBUTION

ANGLE OF ATTACK: $\alpha = \frac{\pi}{3}$ RADIANS (60°)
$M_{\infty} = 8.0$
$Re_{\infty}/m = 12.3 \times 10^{6}$ $(3.75 \times 10^{6}/FT)$
SEMI-SPAN LOCATION: Y/S = 0.5

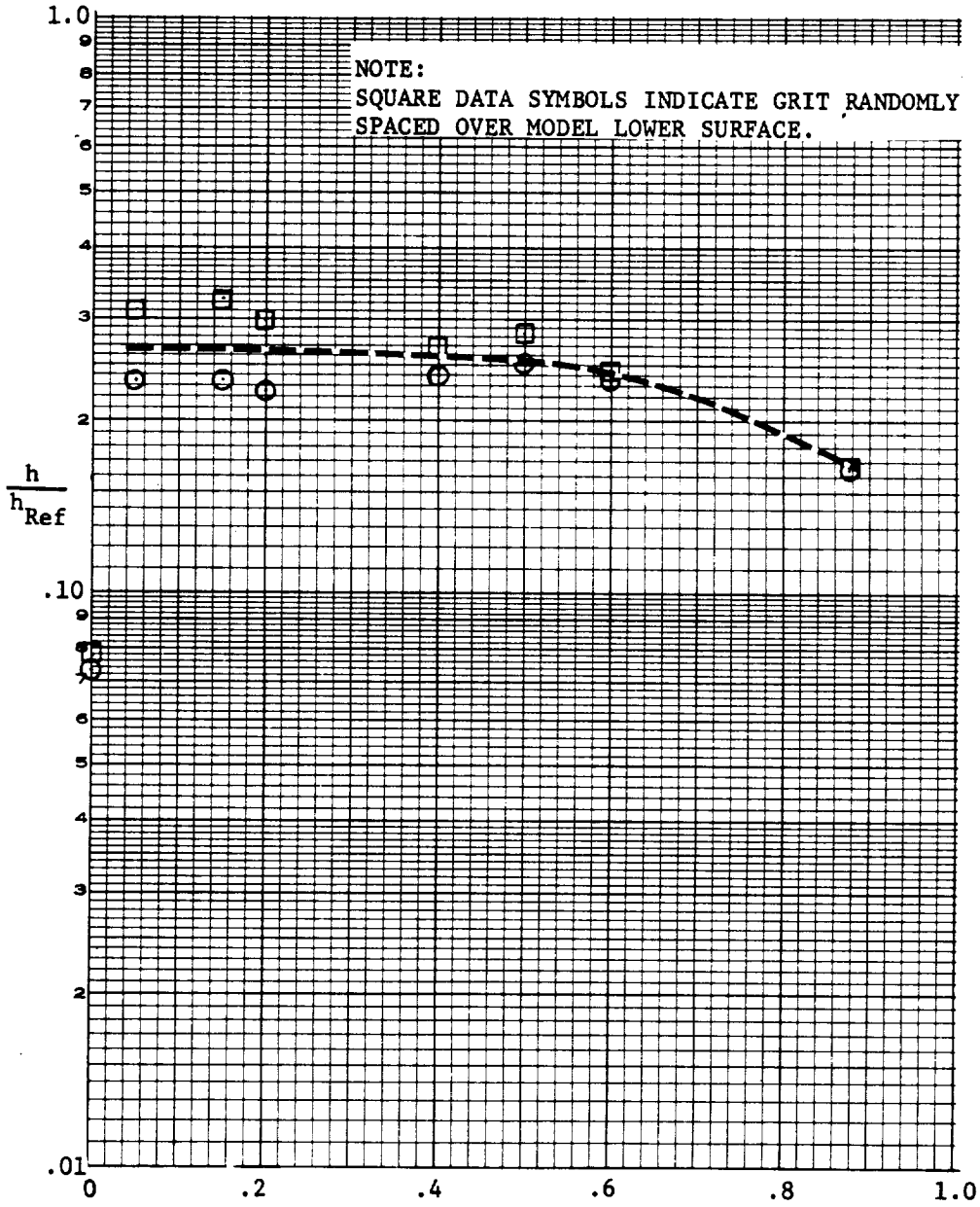

FIGURE 22

GD/C B-15B-2 UPPER SURFACE CENTERLINE HEATING DISTRIBUTION

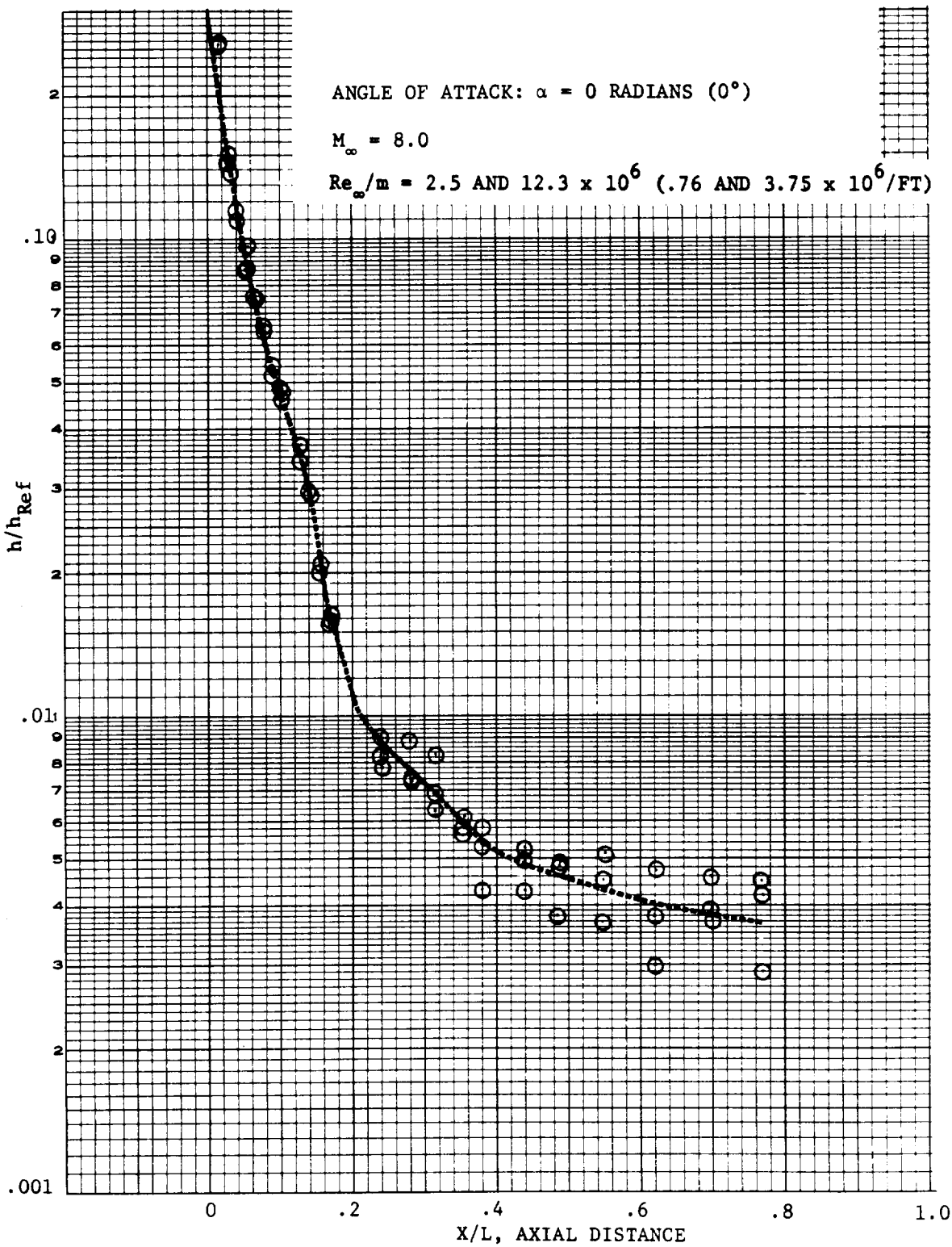

FIGURE 23
GD/C B-15B-2 UPPER SURFACE CENTERLINE HEATING DISTRIBUTION
ANGLE OF ATTACK = $\frac{\pi}{3}$ RADIANS (60°)

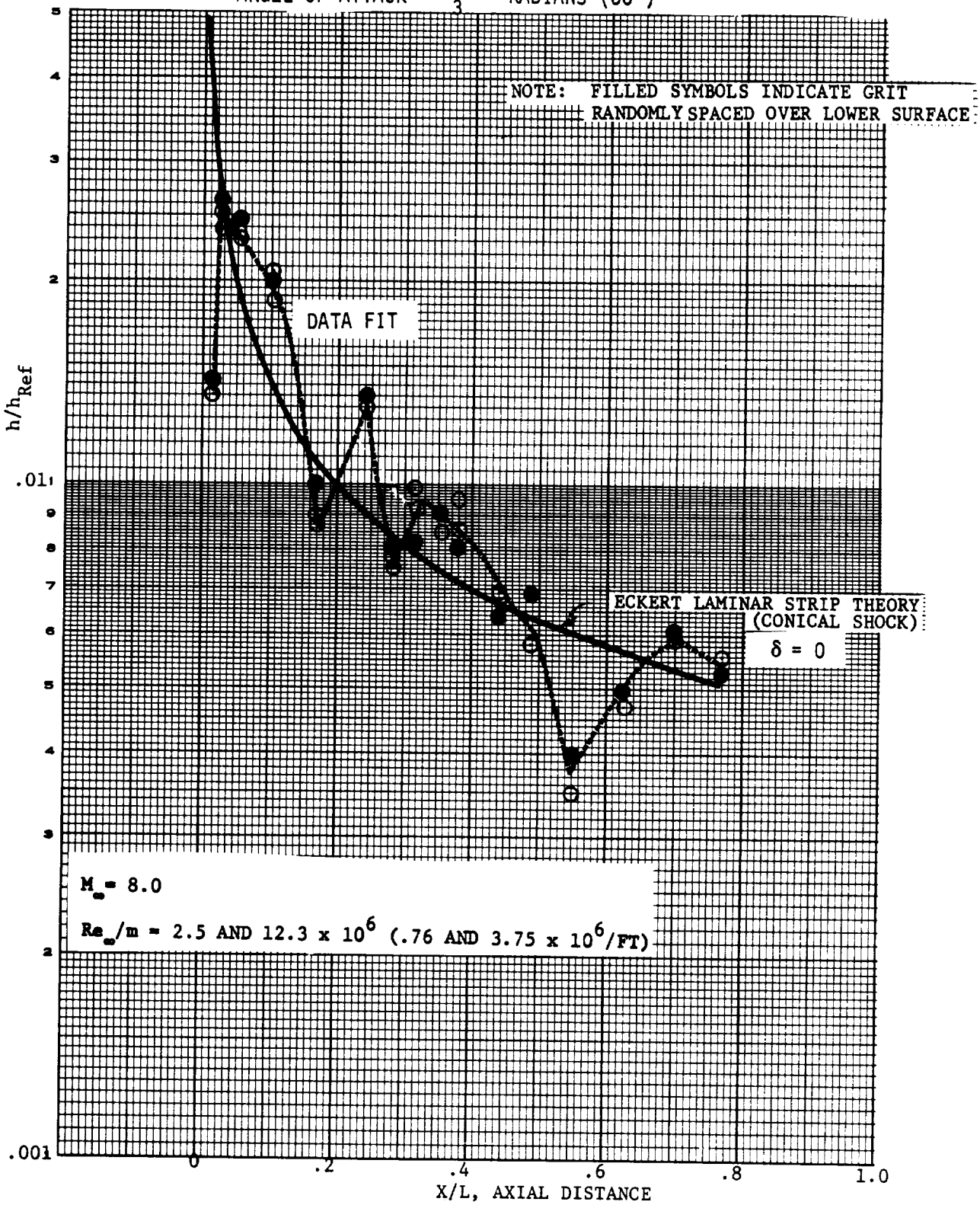

FIGURE 24

GD/C B-15B-2 BOOSTER WING UPPER SURFACE HEATING DISTRIBUTION

M_∞ = 8.0

Re_∞/m = 2.5 AND 12.3 x 10^6 (.76 AND 3.75 x 10^6/FT)

SEMI-SPAN LOCATION: Y/S = 0.5

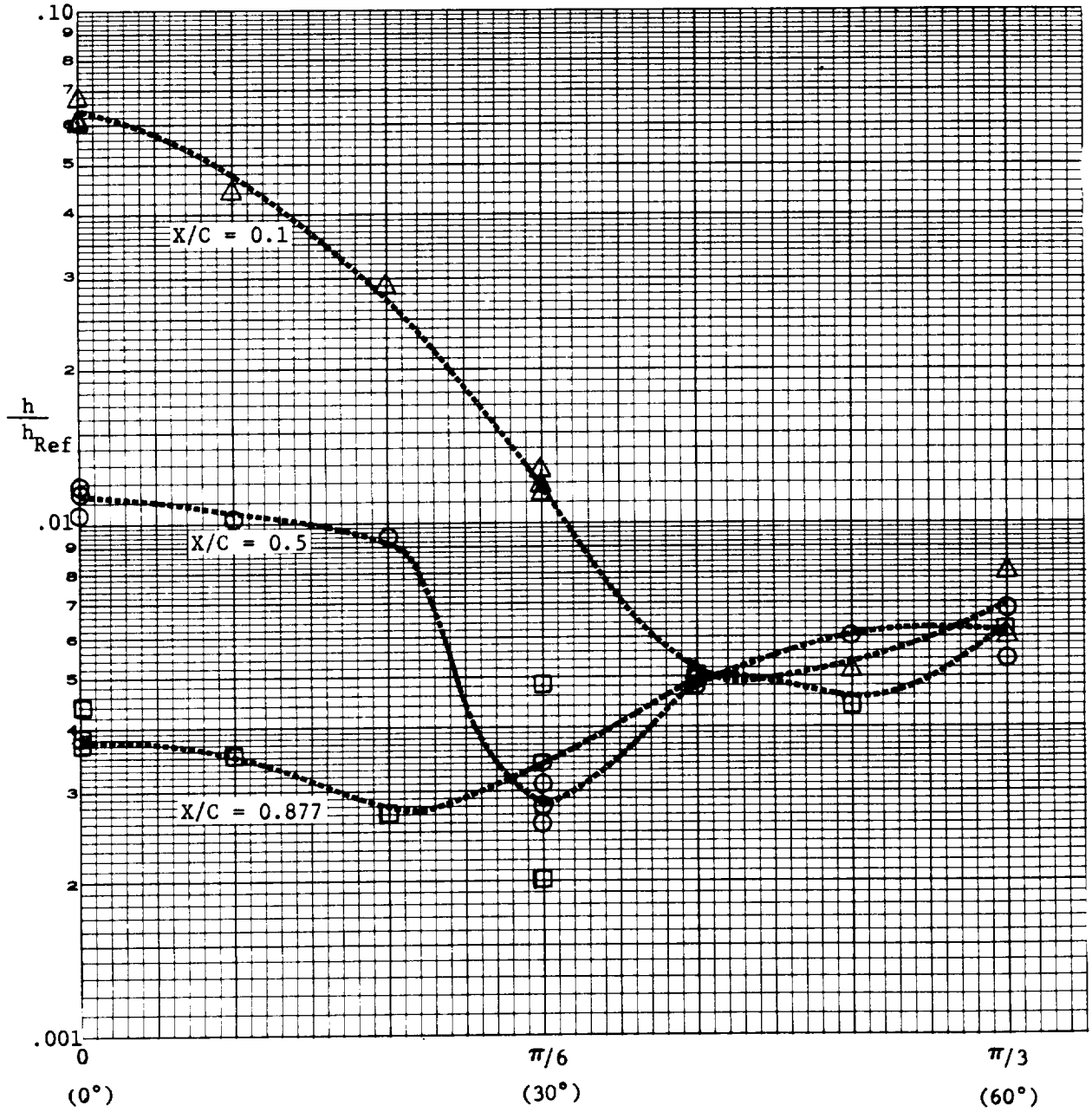

when the upper surface becomes shielded there is very little difference at the three chordwise locations. No systematic correlation of these data with the Eckert strip theory was found, and the data fairings shown on the figure were selected as nominal.

C. Interference Regions

The portions of the booster likely to be affected by interference are in the vicinity of the canard, the aft side body above the wing, and the upper surfaces during mated boost.

At zero angle of attack the mated interference overpowers any canard effects. Figure 25 shows the peripheral distribution of the heat transfer coefficient in the canard region at $\pi/3$ radian (60 degree) angle of attack. Some of the thermocouples were covered by the canard, and the data presented in the SADSAC report from those locations are not valid. These have been identified in the figures. The dashed line shown on the figure was generated by using a mean peripheral heat transfer distribution curve ($h\emptyset/h_{\ell}$) from Reference 3 for a clean cylinder at Mach 8.0. This was then applied to the centerline value of h/h_{ref}. This figure shows that the canard has no discernible effect on the heating distribution. The probable reason is that the canard is at zero angle of attack relative to the tunnel flow and the region of the body likely to be influenced by the canard is in a region of separated flow at this angle of attack.

The ratios of the local heat transfer coefficients on the side body above the wing (measured on the B-9J and B-15B-2 boosters) to those on the lower surface centerline were determined at several axial locations. The peak local values are presented in Figure 26. The trend of the data shows a decrease in peak value of this ratio with increasing angle of attack. This is due to increases in the lower surface heating with angle of attack,rather than to decreasing values of the body heating. For zero angle of attack the multipliers vary between 2.6 and 9 times the lower centerline value.

Interference heating on the mated GD/C booster was evaluated using the data of Reference 6. The configuration was comprised of the GD/C B-15B-2 booster and the NAR 161B delta wing orbiter. The ratios of the local heat transfer coefficients on the mated booster upper body to those on the unmated booster were determined as a function of axial location for four peripheral angles. Typical results are shown in Figures 27 and 28. As may be seen in the figures, heat transfer

FIGURE 25

GD/C B-15B-2 BOOSTER PERIPHERAL HEATING

CANARD REGION

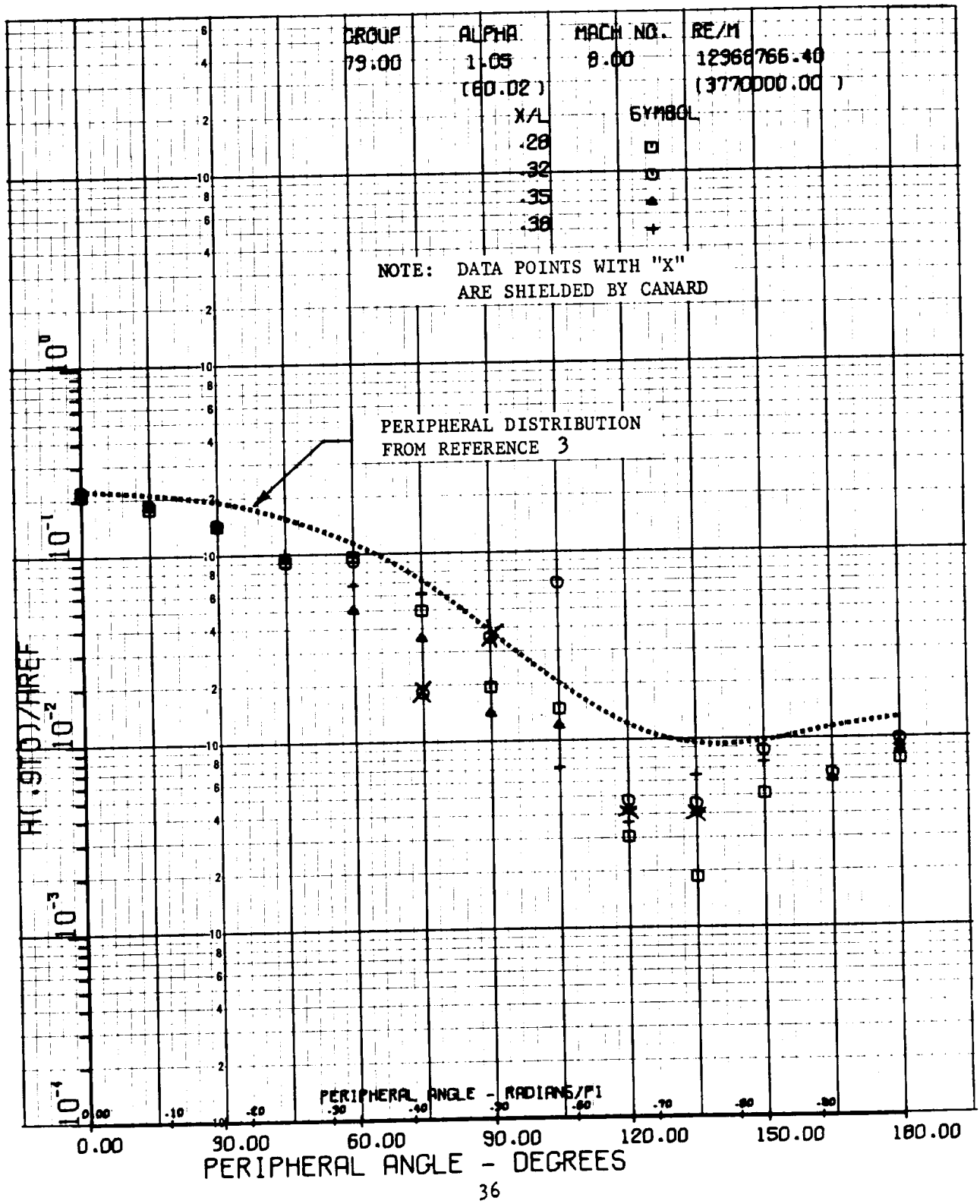

FIGURE 26

PEAK WING INTERFERENCE HEATING

(FUSELAGE ABOVE WING)

SYMBOL	X/L	M_∞	$Re_\infty/L \times 10^{-6}$ (1/m)	$Re_\infty/L \times 10^{-6}$ (1/FT)	CONFIGURATION	FACILITY
○	.625	8.0	12.3	3.75	B-15B-2	AEDC-B
□	.70	↓	↓	↓	↓	↓
△	.77					
◇	.895					
◪	.681	7.4	(2.82-16.19)	(.86-4.93)	B-9J	NASA-AMES
◭	.774	7.4			B-9J	NASA-AMES

NOTE: 1) WING-BODY JUNCTURE AT X/L ~.615
2) NASA-AMES DATA IS BASED ON $\dot{q}/\dot{q}_{Ref}$

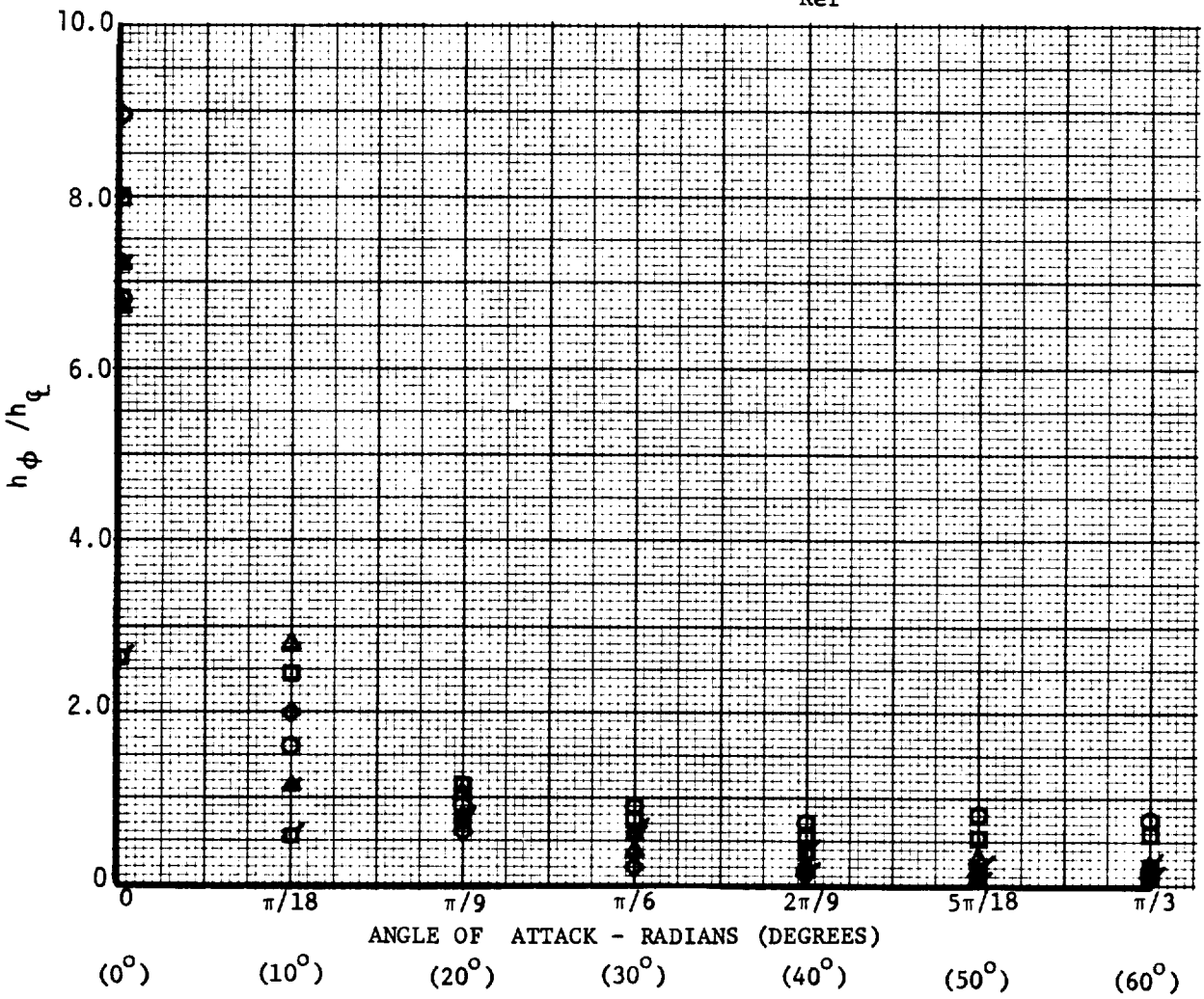

FIGURE 27

MATED INTERFERENCE HEATING - GD/C BOOSTER

$\alpha = 0$

$\phi = \frac{\pi}{2}$ RADIANS (90°)

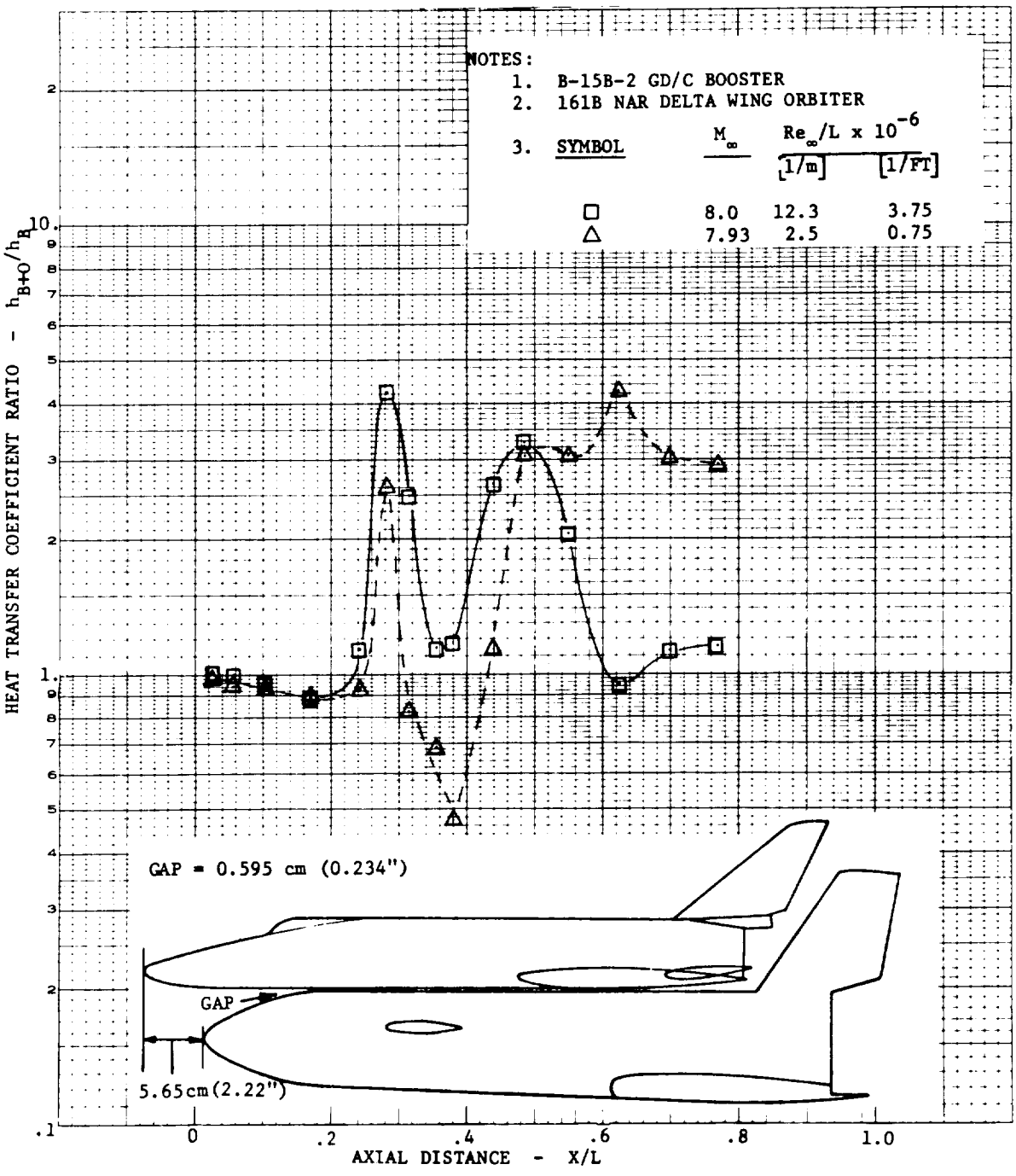

FIGURE 28

MATED INTERFERENCE HEATING - GD/C BOOSTER

$\alpha = 0$

$\phi = \pi$ RADIANS (180°)

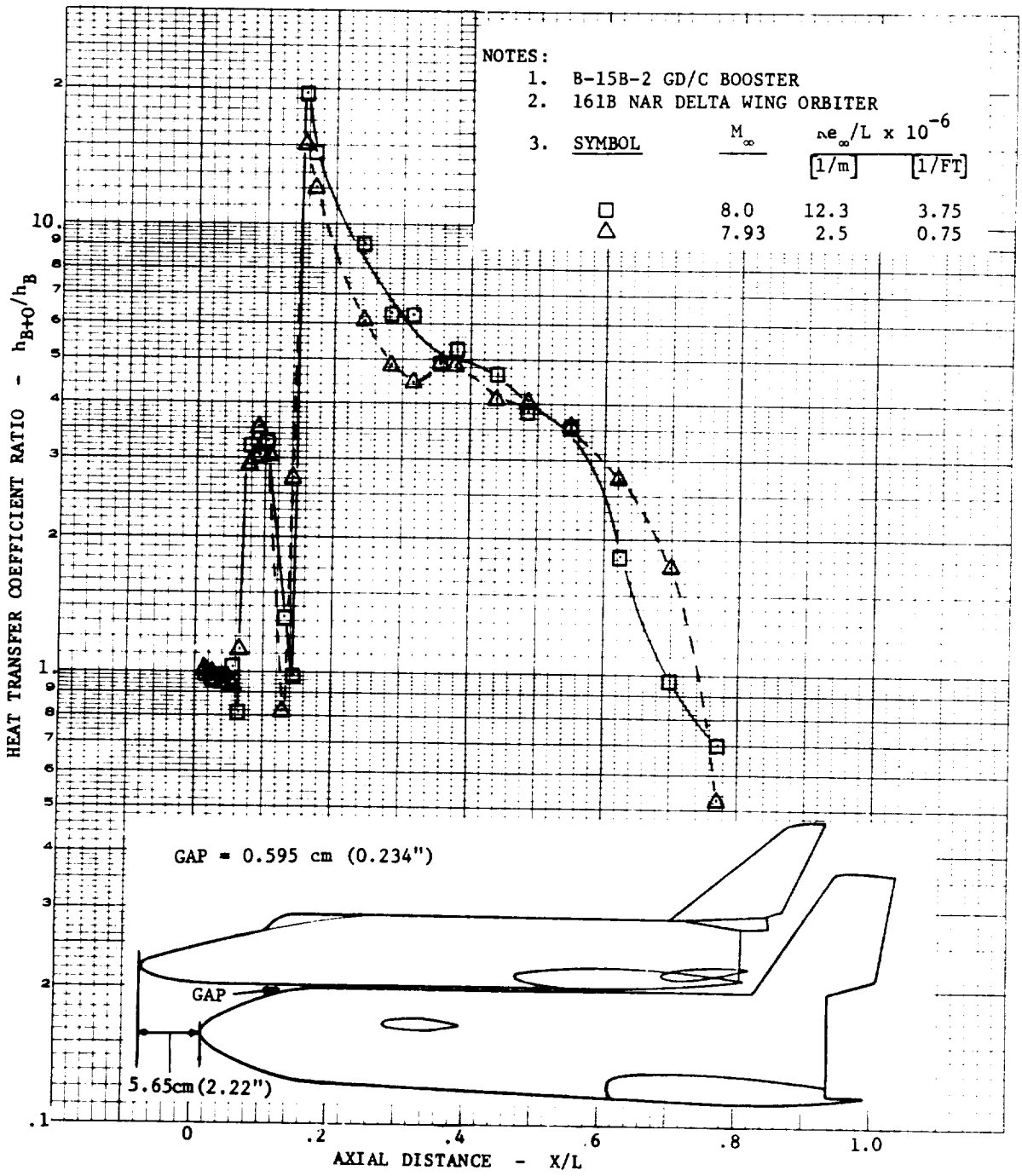

coefficients on the mated booster in some locations are as much as 4 times those on the booster alone at $\phi = \pi/2$ radians (90 degree) increasing to approximately 20 on the top of the vehicle. The data show no systematic trend with Reynolds number.

A correlation of mated interference effects as a function of free stream Mach number, obtained from Reference 8, is shown in Figure 29. Superimposed on the data of the reference are the two peak values on the upper centerline of the B-15B-2 booster (Figure 28). These data show very good agreement with the correlation and were therefore used to determine the nominal mated interference effects. The correlation assumes a Mach number dependence on the ratio of mated to unmated heating. Alternate correlations involving Reynolds number were also evaluated, but provided no better fit.

Upper wing data on the mated B-15B-2 booster exhibited more scatter than on the unmated configuration, however, no net increase of the heating level was noted. In addition, no bow shock interactions were observed on the instrumented portion of the wing which extended outboard to 70 percent of the semispan.

FIGURE 29

CORRELATION OF INTERFERENCE HEATING DATA

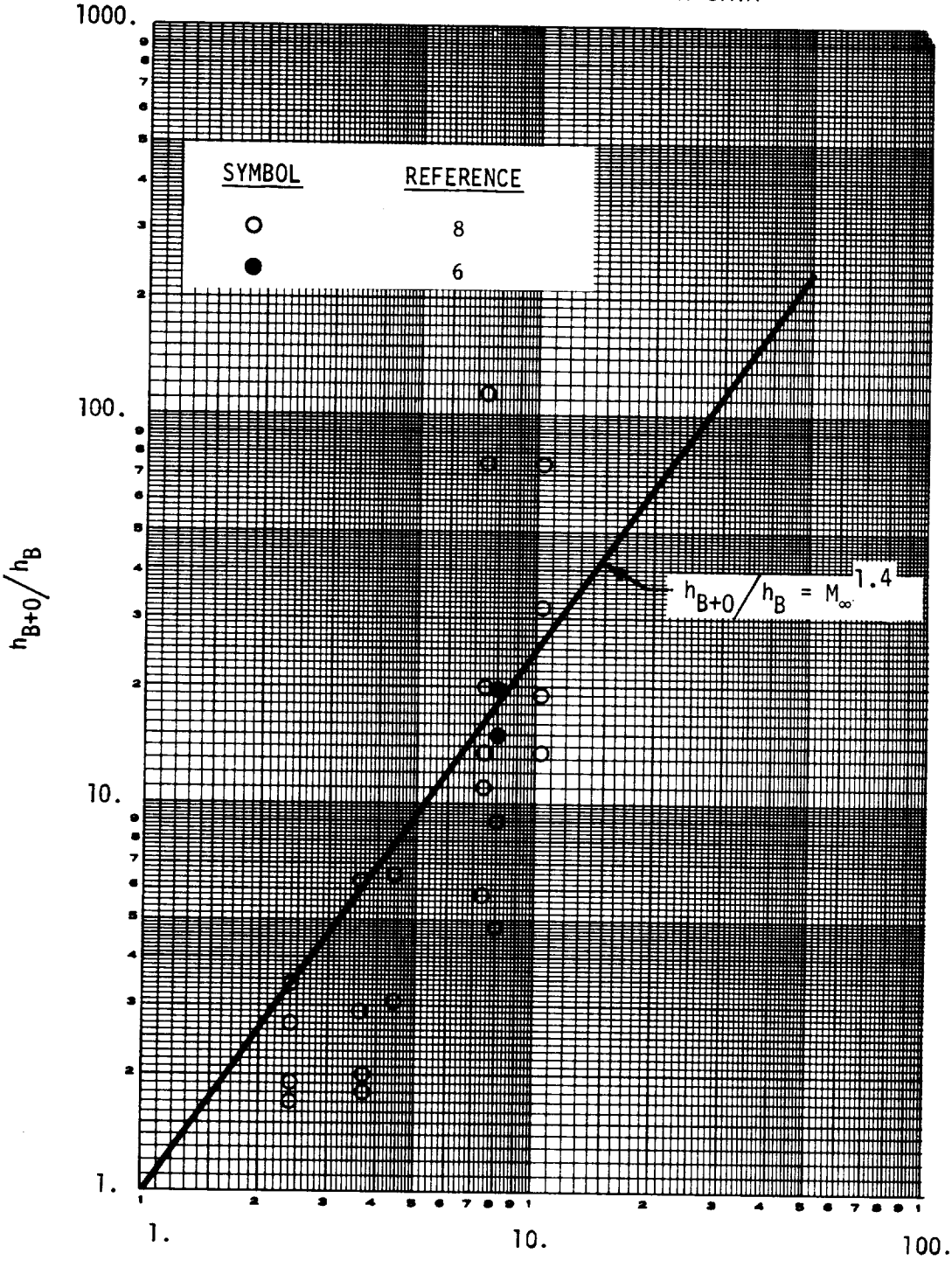

2 Orbiter

a. Windward Surfaces - Lower surface centerline data correlations included both least-square curve fits and multiple regression analysis of the NAR and MDC orbiter data.

Least-square curve fits were made to the ratio of the Reference 9 data to theory on the NAR orbiter lower surface centerline for the $\rho\mu$ and Eckert laminar strip theories and Beckwith and Gallagher laminar swept cylinder theories. Resultant curve fits at an angle of attack equal to $\pi/6$ radians (30 degrees) for the $\rho\mu$ and Beckwith and Gallagher theories are shown in Figures 30 and 31, respectively. Similar fits were made to the MDC delta wing orbiter data of Reference 10. Standard deviations of the data about the curve fits were obtained and typical results are shown for the MDC orbiter in Figure 32. As seen in this figure, there is little difference between the three theories, except for Beckwith and Gallagher at zero angle of attack where this theory is not expected to be valid.

Multiple regression analysis was employed to refine the computed data fits. Given a set of observations of the dependent and independent variables involved in a particular experiment, multiple regression can be employed to obtain a best fit to the data by an equation of the form:

$$y = a_o + a_1x_1 + a_2x_2 + a_3x_3 + \ldots + a_nx_n$$

where y is the dependent variable and x, x_2, . . ., x_n are the independent variables. A multiple regression solution gives the least-square "best" value of the coefficients a_o, a_1, . . ., a_n. In addition to the final equation, intermediate regression equations are obtained after each step in the MRA which give an indication of which variables are most important to the analysis. Also some of the variables included in the analysis may be rejected because they have no significant effect on the dependent variable. For each step in the MRA, predictions of the dependent variable (based on the current equation) are determined along with statistical information regarding goodness of fit, multiple correlation coefficients,and various measures of the reliability of the coefficients. Of particular importance is the standard error of estimate for each step which represents the RMS error of the predictions. MRA is a powerful tool when little is known about the functional form of the dependent variable, but the method is enhanced when such knowledge is available. A more thorough discussion of MRA is presented in Reference 11. The functional

FIGURE 30

LOWER SURFACE CENTERLINE DATA CORRELATION FOR NAR DELTA WING ORBITER

Angle of Attack: $\alpha = \pi/6$ RADIANS (30°)

Theory: $\rho\mu$ Laminar Strip Theory

Flagged Symbols: $M_\infty \cong 10.0$

Unflagged Symbols: $M_\infty = 8.0$

Reference: 9

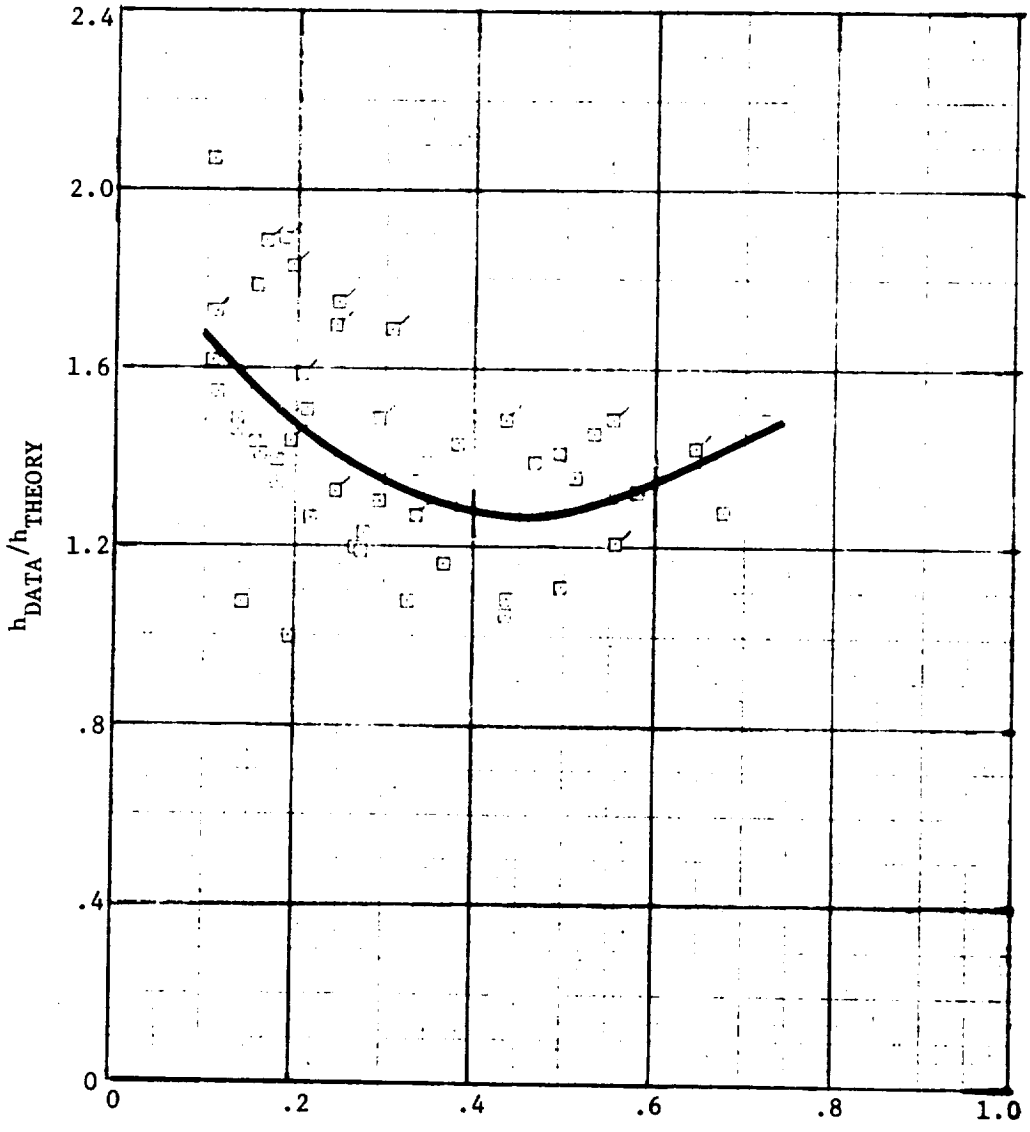

FIGURE 31

LOWER SURFACE CENTERLINE DATA CORRELATION FOR NAR DELTA WING ORBITER

Angle of Attack: $\alpha = \pi/6$ RADIANS (30^{o})

Theory: Beckwith & Gallagher Laminar Strip Theory

Flagged Symbols: M_∞ 10.0

Unflagged Symbols: $M_\infty = 8.6$

Reference: 9

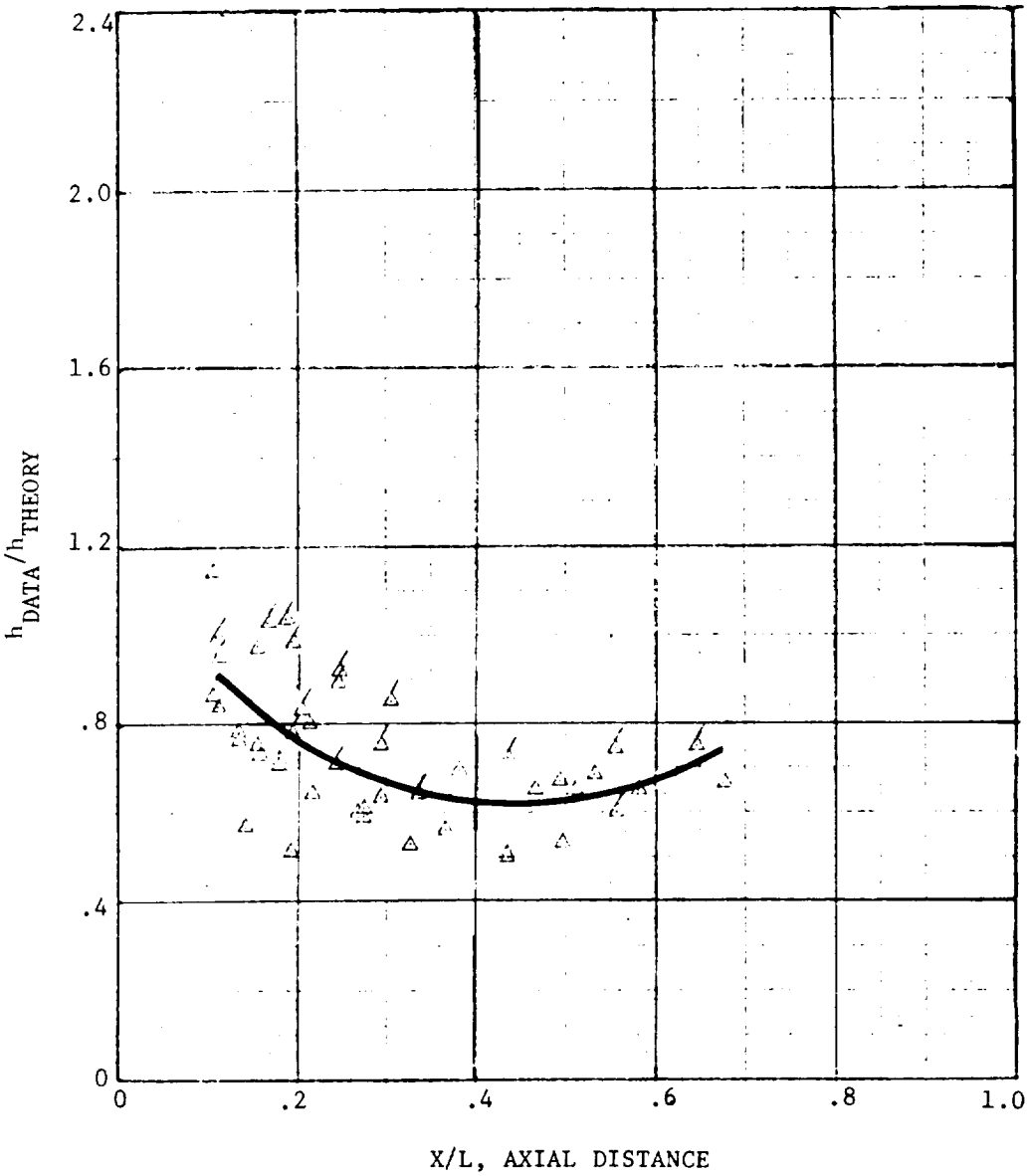

FIGURE 32

COMPARISON OF STANDARD DEVIATION FOR DIVERGENCE PARAMETER

MDAC DELTA WING ORBITER

ANGLE OF ATTACK RADIANS (DEGREES)	STANDARD DEVIATION - PERCENT		
	ECKERT	$\rho\ \mu$	BECKWITH & GALLAGHER
0	2.0	2.0	16.9
$\pi/18$ (10)	9.1	9.0	9.3
$\pi/9$ (20)	18.3	22.3	19.3
$\pi/6$ (30)	6.5	6.0	2.5
$2\pi/9$ (40)	14.5	13.3	16.5
$\pi/3$ (60)	15.5	16.0	16.0

form assumed for the NAR orbiter data was $h_{Data}/h_{Theory} = f\ [X/L,\ (X/L)^2,\ M_\infty,\ Re_\infty/L]$. Results obtained are shown in Figure 33. The standard deviation is reduced with the use of this method but not appreciably.

Correlation of the MDC lower surface centerline data included least-square curve fits to the ratio of data to theory. The curve fits, shown in Figure 34 were obtained using the Eckert theory for laminar flow and the Spalding and Chi theory for turbulent flow. Crossflow corrections as described in Reference 12 were applied to the theories. The curves shown are third order fits to the local flow deflection angle, δ. Multiple regression analysis was also applied to the MDC orbiter data obtained at AEDC Tunnel B and Cornell. Three cases considered are summarized in Figure 35. The stepwise development of the MRA equation is shown for each case. The first case employed flow deflection angle, velocity and unit Reynolds number as independent variables. The second case dropped the variable δ^3 and the third case employed powers of δ up to third order and, hence, gives the same results as the least-square fits. As shown in the figure, Case 1 yields a lower standard error and a somewhat better fit than Case 3, as indicated by the correlation coefficient. As with the NAR data, the differences are small and it was concluded that the use of least-square curve fits was the more expedient method of obtaining results within the accuracies required. Therefore, the curves of Figure 34 were used as nominal for TPS design.

FIGURE 33

COMPARISON OF LEAST SQUARE CURVE FIT WITH MULTIPLE REGRESSION ANALYSIS

NAR DELTA WING ORBITER
ECKERT LAMINAR STRIP THEORY

$\alpha = \pi/6$ RADIANS (30°)

Symb.	M_∞	$Re_\infty/L \times 10^{-6}$	
		1/m	1/FT
◑	10.3	1.64	.50
○	7.91	5.93	1.808
●	7.91	18.96	5.780

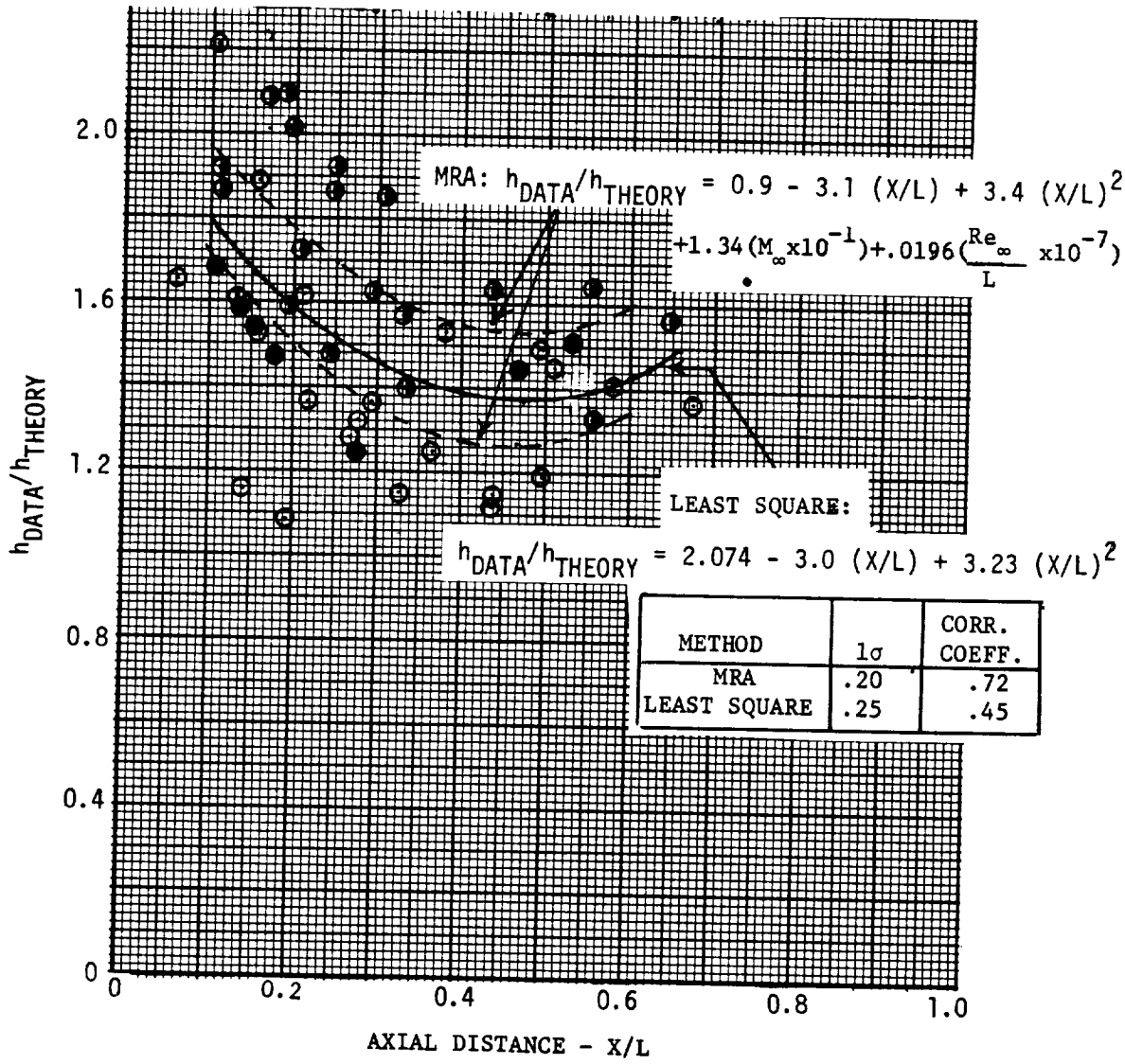

FIGURE 34

MDAC 050/B ORBITER LOWER SURFACE CENTERLINE DATA CORRELATION

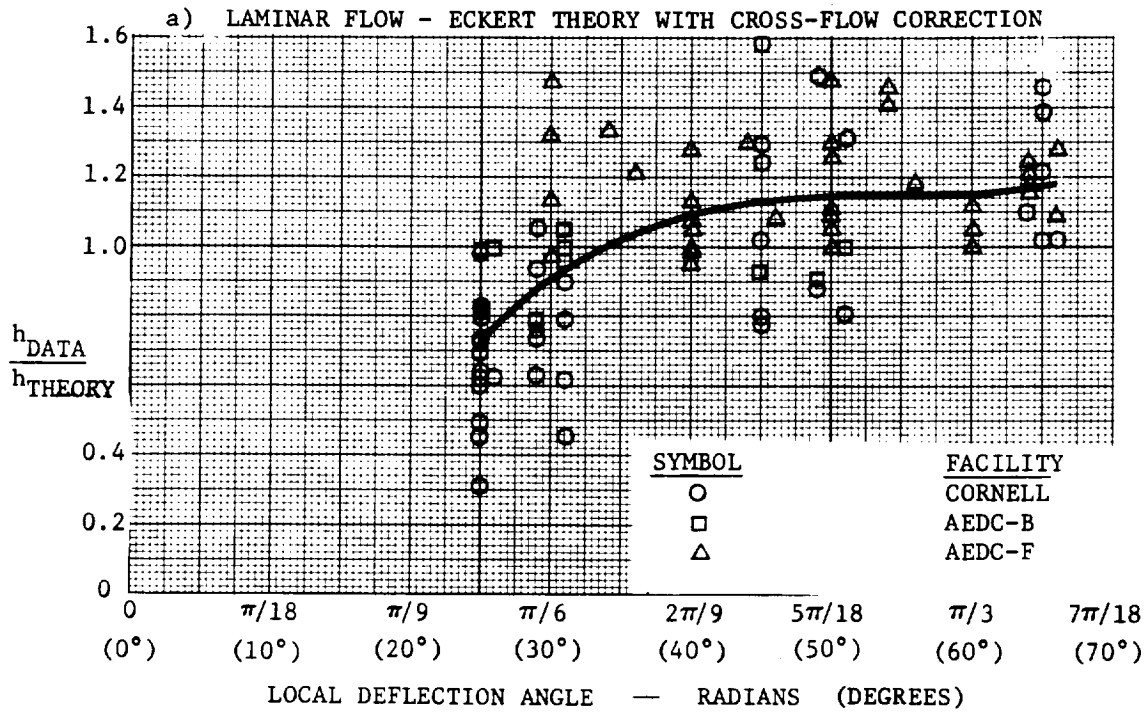

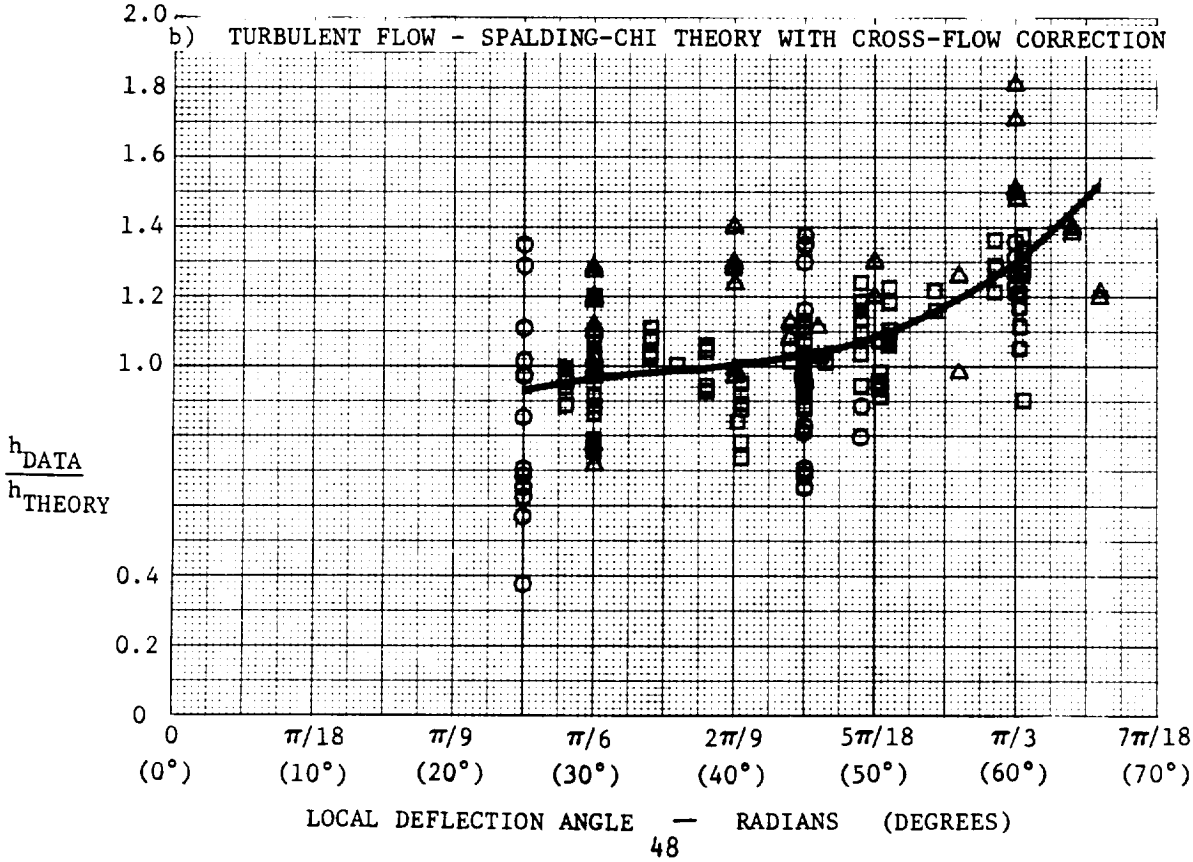

FIGURE 35

STEPWISE MULTIPLE REGRESSION ANALYSIS
OF MDAC/DWO LOWER SURFACE CENTERLINE DATA

FLOW: TURBULENT

FACILITIES: AEDC-B, AEDC-F

CASE	ASSUMED FORM OF EQUATION
1	$q_{DATA}/q_{THEORY} = f(\delta, \delta^2, \delta^3, V_\infty, Re_\infty/FT)$
2	$q_{DATA}/q_{THEORY} = f(\delta, \delta^2, V_\infty, Re_\infty/FT)$
3	$q_{DATA}/q_{THEORY} = f(\delta, \delta^2, \delta^3)$

CASE	STEP	STANDARD ERROR OF ESTIMATE	MULTIPLE CORRELATION COEFFICIENT	VARIABLE ENTERED
1	1	0.1672	0.6324	δ^3
	2	0.1409	0.7594	V_∞
	3	0.1360	0.7796	Re_∞/FT
	4	0.1352	0.7844	δ^2
	5	0.1343	0.7893	δ
2	1	0.1711	0.6096	δ^2
	2	0.1437	0.7438	V_∞
	3	0.1396	0.7663	Re_∞/FT
	4	0.1369	0.7780	δ
3	1	0.1672	0.6324	δ^3
	2	0.1657	0.6435	δ^2
	3	0.1595	0.6791	δ

Lower surface spanwise heat transfer distributions on the MDC orbiter were determined utilizing Shuttle Phase B results for both the MDC and NAR orbiters. Nominal spanwise distributions normalized by the centerline laminar heat transfer coefficient, obtained from Reference 13, are shown versus angle of attack for three spanwise locations at X/L = 0.5 in Figure 36. Similar results are shown in Figure 37 for an angle of attack equal to 0.436 radians (25 degrees) at X/L = 0.75. A comparison of the data scatter on the MDC orbiter with that on the NAR orbiter, obtained utilizing the data of Reference 9, shows good agreement. The nominal spanwise distributions with turbulent centerline flow, also obtained from Reference 13, are shown against angle of attack for three spanwise locations in Figure 38.

Upper Surfaces - Upper surface centerline data for the MDC orbiter, obtained in AEDC Tunnels B and F, are shown in Figures 39 and 40 for angles of attack equal to $\pi/6$ and 0.698 radians (30 and 40 degrees). As shown in the figures, separate curve fits were used forward and aft of the canopy because of the large difference in heating levels. Although there is little difference in the results at the two angles of attack, a design value for the nominal case was interpolated for the 0.593 radian (34 degree) angle of attack.

The upper wing data for the MDC orbiter obtained at Cornell were compared with Eckert laminar strip theory. Such a comparison was made since one traditional method of predicting heating rates on leeward surfaces in separated flow has been the use of a percentage (50 to 55 percent) of flat plate heating rates. The data exhibited a scatter of one order of magnitude, as shown in Figure 41, and the highest data points were less than 20 percent of the theoretical results. Also, no systematic variations with Mach number or Reynolds number could be found. It was, therefore, concluded that the linear fit shown on the figure would be the most reasonable for the nominal case.

In order to obtain a better understanding of the leeward side flow characteristics on the MDC orbiter, oil flow data from tests in the Ames 3.5 ft hypersonic tunnel were studied. The data show that flow separation occurs as the flow rounds the leading edge chine for angles of attack from 0.35 to 0.87 radians (20 and 50 degrees). Location of the separation varied with angle of attack as shown in Figure 42. These results confirm the low heating levels obtained on the upper wing. The data also indicated a weak vortex flow which streams along the upper body centerline and impinges on the canopy. The relative weakness of this impingement phenomenon was verified by the Cornell tests on this configuration.

FIGURE 36

MDAC DELTA WING ORBITER (050/B) LOWER SURFACE SPANWISE HEATING DISTRIBUTION
LAMINAR CENTERLINE FLOW, X/L = 0.5

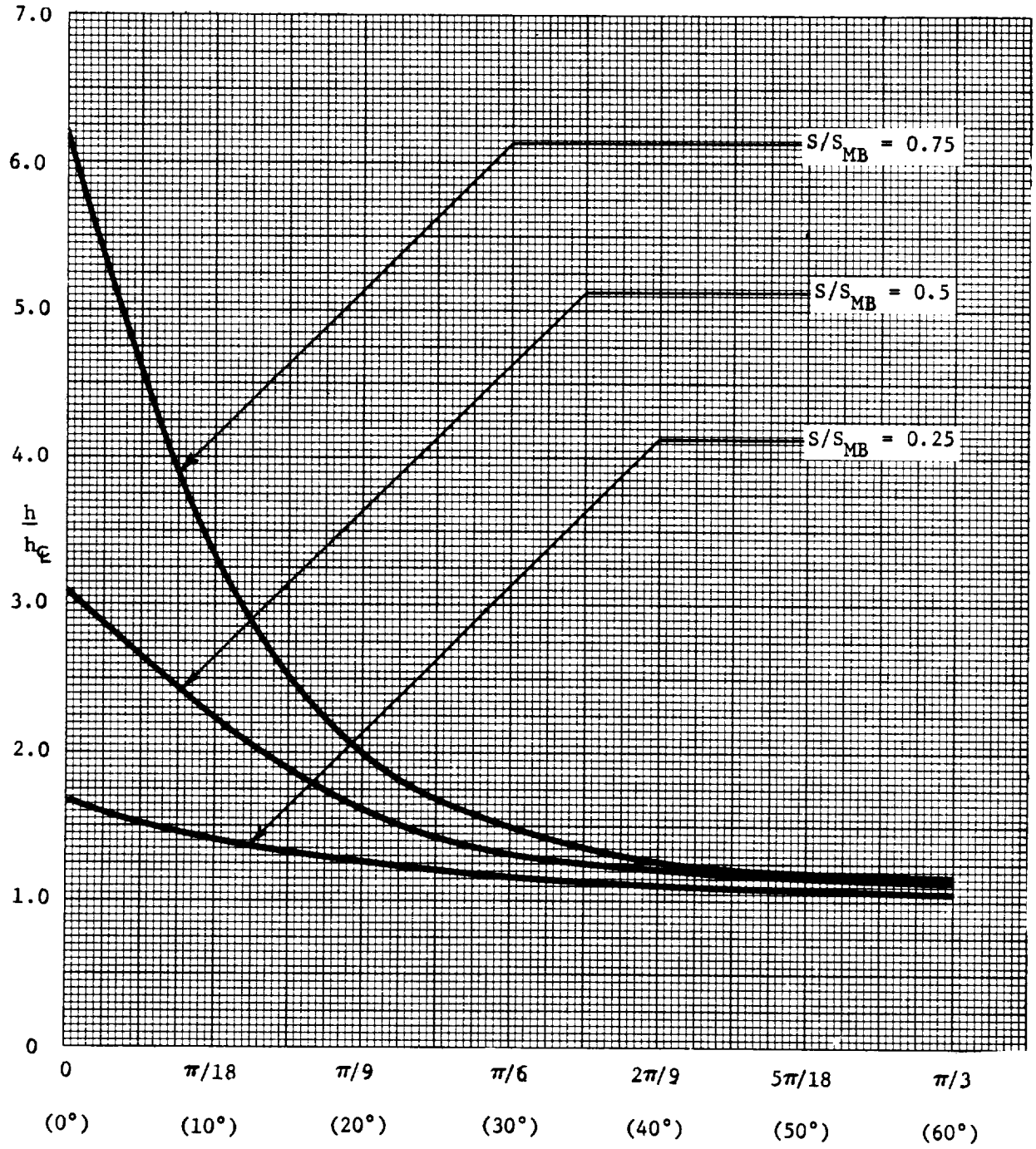

FIGURE 37

LOWER SURFACE SPANWISE HEATING DISTRIBUTION
FOR MDAC DELTA WING ORBITER (050/B)
LAMINAR CENTERLINE FLOW, X/L = 0.75

ANGLE OF ATTACK: 0.436 RADIANS (25°)

SYMBOL	$Re_\infty/L \times 10^{-6}$ [1/m]	$Re_\infty/L \times 10^{-6}$ [1/FT]	M_∞
○	0.985	0.3	8
○	0.985	0.3	12
□	6.56	2.0	8
◇	9.83	3.0	12

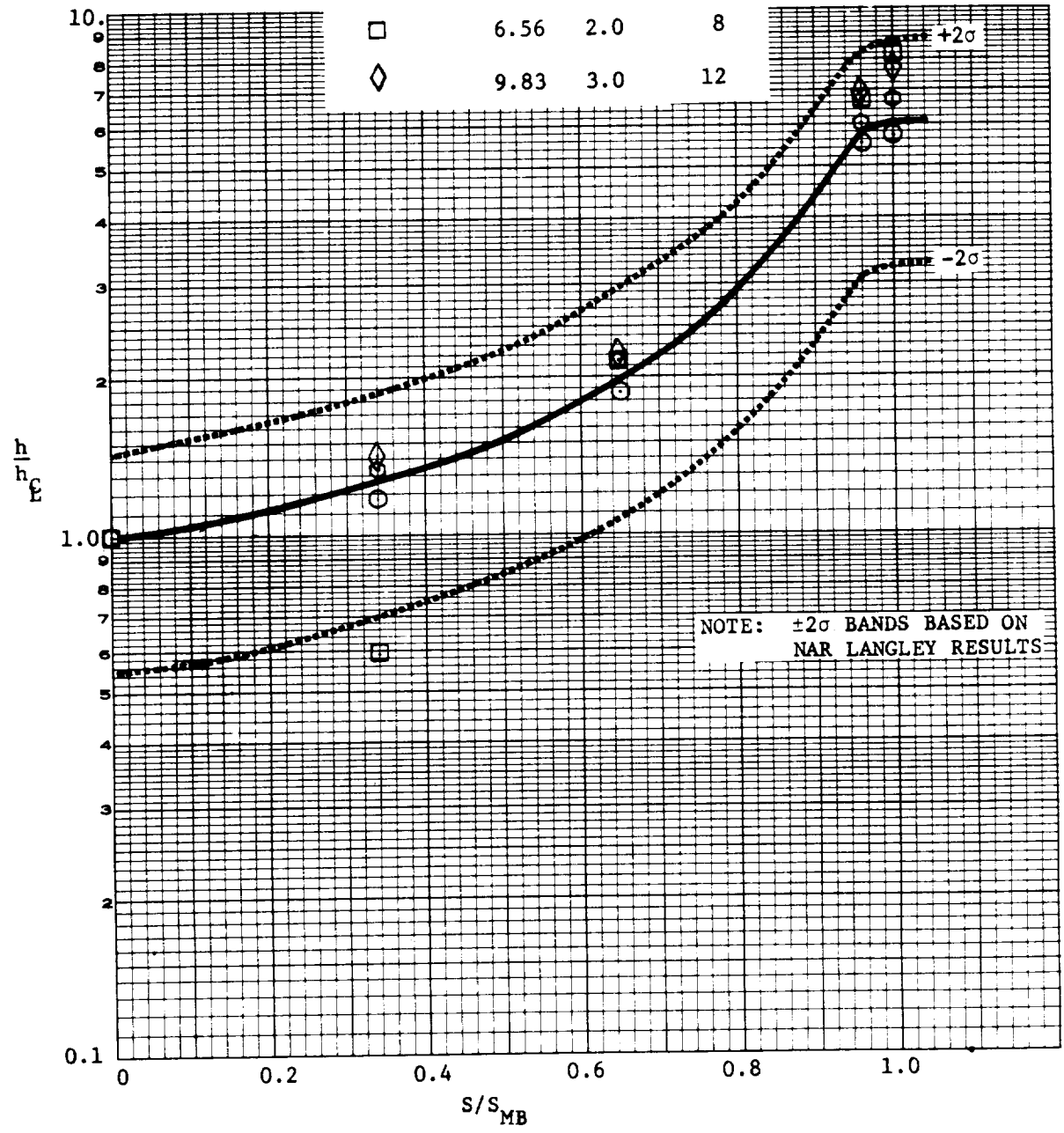

FIGURE 38

MDAC DELTA WING ORBITER (050/B) LOWER SURFACE SPANWISE HEATING DISTRIBUTION
TURBULENT CENTERLINE FLOW, X/L = 0.5

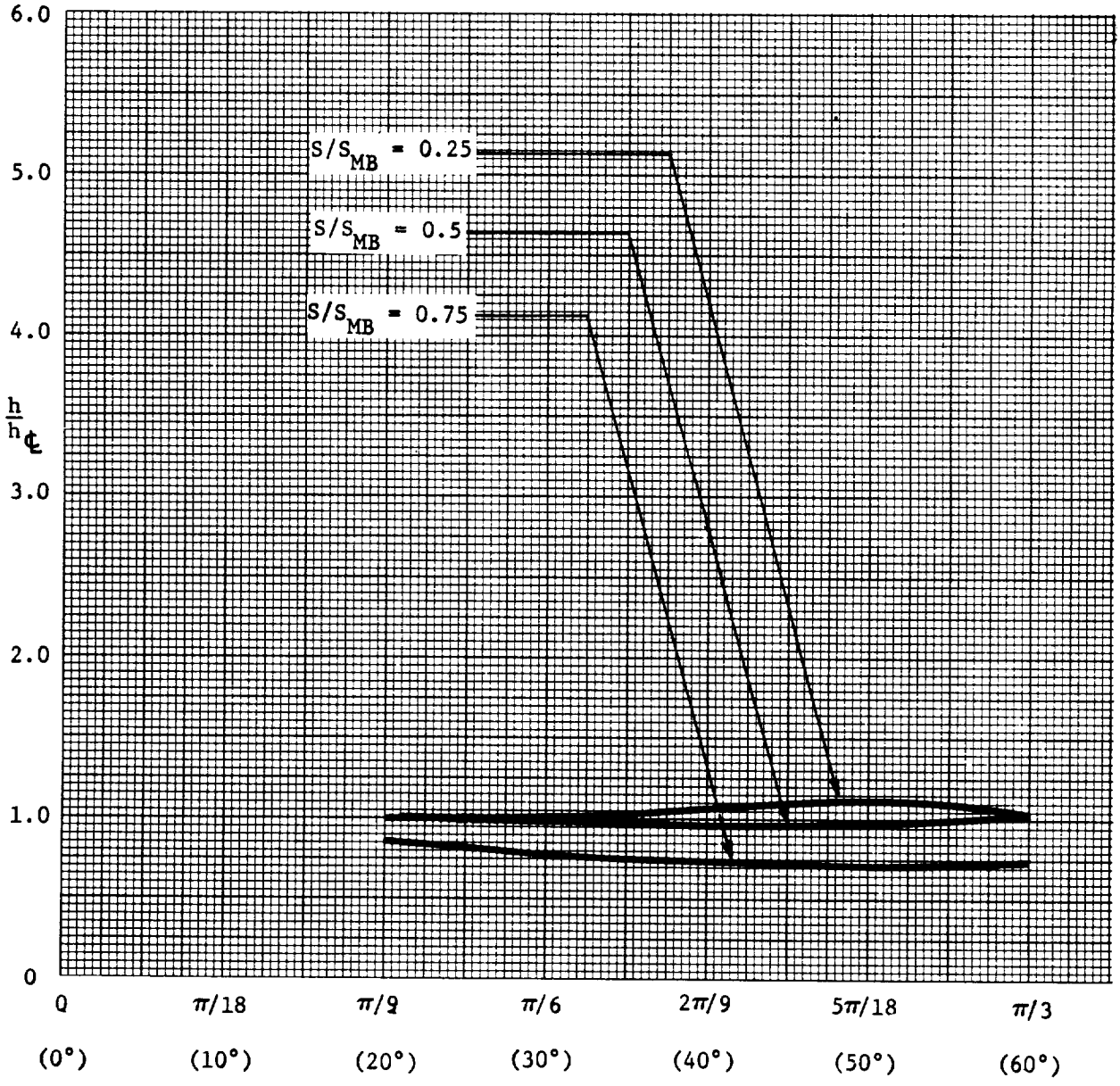

FIGURE 39

MDAC DELTA WING ORBITER (050/B) UPPER SURFACE CENTERLINE HEATING DISTRIBUTION

ANGLE OF ATTACK: $\alpha = \pi/6$ RADIANS (30°)

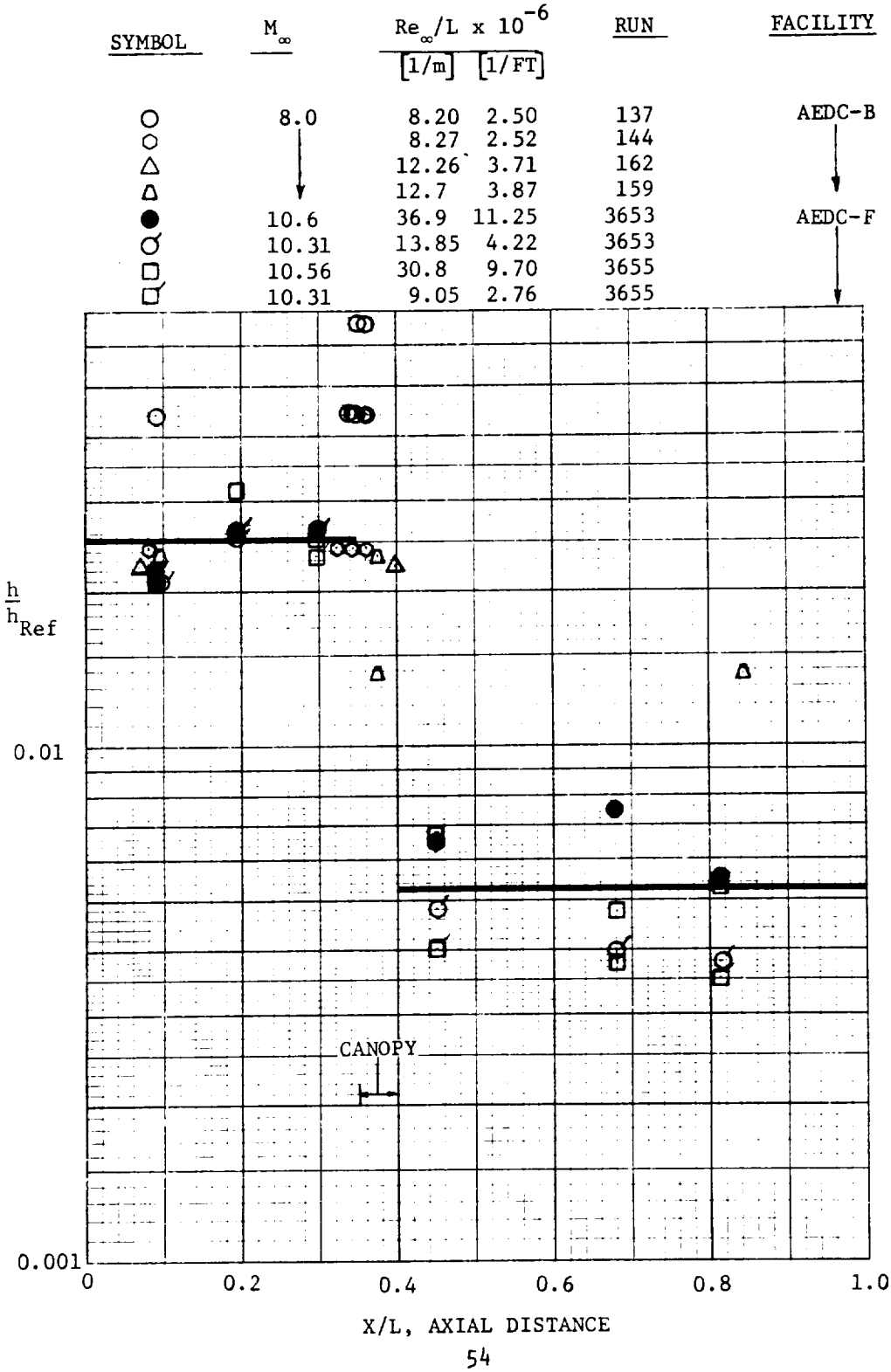

FIGURE 40

MDAC DELTA WING ORBITER (050/B) UPPER SURFACE CENTERLINE HEATING DISTRIBUTION
ANGLE OF ATTACK: α = 0.698 RADIANS (40°)

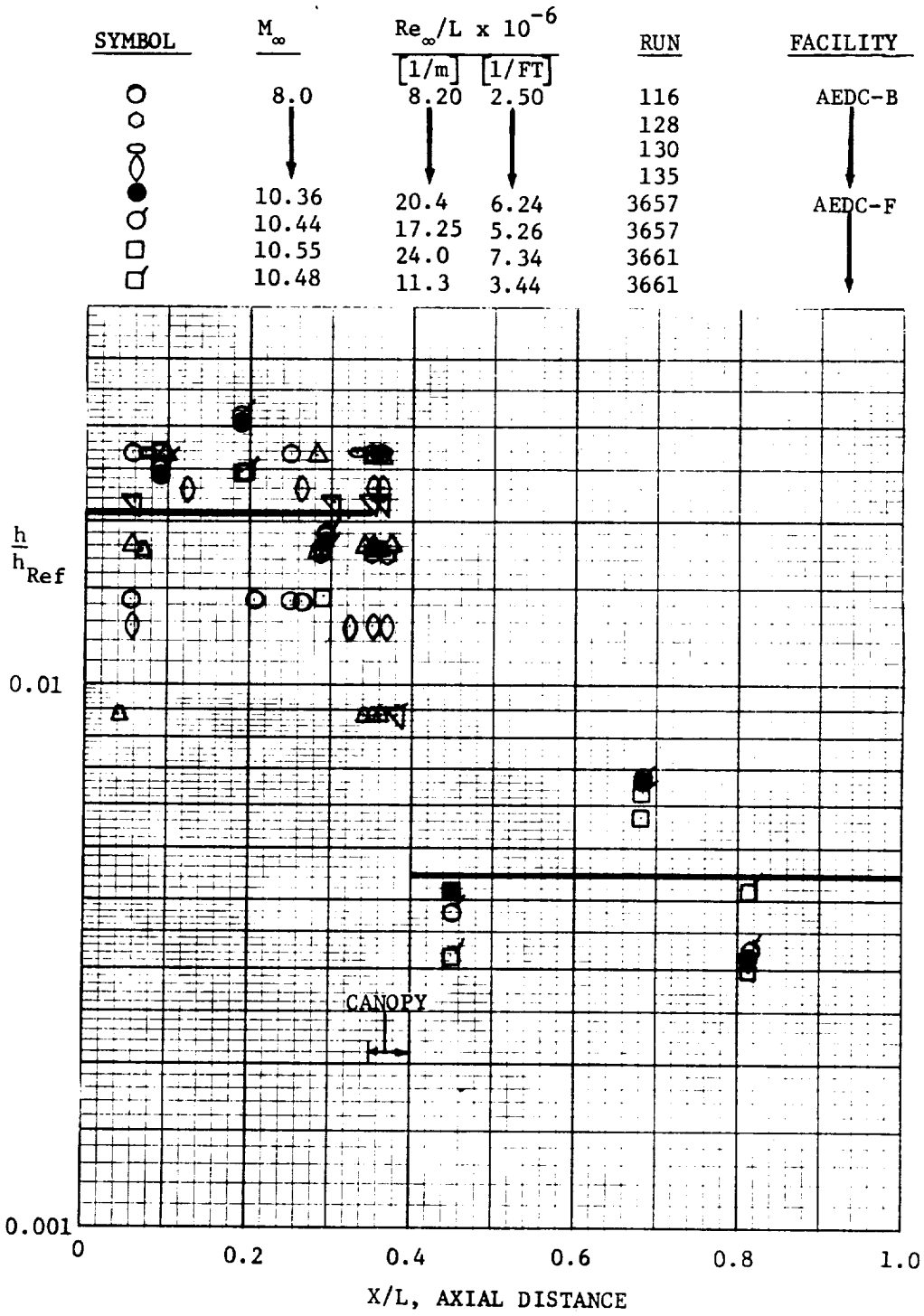

FIGURE 41

MDAC DELTA WING ORBITER (050/B) UPPER SURFACE HEATING DISTRIBUTION

ANGLE OF ATTACK: $\alpha = \pi/4$ RADIANS (45°)

SYMBOL	M_∞	$Re_\infty/L \times 10^{-6}$ [1/m]	[1/FT]	FACILITY	RUN	TIME
□	11.79	1.21	0.37	CORNELL	7	N.A.
▷	13.01	15.6	4.75		8	
△	7.66	2.1	0.64		26	
▽	7.64	89.9	27.4		27	
◇	7.56	40.0	12.2		30	
☆	7.78	25.5	11.4		34	
▽	11.87	18.5	5.64	AEDC-F	3660	106
▽	11.90	14.8	4.52			118
▼	11.84	13.0	3.97			137
⋈	11.52	9.43	2.88		3662	70
⬮	11.27	5.67	1.70			105
●	11.14	3.31	1.01			137
○	11.80	16.7	5.09		3663	84
◁	11.77	9.1	2.78			108
⬬	11.88	5.96	1.82			136

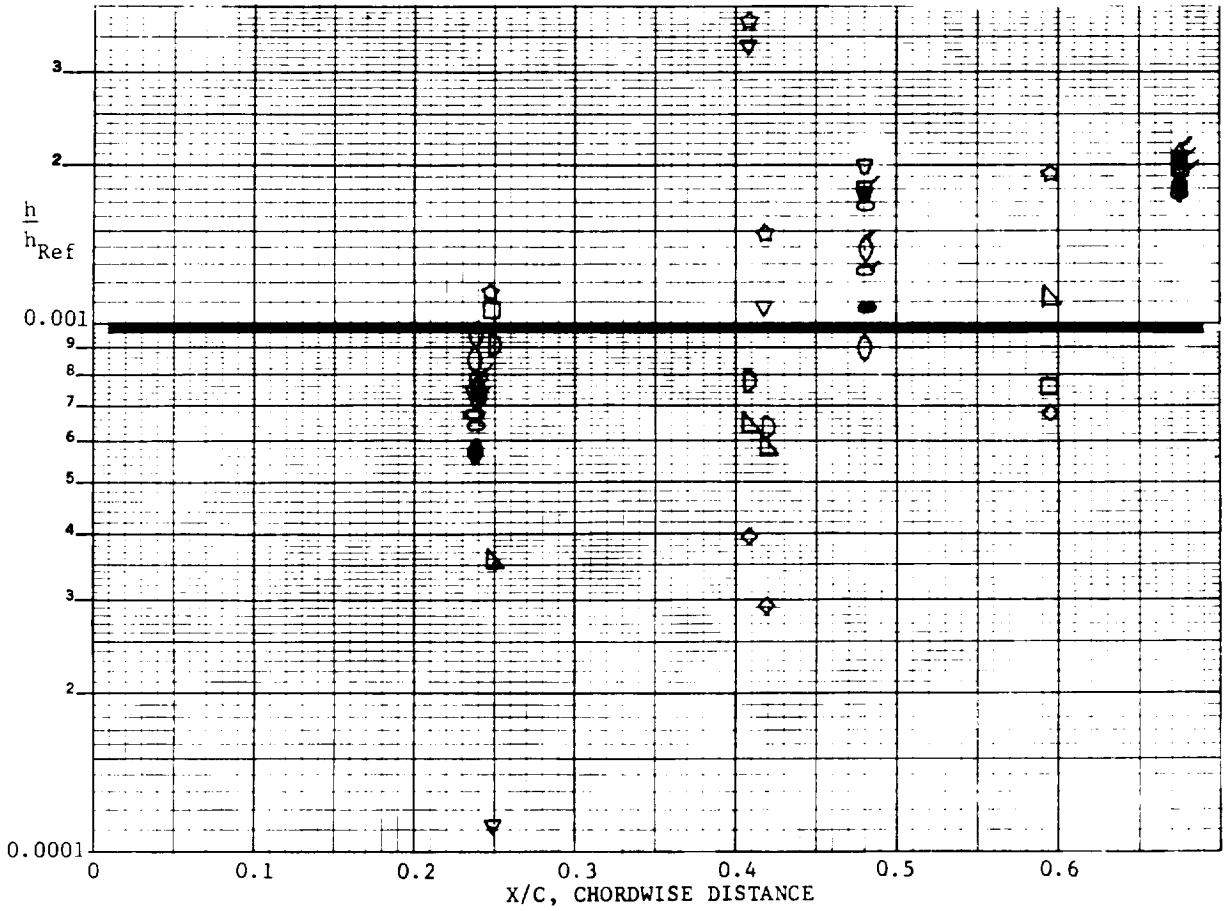

FIGURE 42
LEEWARD SIDE SEPARATION
MDAC DELTA WING ORBITER

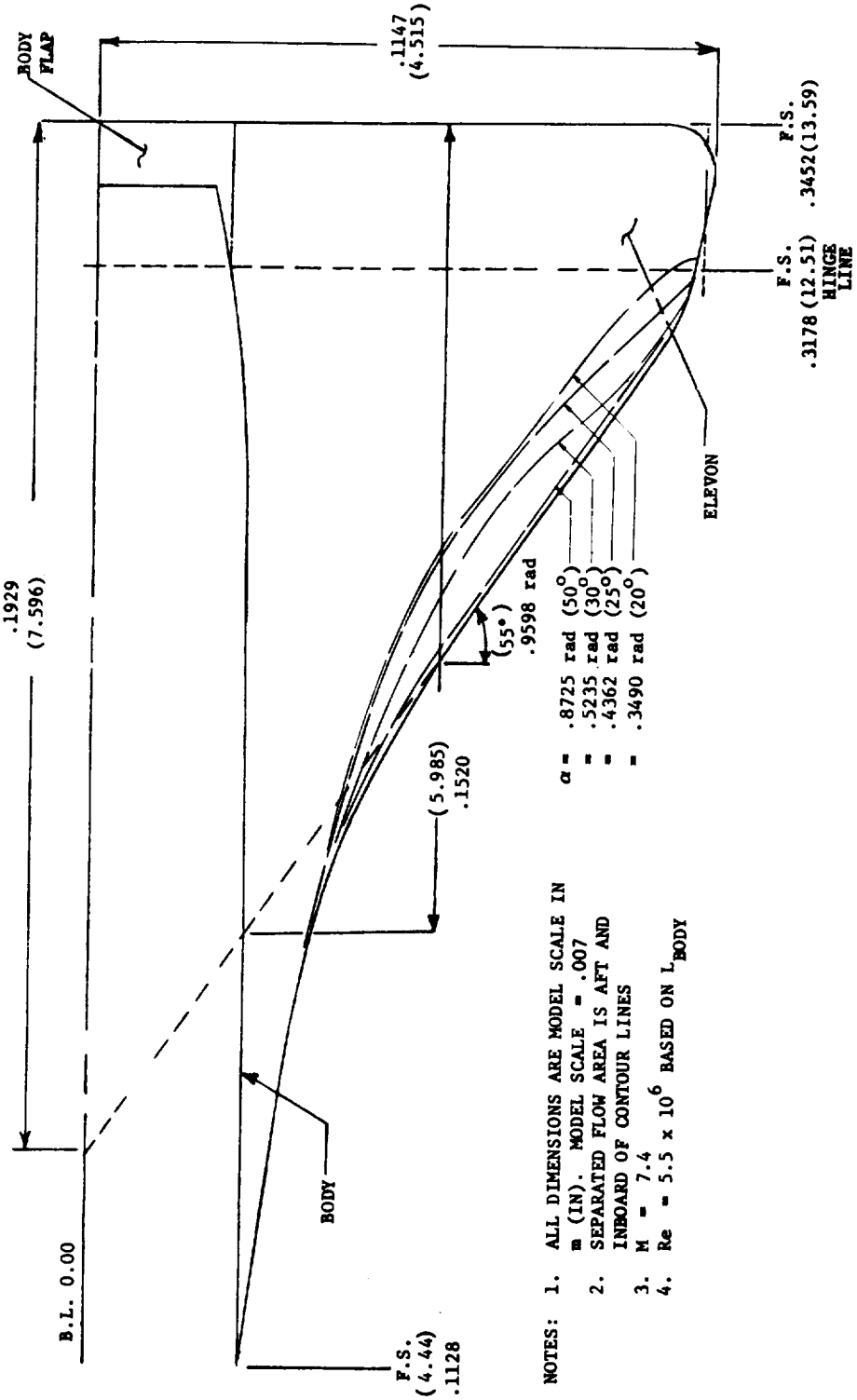

3. Boundary Layer Transition - Several recent studies of the problem of transition during hypersonic entry have focused on parameters derived from sophisticated flow field descriptions. The availability of electronic computers has allowed application of this approach to axisymmetric flow fields (Reference 14). For more complex flow fields, complete solutions are not possible, and restrictive assumptions are necessary (Reference 15). The correlation of data with relatively simple parameters which may be regarded as indices of the complex phenomena was applied for this study of Shuttle transition design criteria. The response of a flow field to variations of a simple parameter may, however, be much more pronounced for one configuration or flow environment than for another. As an extreme example, angle of attack can drastically alter the flow field about a cone, but is an irrelevant parameter for the flow about a sphere. Therefore, correlations based on simplified parameters are likely to be applicable only to the class of configurations and attitudes represented by the data evaluated.

The Phases A and B boundary layer transition data have been recently generated, and no comprehensive survey and correlation study of those data were available prior to this program. This survey, analysis,and correlation identified a group of 29 data points which were felt to be reliable. These data, which were gathered in continuous flow, shock tunnel,and hot shot facilities using (in most cases) delta wing orbiter models, are summarized in Figures 43 and 44. Also included are most of the basic correlating parameters used during this study. Local flow conditions assumed a conical flow field. Plots of these data indicated regular variations with several commonly applied transition parameters. Correlations in terms of local and momentum thickness Reynolds numbers are shown in Figures 45 and 46. Comparison of the figures show that the booster transition data correlate better with the orbiter data if the Reynolds number based on boundary layer momentum thickness at transition onset is used. Figure 47 shows the same data correlated in terms of the MDC Phase B transition criterion. Included in this figure are the criterion and a least-square fit to the data. It should be noted that the Phase B criterion was a fit to a large number of ground and flight test data on delta configurations, whereas the data in the figure were all obtained on Shuttle shapes. For purposes of this study the least square fit was used as the best fit correlation.

Evaluation of the data in each of the above correlations shows that the mean of the transition data taken in the continuous flow AEDC Tunnel B is higher than

FIGURE 43

TRANSITION ONSET PARAMETER SUMMARY

SI UNITS

POINT NO.	CONFIGURATION	TEST CONDITIONS				Re_θ	$Re_{L,tr}$	$Re_{\theta,L}$	M_e	T_W/T_e	T_W/T_{T_∞}	Re_L/m	P_∞	δ	α	X_{tr}/L	X_{tr}
		TUNNEL	M_∞	Re_∞/m (Millions)	T_{T_∞} (°K)		(Millions)	(Millions)				(Millions)	(N/M^2)	(Radians)	(Radians)		(Meters)
1	MDAC DWO	"AL96"	7.5	34.15	916	1536	6.17	1.295	7.52	3.92	0.328	35.8	3.11×10^3	0	0	0.5	0.173
2			7.6	33.8	872	673	2.12	1.281	3.52	1.16	0.345	44.0	2.86×10^3	0.444	0.349	0.14	0.048
3			12.7	9.2	1851	539	1.65	0.198	3.97	0.614	0.162	7.55	0.36×10^3	0.436	0.436	0.634	0.218
4			7.5	34.15	922	551	1.44	1.295	2.89	0.84	0.326	35.4	3.14×10^3	0.536	0.436	0.118	0.041
5			↓	34.15	916	401	0.553	1.295	1.32	0.43	0.327	17.4	3.14×10^3	0.891	0.785	0.092	0.032
6			↓	34.45	911	288	0.786	1.308	0.85	0.379	0.329	12.4	3.11×10^3	1.131	1.047	0.184	0.063
7			7.6	34.15	884	282	0.753	1.295	0.82	0.379	0.340	11.9	2.94×10^3	1.131	1.047	0.184	0.063
8	MDAC DWO	"AEDC"F"	10.8	19.1	987	489	2.06	0.620	2.15	0.515	0.3	8.96	0.54×10^3	0.716	0.698	0.425	0.230
9			↓	15.8	1038	466	1.86	0.514	2.20	0.506	↓	7.61	0.46×10^3	0.713	↓	0.45	0.244
10			↓	14.7	1024	434	1.63	0.478	2.18	0.507	↓	6.99	0.42×10^3	0.716	↓	0.43	0.233
11			10.9	12.7	1014	417	1.58	0.412	2.26	0.528	↓	5.94	0.35×10^3	0.700	↓	0.49	0.266
12	MDAC DWO	"AEDC"B"	8	12.2	747	1131	5.58	0.656	4.3	2.14	0.46	14.9	0.61×10^3	0.349	0.349	0.69	0.374
13			↓	12.1	↓	701	2.93	0.651	2.12	0.996	0.53	7.84	↓	0.698	0.698	0.69	0.374
14			↓	12.2	↓	651	2.78	0.655	2.12	0.926	0.49	7.88	↓	0.698	0.698	0.65	0.352
15			↓	8.1	728	397	1.33	0.434	1.39	0.69	0.505	3.42	0.39×10^3	0.873	0.873	0.72	0.390
16			↓	12.2	747	355	1.53	0.653	1.37	0.677	0.49	5.12	0.61×10^3	0.873	0.873	0.55	0.298
17			↓	8.2	728	353	0.768	0.441	1.02	0.642	0.54	2.08	0.39×10^3	1.047	1.047	0.68	0.368
18			↓	12.1	747	289	0.727	0.651	1.03	0.660	0.53	2.74	0.61×10^3	1.049	1.047	0.49	0.266
19	GD/C Booster	"AEDC"B"	8	12.3	728	706	4.687	0.768	2.69	0.974	0.5	10.6	0.61×10^3	0.559	0.524	0.7	0.441
20			↓	↓	↓	447	2.852	↓	1.77	0.647	0.51	7.21	↓	0.733	0.698	0.626	0.395
21			↓	↓	↓	415	2.022	↓	1.25	0.527	0.52	4.58	↓	0.908	0.873	0.7	0.441
22			↓	↓	↓	385	1.106	↓	0.93	0.474	0.51	2.50	↓	1.082	1.047	0.7	0.441
23	NAR DWO	"AEDC"B"	8	12.3	747	860	4.91	0.894	3.0	1.43	0.51	11.2	0.61×10^3	0.526	0.526	0.6	0.440
24			"	12.2	747	688	3.60	0.887	2.2	1.11	0.565	7.78	0.61×10^3	0.700	0.700	0.63	0.462
25	NAR DWO	"AEDC"B"	8	8.2	726	970	4.25	0.415	6.1	2.92	0.414	12.7	0.39×10^3	0.174	0.174	0.66	0.335
26			↓	12.2	745	1111	5.30	0.616	6.2	2.84	0.414	19.1	0.61×10^3	0.166	0.166	0.545	0.277
27			↓	12.2	746	584	2.20	0.616	2.4	0.856	0.398	7.88	0.61×10^3	0.698	0.698	0.55	0.280
28			↓	8.2	725	348	1.11	0.413	1.5	0.589	0.406	3.42	0.39×10^3	0.873	0.873	0.64	0.325
29			↓	12.2	748	387	1.43	0.615	1.5	0.575	0.396	5.12	0.61×10^3	0.873	0.873	0.55	0.280

FIGURE 44
TRANSITION ONSET PARAMETER SUMMARY
ENGINEERING UNITS

POINT NO.	CONFIGURATION	TEST CONDITONS				Re_θ	$Re_{L,tr}$	$Re_{\theta,L}$	M_e	T_w/T_e	T_w/T_{T_∞}	Re_L/FT	P_∞	δ	α	X_{tr}/L	X_{tr}	θ_{WAVE}
		TUNNEL	M_∞	Re_∞/FT. (Millions)	T_{T_∞} (°R)		(Millions)	(Millions)				(Millions)	(PSIA)				(FT)	
1	MDAC DWO	CAL 96"	7.5	10.4	1650	1536	6.17	1.295	7.52	3.92	0.328	10.9	0.454	0°	0°	0.5	0.566	7.5°
2			7.6	10.3	1570	673	2.12	1.281	3.52	1.16	0.345	13.4	0.415	25.4°	20°	0.14	0.158	29°
3			12.7	2.8	3335	539	1.65	0.198	3.97	0.614	0.162	2.30	0.0515	25°	25°	0.634	0.716	27.6°
4			7.5	10.4	1660	551	1.44	1.295	2.89	0.84	0.326	10.8	0.456	30.7°	25°	0.118	0.133	34.8°
5			↓	10.4	1650	401	0.553	1.295	1.32	0.43	0.327	5.31	0.456	51.1°	45°	0.092	0.104	59.3°
6			↓	10.5	1640	288	0.786	1.308	0.85	0.379	0.329	3.78	0.454	64.8°	60°	0.184	0.208	72.8°
7			7.6	10.4	1590	282	0.753	1.295	0.82	0.379	0.340	3.62	0.426	64.8°	60°	0.184	0.208	72.8°
8	MDAC DWO	AEDC"F"	10.8	5.82	1778	489	2.06	0.620	2.15	0.515	0.3	2.73	.0778	41.1°	40°	0.425	0.756	45°
9			↓	4.82	1867	466	1.86	0.514	2.20	0.506	↓	2.32	.0673	40.8°	↓	0.45	0.8	44.7°
10			↓	4.47	1842	434	1.63	0.478	2.18	0.507	↓	2.13	.0606	41°	↓	0.43	0.765	44.9°
11			10.9	3.86	1824	417	1.58	0.412	2.26	0.528	↓	1.81	.0504	40.1°	↓	0.49	0.872	44°
12	MDAC DWO	AEDC"B"	8	3.73	1345	1131	5.58	0.656	4.3	2.14	0.46	4.55	.088	20°	20°	0.69	1.227	23.3°
13			↓	3.70	↓	701	2.93	0.651	2.12	0.996	0.53	2.39	↓	40°	40°	0.69	1.227	45°
14			↓	3.72	↓	651	2.78	0.655	2.12	0.926	0.49	2.40	↓	40°	40°	0.65	1.156	45°
15			↓	2.47	1310	397	1.33	0.434	1.39	0.69	0.505	1.04	.057	50°	50°	0.72	1.28	57.2°
16			↓	3.71	1345	355	1.53	0.653	1.37	0.677	0.49	1.56	.088	"	50°	0.55	0.978	57.2°
17			↓	2.51	1310	353	0.768	0.441	1.02	0.642	0.54	0.635	.057	60°	60°	0.68	1.21	68°
18			↓	3.70	1345	289	0.727	0.651	1.03	0.660	0.53	0.835	.088	60.1°	60°	0.49	0.871	68.1°
19	GD/C Booster	AEDC"B"	8	3.75	1310	706	4.687	0.768	2.69	0.974	0.5	3.23	.088	32°	30°	0.7	1.45	37°
20			↓	↓	↓	447	2.852	↓	1.77	0.647	0.51	2.20	↓	42°	40°	0.626	1.298	48°
21			↓	↓	↓	415	2.022	↓	1.25	0.527	0.52	1.396	↓	52°	50°	0.7	1.45	59°
22			↓	↓	↓	385	1.106	↓	0.93	0.474	0.51	0.763	↓	62°	60°	0.7	1.45	70°
23	NAR DWO	AEDC"B"	8	3.75	1345	860	4.91	0.894	3.0	1.43	0.51	3.40	.088	30.1°	30.1°	0.6	1.445	34.2°
24			"	3.72	1345	688	3.60	0.887	2.2	1.11	0.565	2.37	.088	40.1°	40.1°	0.63	1.518	44.8°
25	NAR DWO	AEDC"B"	8	2.51	1307	970	4.25	0.415	6.1	2.92	0.414	3.87	0.057	9.96°	9.96°	0.66	1.1	14.5°
26			↓	3.73	1342	1111	5.30	0.616	6.2	2.84	0.414	5.83	.088	9.52°	9.52°	0.545	0.909	14.1°
27			↓	3.73	1343	584	2.20	0.616	2.4	0.856	0.398	2.40	.088	39.97°	39.97°	0.55	0.916	44.7°
28			↓	2.50	1305	348	1.11	0.413	1.5	0.589	0.406	1.04	.057	49.99°	49.99°	0.64	1.067	55.6°
29			↓	3.72	1347	387	1.43	0.615	1.5	0.575	0.396	1.56	.088	49.99°	49.99°	0.55	0.916	55.6°

FIGURE 45

LOCAL REYNOLDS NUMBER
vs
LOCAL MACH NUMBER

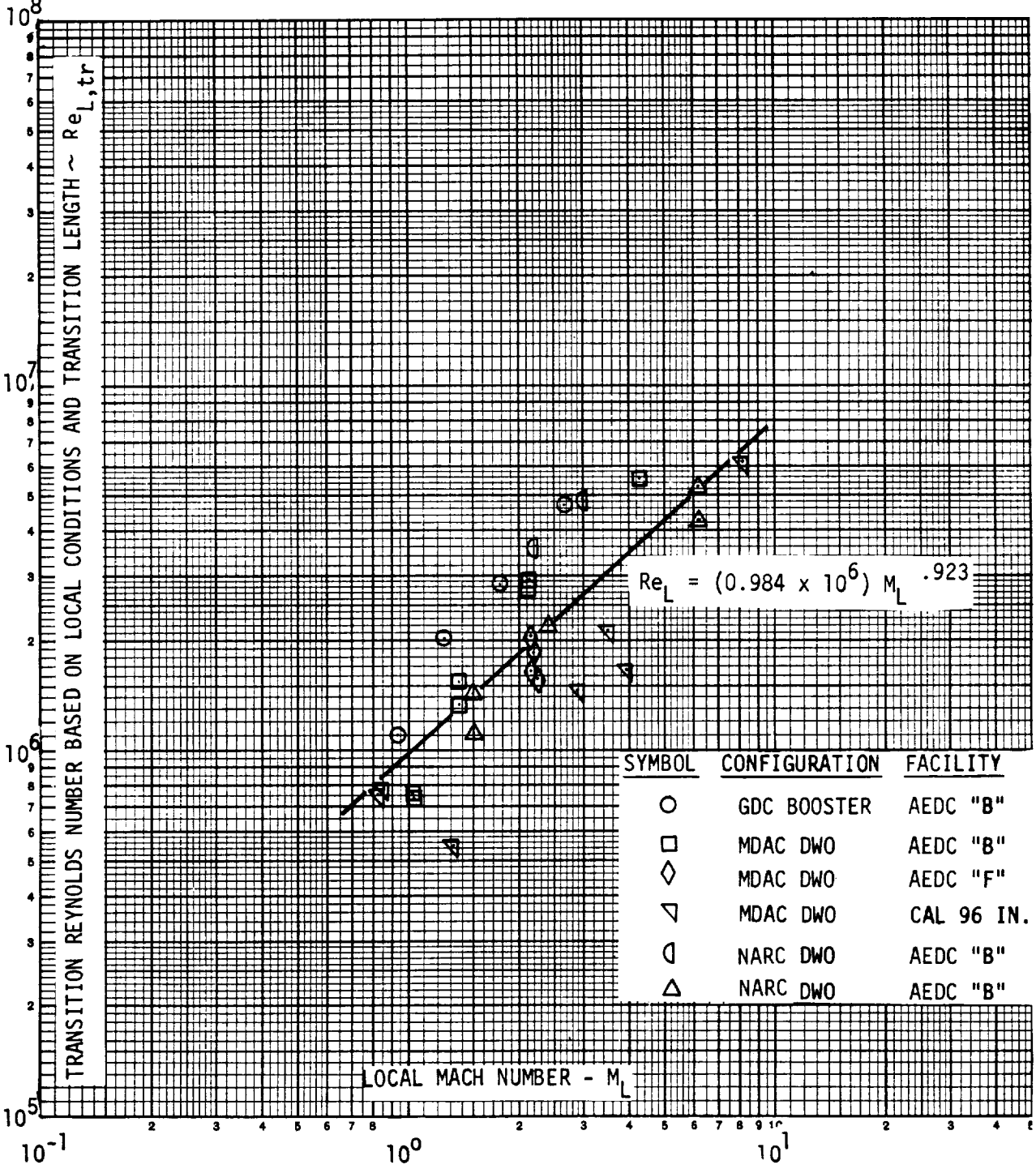

FIGURE 46

MOMENTUM THICKNESS REYNOLDS NUMBER
vs
LOCAL MACH NUMBER

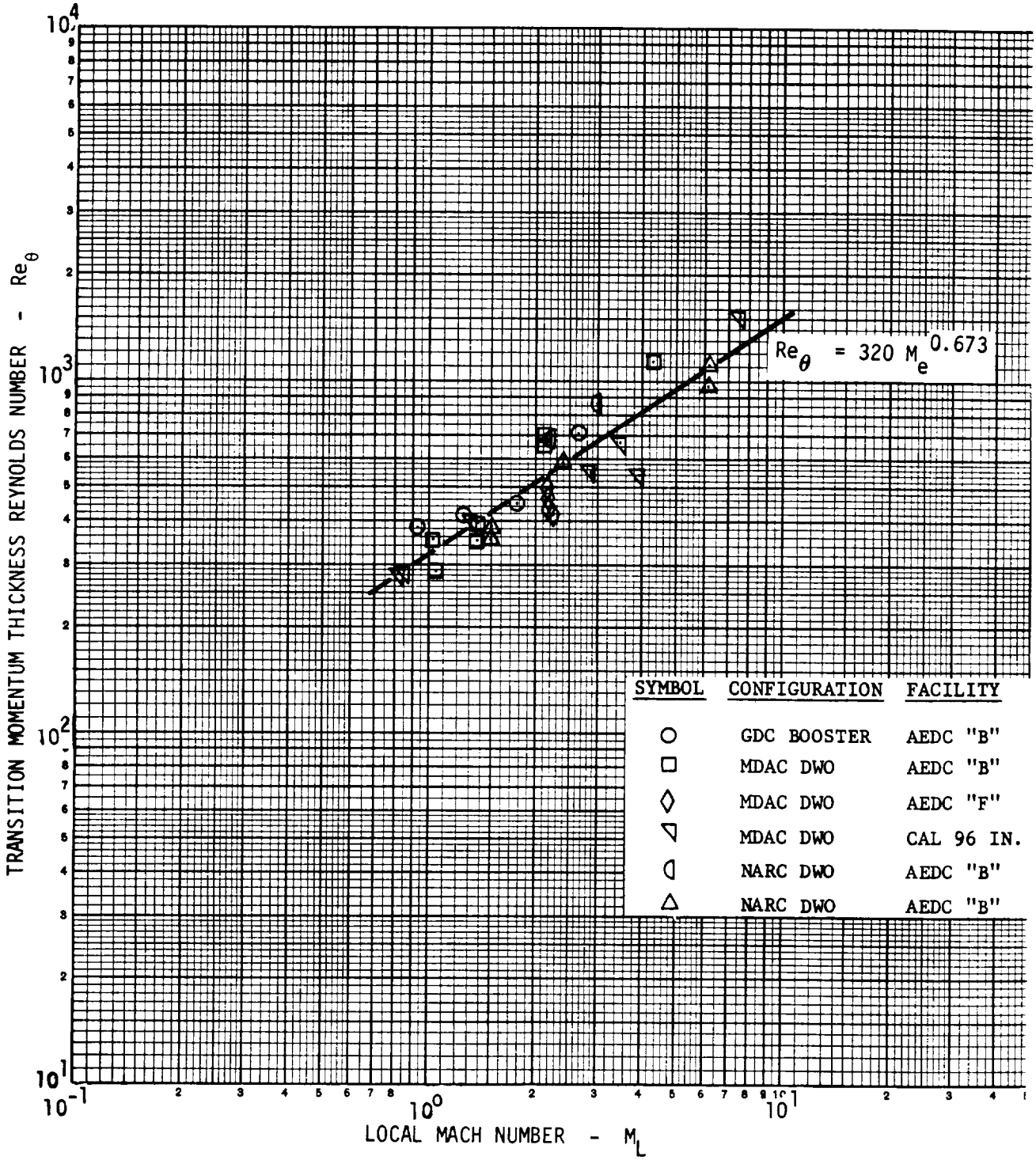

FIGURE 47

MDAC PHASE B TRANSITION CORRELATION PARAMETER

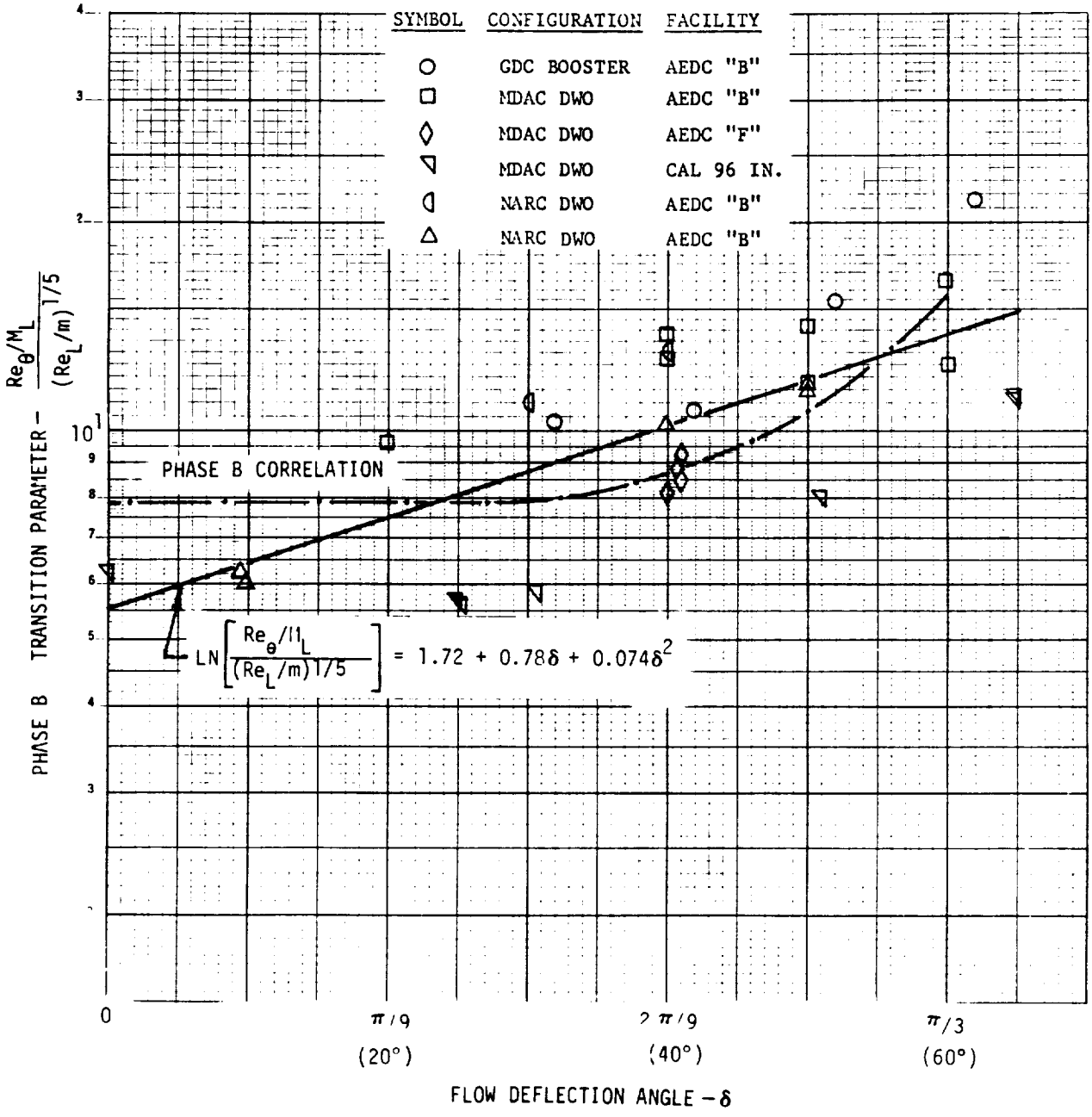

the mean of the data taken either in the Cornell Hypersonic Shock Tunnel or AEDC Tunnel F. These differences were found to be less pronounced if a wall cooling parameter was introduced. In particular, the use of a parameter T_w/T_e was found to reduce these tunnel differences. Alternate correlation forms were evaluated as a part of IRAD at MDAC-E, and are included herein for information.

The same data points were processed by multiple regression analysis computer program assuming various combinations of parameters and forms of correlating equations. Those multiple regression fits which provided a significant degree of correlation are presented in Figures 48 through 50 along with their one-standard-error-of-estimate deviations. It should be noted that momentum thickness Reynolds number is roughly proportional to the square root of transition length (this is not a direct proportionality due to application of streamline divergence factors calculated by the method of Reference 16). Thus, momentum thickness Reynolds number is less sensitive to transition length than either length Reynolds number or fractional body length (X/L). As a result, equations based on momentum thickness Reynolds number exhibit generally lower standard errors of estimate than equations with the other dependent variables. For a given dependent variable, however, the standard errors of estimate gave a quantitative basis for ranking the equations.

Equations including Reynolds number, Mach number, flow deflection angle, and either the ratio of wall temperature to static temperature or the ratio of wall temperature to total temperature were found to yield low standard errors of estimate and probability plots consistent with the assumption of normal distributions. A minor improvement in the standard error of estimate was achieved by inclusion of unit Reynolds number, but the indicated dependency is slight. Equations including a cubic expression in flow deflection angle were also effective, but such complexity often yields misleading results when applied to a small data sample.

The significance of the correlations to vehicle design must be evaluated in terms of flight parameters. Thus, studies discussed in this section can only be used for the screening of correlations. Altitude uncertainties associated with the correlations are a better measure of the degree of correlation provided. Results of this approach are included in Section V of this report.

FIGURE 48

UNCERTAINTY IN TRANSITON ONSET BASED ON LOCAL REYNOLDS NUMBER CORRELATIONS

EQUATION	σ
$Re_{L,tr} = 0.984 \times 10^6 \, M_e^{0.923}$	0.415
$Re_{L,tr} = 2.305 \times 10^6 \, (T_w/T_{T_\infty})^{1.04} M^{1.05}$	0.261
$Re_{L,tr} = 1.86 \times 10^6 \, (T_w/T_e)^{0.89} \, (Re_L/\text{Meter})^{0.0143}$	0.401
$Re_{L,tr} = 6 \times 10^6 - (6.19 \times 10^6) \, \delta + (1.275 \times 10^6)\delta^2$	0.35
$Re_{L,tr} = 0.89 \times 10^6 \, (T_w/T_{T_\infty})^{1.07} (\delta + 1)^{1.28} M_e^{1.45}$	0.260
$Re_{L,tr} = 0.116 \times 10^6 \, (T_w/T_e)^{0.75} (\delta + 1)^{3.76} M_e^{1.41}$	0.369
$Re_{L,tr} = -14.6 \times 10^6 + (2.63 \times 10^4) \, T_w/T_e + (1.32 \times 10^6)(T_w/T_e)^2 + (6.49 \times 10^7)\delta - (8.2 \times 10^7)\delta^2 + (3.2 \times 10^7)\delta^3$	0.27
$Re_{L,tr} = 2.48 \times 10^7 + (1.9 \times 10^6) \, T_w/T_e - 376.4 \, P_\infty - (3.36 \times 10^6) M_e - (2.49 \times 10^7)\delta - (3.33 \times 10^6)\delta^2 + (7.61 \times 10^6)\delta^3$	0.27

FIGURE 49
UNCERTAINTY IN TRANSITION ONSET BASED ON
MOMENTUM THICKNESS REYNOLDS NUMBER CORRELATIONS

EQUATION	σ
$Re_{\theta,tr} = 320\ M_e^{0.67}$	0.183
$Re_{\theta,tr} = 470\ M_e^{0.73}(T_w/T_{T_\infty})^{0.47}$	0.127
$Re_{\theta,tr} = 258\ M_e^{0.675}\ P_\infty^{0.037}$	0.178
$Re_{\theta,tr} = 245\ M_e^{0.475}(\delta + 1)^{-0.65}\ (T_w/T_{T_\infty})^{0.495}(Re_L/Meter)^{0.075}$	0.113
$Re_{\theta,tr} = 257\ M_e^{0.54}(\delta + 1)^{1.03}\ (T_w/T_e)^{0.456}(Re_L/Meter)^{0.06}$	0.122
$Re_{\theta,tr} = 602\ (T_w/T_e)^{0.66}$	0.157
$Re_{\theta,tr} = -1051 + 4.15\ T_w/T_e + 160.8\ (T_w/T_e)^2 + 6447\delta - 8537\delta^2 + 3420\delta^3$	0.113
$Re_{\theta,tr} = 569.5\ (T_w/T_{T_\infty})^{0.265}\delta^{-0.25}$	0.315
$Re_{\theta,tr} = 926\ P_\infty^{-0.11}\delta^{-0.26}$	0.323
$Re_{\theta,tr} = 982\ (T_w/T_{T_\infty})^{0.44}(\delta + 1)^{-1.028}M_e^{0.414}$	0.120
$\frac{Re_{\theta,tr}/M_e}{(Re_L/Meter)^{0.2}} = 5.525 + 4.54\delta + 3.4\delta^2$	0.25
$Re_{\theta,tr} = 299\ (T_w/T_e)^{0.417}(\delta + 1)^{0.571}M_e^{0.482}$	0.125
$Re_{\theta,tr} = 1066 + 1400\ T_w/T_{T_\infty} - 919\ (T_w/T_{T_\infty})^2 - 1993\delta + 1033\delta^2 - 187\delta^3$	0.163
$Re_{\theta,tr} = 1187 + 0.76\ P_\infty - 2 \times 10^{-4}\ P_\infty^2 - 2.593\delta + 2238\delta^2 - 810\delta^3$	0.185
$\ln\left(\frac{Re_\theta/Me}{Re_L/Meter}\right)^{0.2} = 1.721 + 0.7786\delta + 0.0743\delta^2$	0.234

FIGURE 50

UNCERTAINTY IN TRANSITION ONSET LOCATION
BASED ON COMBINED REYNOLDS NUMBER AND ANGLE OF ATTACK CORRELATIONS

EQUATION	σ
$X_{tr/L} = (6.01 \times 10^{4})\ Re_{0,L}^{-0.88}\ \alpha^{-0.079}$	0.431
$X_{tr/L} = 0.875 - (0.434 \times 10^{-6})\ Re_{0,L} - 0.049\alpha$	0.33
$X_{tr/L} = 2.067\ (Re_{0,L} \times \alpha)^{-0.118}$	0.40

V. DEFINITION OF AERODYNAMIC HEATING UNCERTAINTIES

As shown in the correlation curves of Section IV, the analyst is faced with aerodynamic heating data which scatter significantly about theory or the selected correlations. Therefore, he must decide on factors to apply to his best fits which assure a safe design for flight. In this study an approach was developed and applied to quantify the uncertainties for various confidence levels using a statistical approach. This approach is modeled after procedures utilized in the Dynasoar program and successfully applied to the design of the hypersonic BGRV flight vehicle.

In the BGRV program ground test data were correlated in terms of significant aerothermodynamic parameters. Best fits to the data were then made and the standard deviations of the data about the best fits were determined. Factors were developed to apply to the nominal data fit to estimate the off-nominal effects of aerodynamic heating on temperature and TPS weight. The increments (in temperature and weight) were then statistically combined with other independent factors which affect the temperature and TPS weight using the root sum square method. These included, for example, trajectory dispersions, off-nominal atmospheric properties, and variations in material properties affecting TPS performance (surface emittance, skin thickness, skin and insulation properties).

Postflight evaluation of the BGRV data showed that the data scatter about the ground test developed correlations were essentially bounded in terms of peak heating by the band representing two standard deviations of the ground test data about its mean. These results provide support for the use of ground test data and data scatter to establish uncertainties in flight even though some of the factors which produce the ground test scatter do not occur in flight. It should be recognized, however, that the BGRV was a relatively simple (axisymmetric) shape with a high quality ground test data base which made the uncertainty low, compared with the currently available Shuttle data base. Thus, direct application of the results of this study are expected to be conservative. However, as the Shuttle Phase C/D data base is developed, it is anticipated that better estimates of the effect of uncertainties in the heating prediction methods can be obtained with this statistical approach.

1. The Statistical Approach - Since it is suggested that a statistical approach be used to develop heating factors for flight, it is necessary to select and apply correctly, statistical methods which model the problem.

The specific problem is to apply a factor to heating analysis methods that will assure,with some level of confidence,that the predicted heating will not be exceeded in flight for known free-stream conditions. The prediction methods which are currently considered state of the art are not exact for Shuttle-like configurations and it is necessary to rely on correlations developed from comparisons of ground test measurements with these imperfect theories. With this approach a factor, or factors, is determined to apply to the theory in order to scale to flight. Since we are dealing with data there is scatter. This may be due to tunnel measurement errors or to an inexact match of the theory to the physical problem. If the latter case is assumed, the ground test scatter and deviation about the data mean can be used to define a scatter or uncertainty band for flight. To assist in selecting the appropriate statistics to apply, a few definitions and statistical concepts are described below.

a. The Normal Distribution - The normal (Gaussian) probability distribution is completely determined by its mean, μ, and its variance, σ^2. The statement that a variable, x, is normally distributed with mean μ and variance σ^2 can be written

$$x : N(\mu,\sigma^2)$$

Tables of the normal distribution are available which provide tabulated values of K, the probability, P, that a randomly occurring value of the variable, x, will be within an interval of length, $K\sigma$, on either side of the mean, μ. That is, the probability that

$$\mu - K\sigma < x < \mu + K\sigma .$$

b. Normal Distribution Sample Statistics - A sample of size n from a normal distribution is a collection $(x_1, x_2, .x_n)$ of normally distributed variables. The sample mean is given by

$$\bar{x} = \frac{1}{n} \sum_{i=1}^{n} x_i \qquad (1)$$

and the sample variance, s^2, is given by

$$s^2 = \frac{1}{n} \sum_{i=1}^{n} (x_i - \bar{x})^2 \qquad (2)$$

When drawing inferences about the normally distributed parent population (or universe) from which the sample was taken, we use $\bar{x}$ and an unbiased sample estimate of the population variance, $\hat{\sigma}^2$, as defined by

$$\hat{\sigma}^2 = \frac{1}{n-1} \sum_{i=1}^{n} (x_i - \bar{x})^2 \qquad (3)$$

It is important to recognize that $\bar{x}$ is not μ and $\hat{\sigma}^2$ is not σ^2 since the sample size is limited and does not include the total population of data. However, these parameters and the assumption that we are dealing with normally distributed data can be used to predict the characteristics of other data samples from the total data population.

An important property of the normal distribution is that a sample mean, $\bar{x}$, for a random sample of size n is normally distributed about the true mean μ with a variance σ^2/n. Another important property is that the quantity ns^2/σ^2 has an x^2 (Chi-square) distribution with (n-1) degrees of freedom, where from equation (2)

$$n s^2 = \sum_{i=1}^{n} (x_i - \bar{x})^2 \tag{4}$$

The Chi-square variable has (n-1) degrees of freedom rather than n because only (n-1) of the x_i are "free", the other one being determined from the fact that $\bar{x}$ is known and

$$n \bar{x} = \sum_{i=1}^{n} x_i \tag{5}$$

c. Confidence Limits for Normal Population Parameters - A major use of statistics is to use sample data to draw inferences about the parent population. Limits can be specified which include the population mean and variance within a stated level of confidence if the data are normally distributed. In this study, the sample data are derived from ground tests and are assumed to be a part of the total population which includes ground and flight data.

Confidence Limits on the Mean - It is possible to place confidence limits on the mean of the total population based on the sample measurement, e.g., to determine limits on the mean in flight based on the ground sample. To do this, it is necessary to recognize that the variable

$$t = \frac{(\bar{x} - \mu)\sqrt{n - 1}}{s} \tag{6}$$

has a Student's t distribution (reference 14) with (n-1) degrees of freedom. Because s^2 and $\hat{\sigma}^2$, are related by the expression

$$\hat{\sigma}^2 = \frac{n}{n-1} s^2 \tag{7}$$

equation (6) can also be written

$$t = \frac{(\bar{x} - \mu)\sqrt{n}}{\hat{\sigma}} \tag{8}$$

where $\hat{\sigma}$ is defined, for this purpose, by the equation $\hat{\sigma} = \sqrt{\hat{\sigma}^2}$

Using equation (8), we can define an interval which includes the mean based on the sample data. For example, if $t_{0.05}$ represents the value of Student's t corresponding to a probability of 0.05 that $|t| > t_{0.05}$, there is a 95-percent chance that

$$\left| \frac{(\bar{x} - \mu)\sqrt{n}}{\hat{\sigma}} \right| < t_{0.05} \tag{9}$$

where t 0.05 is obtained from tabulated results for Student's t for (n-1) degrees of freedom. Thus, a 95-percent confidence interval for the population mean is defined by the expression

$$\bar{x} - t_{0.05}\frac{\hat{\sigma}}{\sqrt{n}} < \mu < \bar{x} + t_{0.05}\frac{\hat{\sigma}}{\sqrt{n}} \tag{10}$$

If some probability other than 0.05 is desired we replace $t_{0.05}$ by the corresponding t in the above expression Equation (10) can also be used to define a confidence interval for the ratio of the population mean to the sample mean by rewriting it in the form

$$\frac{\mu}{\bar{x}} = 1 \pm \frac{t}{\bar{x}}\frac{\hat{\sigma}}{\sqrt{n}} \tag{11}$$

Confidence Limits on the Variance - Confidence limits on the variance (σ^2) can be derived from the fact that $n s^2 / \sigma^2$ has a χ^2 distribution with (n-1) degrees of freedom. If the confidence level is to be 0.95, that is, if an interval is desired such that in repeated experiments 95-percent of the intervals derived in the same manner would contain the true population variance, σ^2, then the interval for a particular sample of size n would be derived from the relation,

$$\frac{n s^2}{\chi^2_2} \leq \sigma^2 \leq \frac{n s^2}{\chi^2_1} \tag{12}$$

where χ_1^2 and χ^2_2 are derived from Chi-square tables for (n -1) degrees of freedom so that the probability is 0.975 that $\chi^2 \geq \chi^2_1$ and 0.025 that $\chi^2 \leq \chi^2_2$.

One-Sided Confidence Limits - The above discussion assumed that both upper and lower confidence limits for the mean and variance were of interest. If, as is the case for heating uncertainties, we are really interested that a heating rate or value not be exceeded at some confidence level, we are dealing in one-sided confidence limits, i.e., we are interested in the precent of samples below some limit rather than between two equally spaced limits. The symmetric nature of the normal

distribution curve allows calculation of one-sided confidence limits on the mean by evaluating Student's t for a probability twice the two-sided value. For example, if a one-sided upper 95-percent confidence interval for the mean is desired, the value of Student's t for (n-1) degrees of freedom would be used such that the probability is 0.10 that $|t| > t_{0.10}$. Then the probability is 0.95 that

$$\frac{(\bar{x} - \mu)\sqrt{n}}{\hat{\sigma}} < t_{0.10} \qquad (13)$$

or that

$$\bar{x} + t_{0.10} \frac{\hat{\sigma}}{\sqrt{n}} < \mu \qquad (14)$$

The value of $t_{0.10}$ such that $|t| > t_{0.10}$ corresponds to a probability that 5-percent of the Student's t distribution is in each tail of the normal distribution curve. It is the correct value of Student's t for a one-side (upper or lower) 95-percent confidence interval for μ.

d. Tolerance Limits With Confidence Coefficients - The previous paragraph discussed in general the relations between sample data and a total population and ways of placing confidence limits on the mean and variance of the total population of which the data sample is a part. It does not, however, tell where the next data point is likely to fall, which is the real problem to be addressed in developing heating uncertainties. That is, it is desired to apply a factor to the average heating data that will assure that some percentage of the data population will not exceed the resulting off-nominal heating rate. The appropriate statistics to use in developing such factors must consider tolerance limits with confidence. If the normal distribution parameters μ and σ^2 are known for the total population we can find the appropriate values of K to establish the desired tolerance limits on x so that

$$\mu - K\sigma < x < \mu + K\sigma \qquad (15)$$

In practice μ and σ^2 are not known and tolerance limits must be estimated from the sample mean, $\bar{x}$, and the unbiased sample estimate of the population variance, $\hat{\sigma}^2$. This problem has been evaluated by A. H. Bowker and tables of tolerance limits with confidence coefficients have been tabulated and published in References 17 and 18. Bowker's table gives values of K such that in a large series of samples from a normally distributed total population

a certain proportion of the intervals $\bar{x} \pm K\hat{\sigma}$ will include at least a fixed percentage of the total data. In simpler terms the approach defines the percentage of data which falls within some tolerance band for a given confidence level. As discussed in Paragraph 1C, one-sided confidence limits are more applicable to the problem of heating uncertainties.

2. Development of the Standard Deviation - The standard deviation of the data about best fits to heating data was obtained for several locations on the booster and orbiter configurations to assist in selection of the theory which best matched the data, and to define uncertainty factors to apply for the flight trajectory. The configurations were divided into areas for which a given prediction method (and corresponding uncertainty) was expected to apply. These included (1) lower surface centerline, (2) off-centerline windward regions, (3) shielded regions, (4) upper surface centerline, and (5) regions of shock impingement and interaction. In addition, the location of boundary layer transition on the lower surface centerline was correlated and the standard deviation of the data around the best fits determined. For the lower surfaces, turbulent and laminar data were separately correlated and the corresponding standard deviations determined.

The standard deviation about least square fits of the data (or ratio of data to theory) was obtained graphically. The graphical technique, an example of which is shown in Figure 51, provides a visual description of the data scatter distributions and a consistent technique for deriving the standard deviation of the data set(s). This example curve, which is based on the orbiter lower surface centerline correlations of Figure 34 of Section IV, contains the ratio of data to theory as a function of the percent of the data which lies below each value. Fits to the laminar and turbulent data are superimposed in the figure. It can be seen that the uncertainty in the laminar data is slightly greater for the laminar than for the turbulent data. They are, however, sufficiently close that a single value could be used for each set. This value of the factor corresponding to one standard deviation is approximately 18 percent. The laminar theories used to develop this curve were Eckert's Reference Enthalpy Method for laminar and the Spalding-Chi correlations for turbulent flow. The data were obtained from tests of the MDC 050 B orbiter configuration in the AEDC Tunnels B and F and the Cornell Aeronautical Laboratory Hypersonic Shock Tunnel. The Mach number range was from 7.6 to 12.5 and Reynolds numbers based on free stream conditions and model length varied between 0.25 and 40 million.

The slightly higher value for laminar flow had not been anticipated, since laminar theories are further advanced than those for turbulent flow (at least for stagnation point heating). Investigation of the reasons for this has indicated that the range of environmental parameters was wider for the laminar than for the turbulent data and, in addition, that the laminar heating is more

FIGURE 51

PROBABILITY PLOT FOR DETERMINING STANDARD DEVIATION FOR MDAC ORBITER DATA OF FIGURE 34, SECTION IV

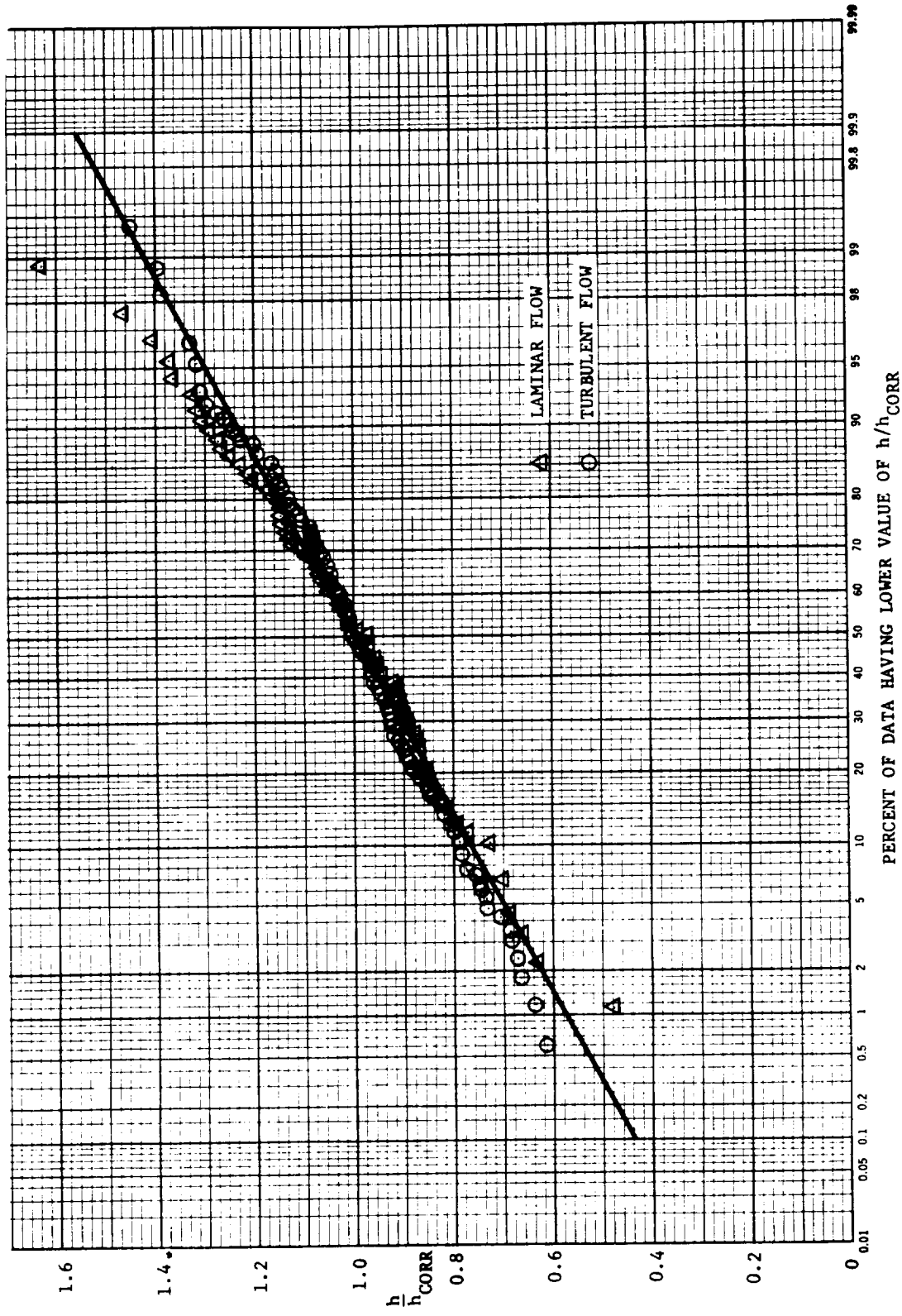

sensitive to three-dimensional flow effects, which are not perfectly modeled in theory. Further evaluation of this phenomenon will require a more complete data base or the development of more sophisticated flow field and heating models for the complex shuttle configuration.

The B-15B-2 booster laminar heating was correlated as a function of h/h_{ref}. This type correlation is extremely sensitive to the configuration. Sufficient data were not available on the B-15B-2 configuration to establish uncertainties which could be applied to flight. Therefore, data correlations of similar configurations were used to establish the standard deviation. The data used to establish standard deviations for the lower surface centerline are shown in Figures 52 and 53. These data were obtained on three booster configurations: the B-15B-2, B-9J, and B-8B, all correlatable in terms of h/h_{ref} since the nose geometry (forward of X/L = 0.4) was essentially the same for all configurations except for the B-15B-2 which differed aft of X/L = 0.20. This can be seen by reviewing the data in the figure which show little geometric sensitivity forward of X/L =0.04. These laminar data were obtained over a Reynolds number range between 0.8 and 10 million based on free-stream conditions and model length. During the time span in which these uncertainties were developed, the booster data were available in a limited Mach number range, M = 7.4 to 10. It would be desirable to include additional low Mach number data since the Mach numbers of interest for heat sink boosters are below Mach 7. The curve used to define the heating factor corresponding to one standard deviation is included in Figure 54 for the zero degree angle of attack data. By comparing this curve with Figure 51 similar characteristics are noted but slightly lower uncertainties are indicated for these booster data. This might be expected since the booster nose section is cylindrical and thus more easily modeled with Fay-Riddell stagnation point theory. Fewer turbulent data were available for the booster than for the orbiter configurations. The only configuration for which a large sample of turbulent data were available was the MDC booster. These data were best fit with the Beckwith and Gallagher theory at 60 degrees angle of attack, and uncertainty factors developed for fits to this theory. The range of tunnel variables encompassed Mach numbers between 8.0 and 11.2 and free stream Reynolds numbers based on model length between 5.0 and 15 million. The ratio of wall to total temperature ratio for these data varied between 0.2 and 0.6. The heating multiplier for these data was found to be 1.25 for one standard deviation.

FIGURE 52

LOWER SURFACE CENTERLINE HEATING DISTRIBUTIONS FOR GD/C BOOSTERS

SYMBOL	M_∞	$Re_\infty/L \times 10^{-6}$ [1/m]	[1/FT]	CONFIGURATION	FACILITY	RUN
○	8.0	2.49-12.3	.76-3.74	B-15B-2	AEDC-B	58, 55, 83
□	7.4	2.1-11.15	.64-3.4	B-9J	AMES	23, 24, 25, 26
△	7.4	2.3-23.0	.7-7.0	B-8B	AMES	5, 6, 7, 8, 39, 40

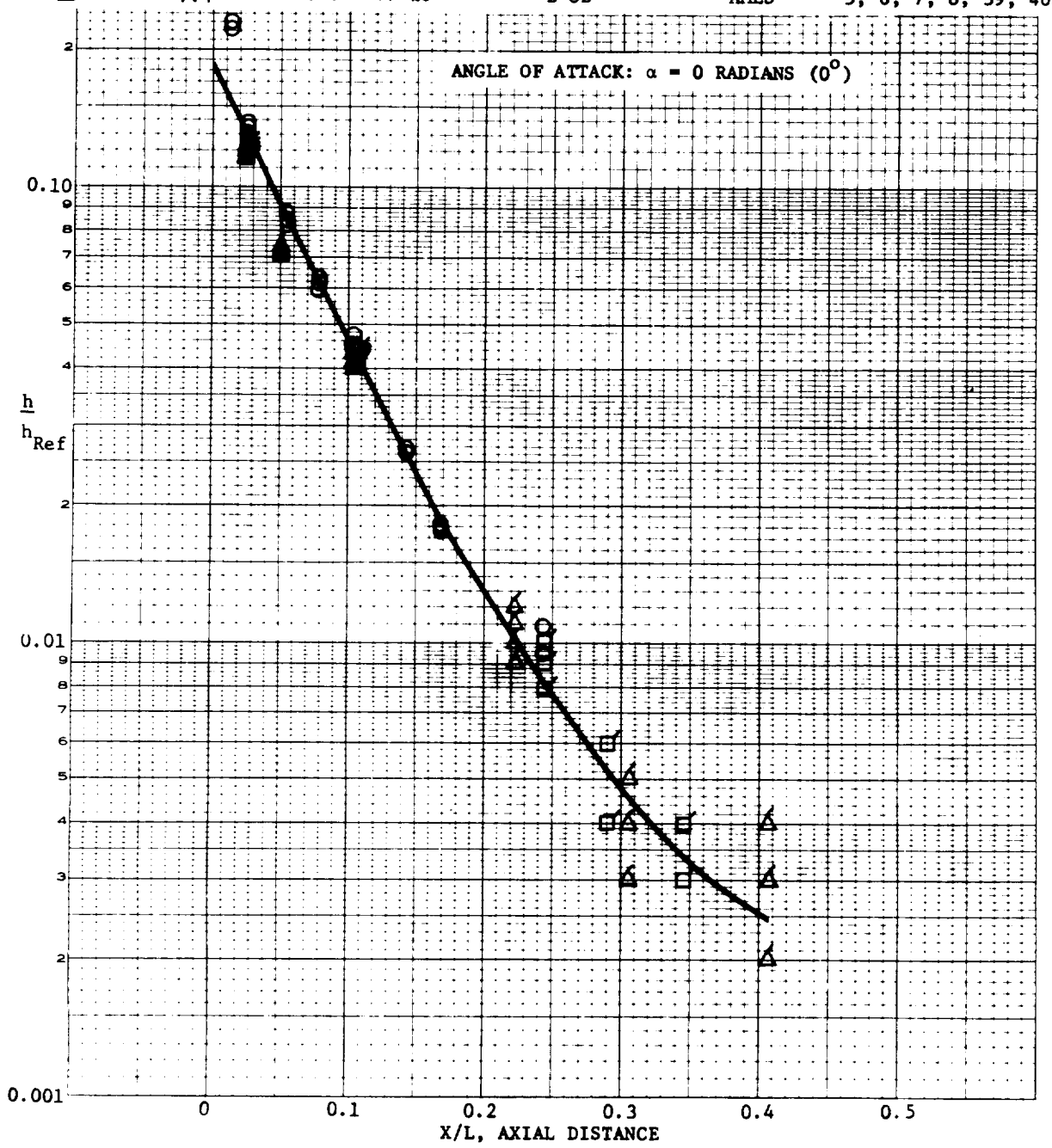

FIGURE 53

LOWER SURFACE CENTERLINE HEATING DISTRIBUTIONS FOR GD/C BOOSTERS

ANGLE OF ATTACK: $\alpha = \pi/3$ RADIANS (60°)

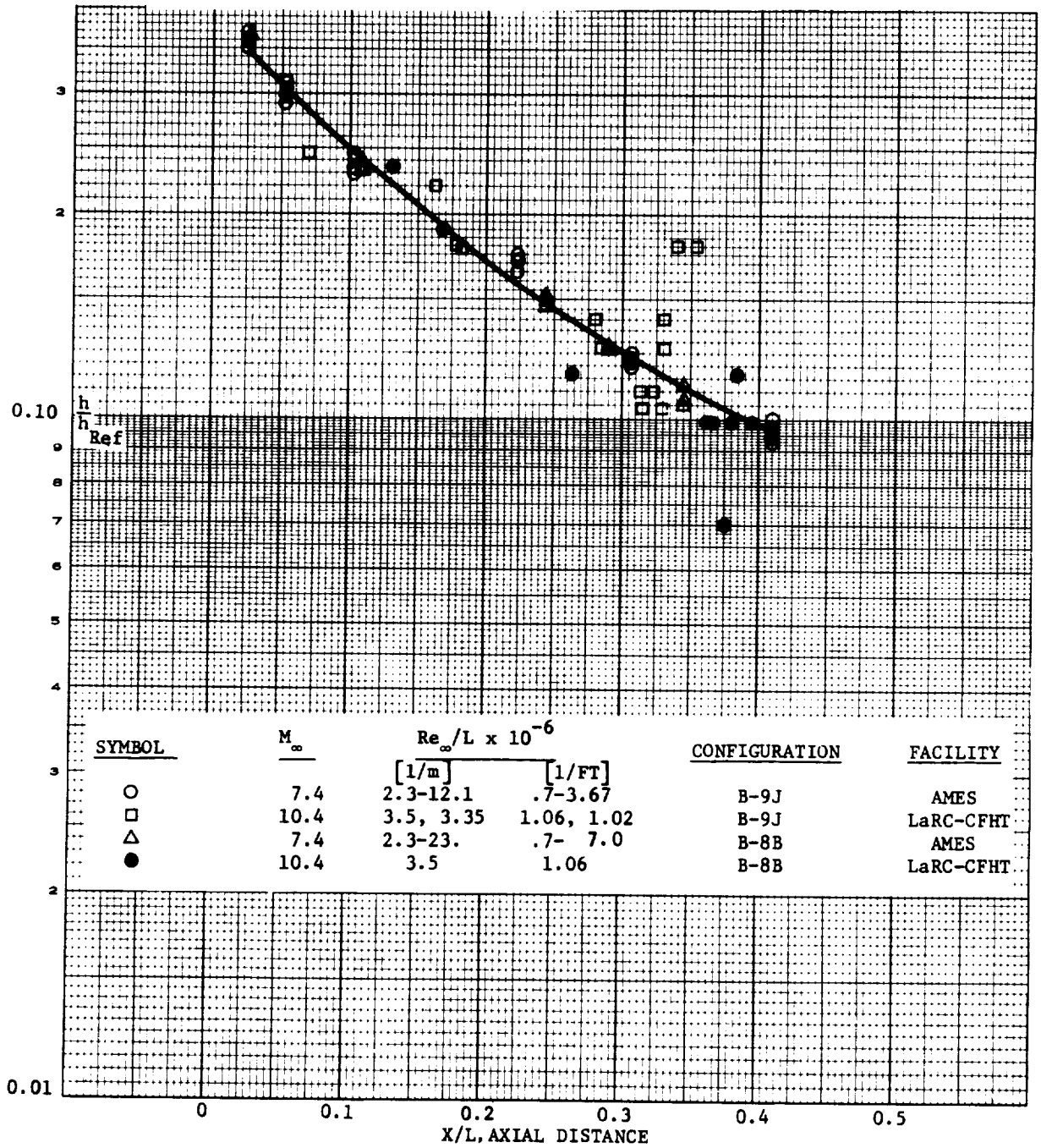

FIGURE 54

PROBABILITY PLOT FOR DETERMINING STANDARD DEVIATION FOR GD/C BOOSTER CONFIGURATION DATA OF FIGURE 52

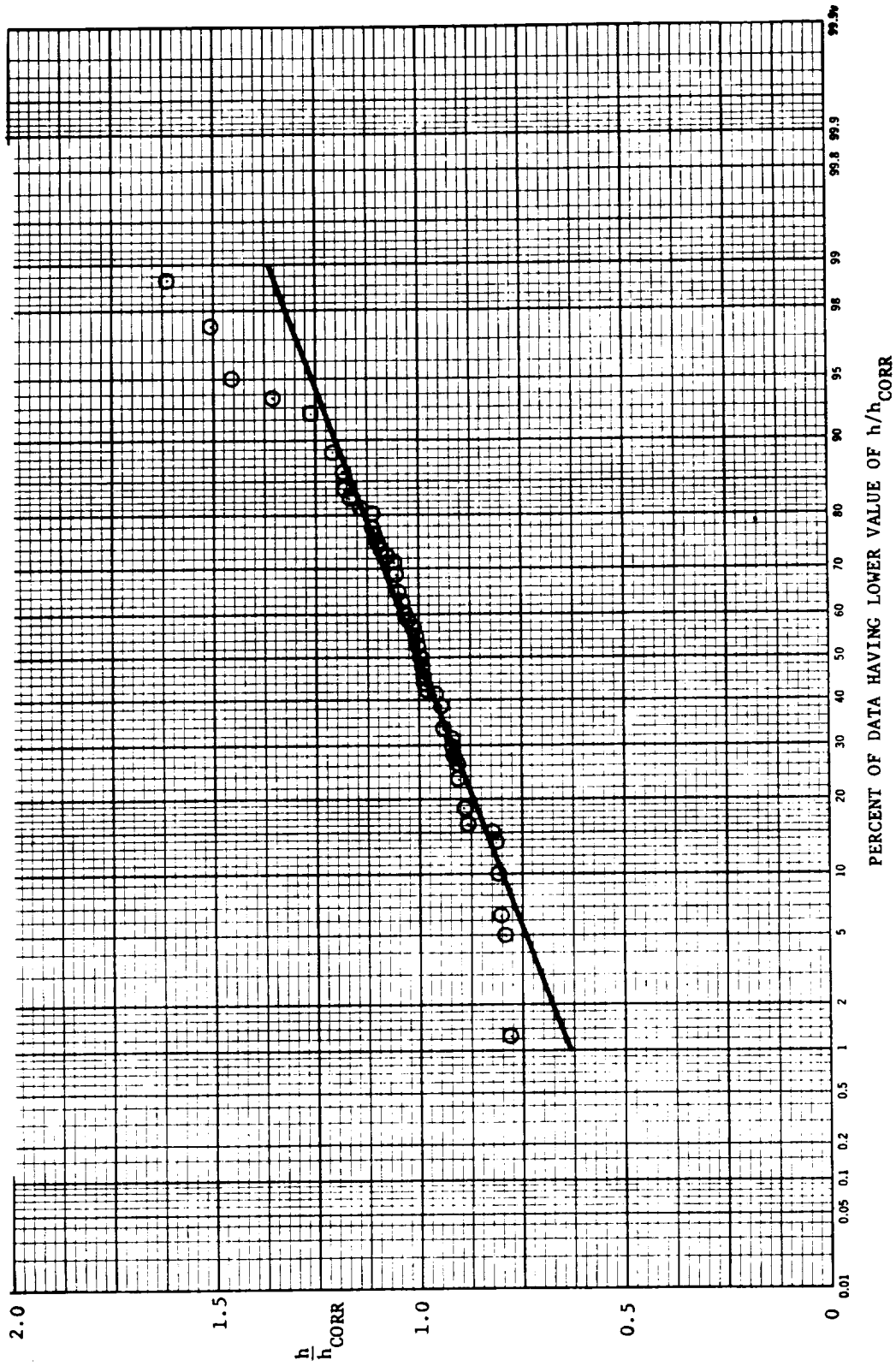

Heating multipliers developed in a similar manner for the various locations on the booster and orbiter are shown in Figures 55 and 56. These tables show that the largest uncertainty occurs in regions above the wing at high angle of attack. This is due to two factors: (1) the complex phenomena related to separated and reattaching flows which are poorly modeled in current correlations, and (2) the low heating levels in tests which are near the sensitivity level of the instrumentation. Also, as expected, the regions where interference heating is present (upper surfaces of the booster at α = 0) have high multipliers corresponding to one standard deviation of the data. The data scatter is slightly greater for the orbiter than for the booster. This is probably due to the greater complexity of the flow field (during reentry). Insufficient spanwise heating data were available on the lower surface of the 050/B orbiter to define a heating factor. Thus the factors for spanwise heating were defined from tests of the NAR 134B delta orbiter configuration.

In addition to heating factors applied to laminar and turbulent heating methods, an uncertainty exists in the state of the flow. This is best quantified as an uncertainty in the time of transition from laminar to turbulent flow, which can constitute a major contribution to the total uncertainty since turbulent heating is a factor of two or more greater than the corresponding laminar values.

The transition data were treated similarly to the heat transfer results. Best fits to a number of correlating approaches were made, and the standard deviation of the data about the best fit determined graphically. The probability plot developed for correlating forms Re_θ vs M_e, is included in Figure 57. The curve is nonlinear, suggesting that the data are not normally distributed about the best fit and a rather large standard deviation is noted. This is not surprising when one considers the complexity of the phenomena and the acknowledged sensitivity of the transition process to wind tunnel disturbances.

The times at which transition is predicted to occur for three of the more common correlations (and uncertainties corresponding to one, two and three standard deviations about the best fit) are summarized in Figure 58 through 60 for three locations on the MDC orbiter centerline. The most optimistic correlation would predict transition at 1,136 seconds and the most conservative at 384 seconds in the reentry trajectory for X/L = 0.5. The corresponding altitudes at which transition would be expected are 78 km (255,000 ft) and 57 km (186,000 ft) and were derived from the curves of Figures 61 through 63. These curves contain a superposition

FIGURE 55

GD/C BOOSTER UNCERTAINTIES

VEHICLE LOCATION	ANGLE OF ATTACK	FLOW	HEATING * MULTIPLIER	SAMPLE SIZE
LOWER SURFACE $\overset{C}{L}$	0	LAM	1.16	80
		TURB	1.19	62
	$\pi/3(60^{\circ})$	LAM	1.12	77
		TURB	1.25	19
WINDWARD PERIPHERAL	$\pi/6$ (30°)		1.28	78
UPPER SURF $\overset{C}{L}$	0	LAM	1.44**	22
		TURB	1.44**	22
	$\pi/3$ (60°)	N.A.	1.27	40
LOWER WING SURFACE	0	LAM	1.16	80
		TURB	1.19	62
	$\pi/3$ (60°)	LAM	1.12	77
		TURB	1.25	19
UPPER WING SURFACE	0	LAM	1.16	80
		TURB	1.19	62
	$\pi/3$ (60°)	N.A.	$1\sigma = 1.83$ $2\sigma = 3.37$ $3\sigma = 6.21$	89
ABOVE WING	0	N.A.	1.44**	22

* FOR 1σ EXCEPT AS NOTED
** MATED INTERFERENCE

FIGURE 56

MDAC DELTA WING ORBITER UNCERTAINTIES

VEHICLE LOCATION	ANGLE OF ATTACK	THEORY/CORRELATION	HEATING* MULTIPLIER	FACILITIES	SAMPLE SIZE
Lower Surface					
Centerline-All X/L	0 to $\pi/3$ (60°)	Eckert Laminar	1.18	Cornell,	87
		Spalding Chi	1.18	Tunnels B and F	166
		Turbulent			
Span - X/L = 0.5	$\pi/6$ (30°)	h/h_{Ref} vs Y/S	1.31	**	27
X/L = 0.75			1.22		29
Upper Surface					
Centerline-Forward of Canopy	0.593 (34°)	$\ln h/h_{Ref}$ = Const	1.25	Tunnels B and F	45
Aft of Canopy	0.593 (34°)		1.45		45
Side Body					
Forward of Wing	$\pi/6$ (30°)	$\ln h/h_{Ref}$ vs Z/Z_{MAX}			
X/L = 0.3			1.35		24
X/L = 0.45			1.28		35
Aft of Wing					
X/L = 0.68			1.49		26
Upper Wing	.593 (34°)	$\ln h/h_{Ref}$ = Const	$1\sigma = 2.04$	Cornell, Tunnel F	89
			$2\sigma = 4.20$		
			$3\sigma = 8.75$		

* For 1σ Except as noted.
**Based on North American DWO Spanwise Data.

FIGURE 57

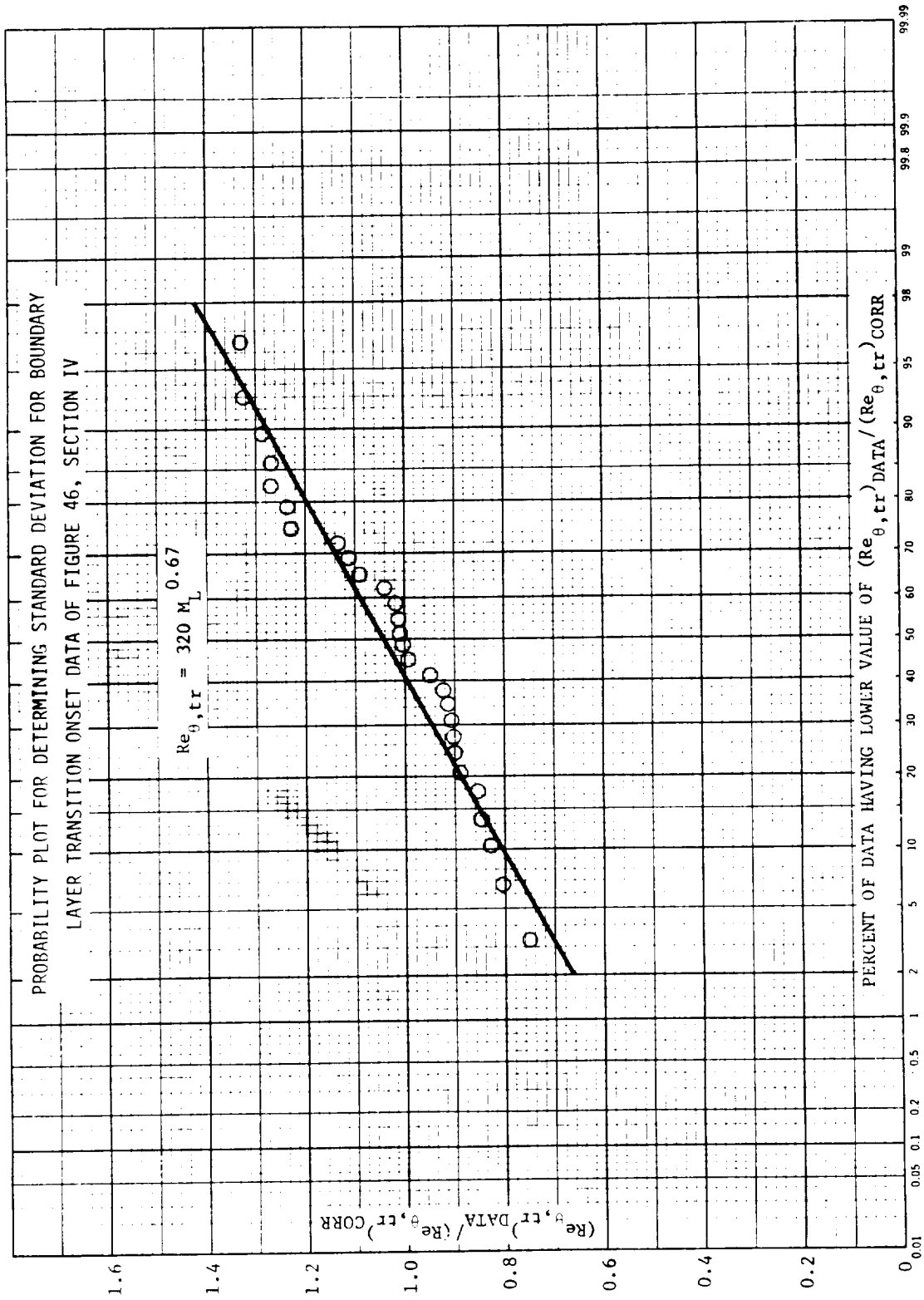
PROBABILITY PLOT FOR DETERMINING STANDARD DEVIATION FOR BOUNDARY LAYER TRANSITION ONSET DATA OF FIGURE 46, SECTION IV
$Re_{\theta,tr} = 320\ M_L^{0.67}$
$(Re_{\theta,tr})_{DATA}/(Re_{\theta,tr})_{CORR}$
PERCENT OF DATA HAVING LOWER VALUE OF $(Re_{\theta,tr})_{DATA}/(Re_{\theta,tr})_{CORR}$
1.6
1.4
1.2
1.0
0.8
0.6
0.4
0.2
0
99.99
99.9
99.8
99
98
95
90
80
70
60
50
40
30
20
10
5
2
1
0.5
0.2
0.1
0.05
0.01

FIGURE 58

UNCERTAINTY IN TIME OF TRANSITION ONSET
BASED ON LOCAL REYNOLDS NUMBER CORRELATION

$$Re_{L,tr} = (0.984 \times 10^6) M_e^{0.923}$$

UNCERTAINTY LEVEL	$Re_{L,tr}$ AND TRANSITION TIME					
	X/L = 0.1		X/L = 0.5		X/L = 0.9	
	$Re_{L,tr}$	TIME (SEC)	$Re_{L,tr}$	TIME (SEC)	$Re_{L,tr}$	TIME (SEC)
+ 3σ	4.75×10^6	1612	6.08×10^6	1310	7.90×10^6	1170
+ 2σ	3.84×10^6	1570	5.06×10^6	1247	6.90×10^6	1075
+ 1σ	3.02×10^6	1527	4.33×10^6	1188	5.76×10^6	852
- 1σ	1.25×10^6	1376	2.39×10^6	692	2.44×10^6	500
- 2σ	0.531×10^6	825	0.71×10^6	400	0.772×10^6	350
- 3σ	<0	All Turb	<0	All Turb	<0	All Turb

FIGURE 59

UNCERTAINTY IN TIME OF TRANSITION ONSET
BASED ON MOMENTUM THICKNESS REYNOLDS NUMBER CORRELATION

$$Re_{\theta,tr} = 320\ M_e^{0.67}$$

UNCERTAINTY LEVEL	$Re_{\theta,tr}$ AND TRANSITION TIME					
	X/L = 0.1		X/L = 0.5		X/L = 0.9	
	$Re_{\theta,tr}$	TIME (SEC)	$Re_{\theta,tr}$	TIME (SEC)	$Re_{\theta,tr}$	TIME (SEC)
+ 3σ	860	1564	1005	1365	1365	1125
+ 2σ	768	1522	918	1288	1220	745
+ 1σ	664	1478	835	1207	1060	625
Nominal	**555**	**1415**	**787**	**1136**	**913**	**533**
- 1σ	470	1302	690	732	755	452
- 2σ	432	997	540	563	603	390
- 3σ	344	765	403	436	442	346

FIGURE 60

UNCERTAINTY IN TIME OF TRANSITION ONSET
BASED ON CORRELATION OF THE MDAC PARAMETER

$$\ln\left[\frac{Re_\theta/Me}{(Re_L/Meter)^{0.2}}\right] = 1.721 + 0.7786\delta + 0.0743\delta^2$$

UNCERTAINTY LEVEL	$\frac{Re_{\theta,tr}/Me}{(Re_L/Meter)^{0.2}}$ AND TRANSITION TIME					
	X/L = 0.1		X/L = 0.5		X/L = 0.9	
	$Re_\theta/Me(Re_L/m)^{0.2}$	Time (SEC)	$Re_\theta/Me(Re_L/m)^{0.2}$	Time (SEC)	$Re_\theta/Me(Re_L/m)^{0.2}$	Time (SEC)
+ 3σ	17.0	1344	15.6	806	14.95	387
+ 2σ	14.7	1238	13.45	606	12.65	356
+ 1σ	12.35	1063	11.2	445	10.6	327
Nominal	**10.0**	**774**	**9.0**	**384**	**8.53**	**294**
- 1σ	7.65	575	6.74	333	6.55	All Turb.
- 2σ	5.25	374	4.73	275	4.59	All Turb.
- 3σ	2.88	279	2.63	All Turb.	2.55	All Turb.

FIGURE 61

PREDICTIONS OF TRANSITION REYNOLDS NUMBERS
FOR ORBITER FLIGHT CONDITIONS

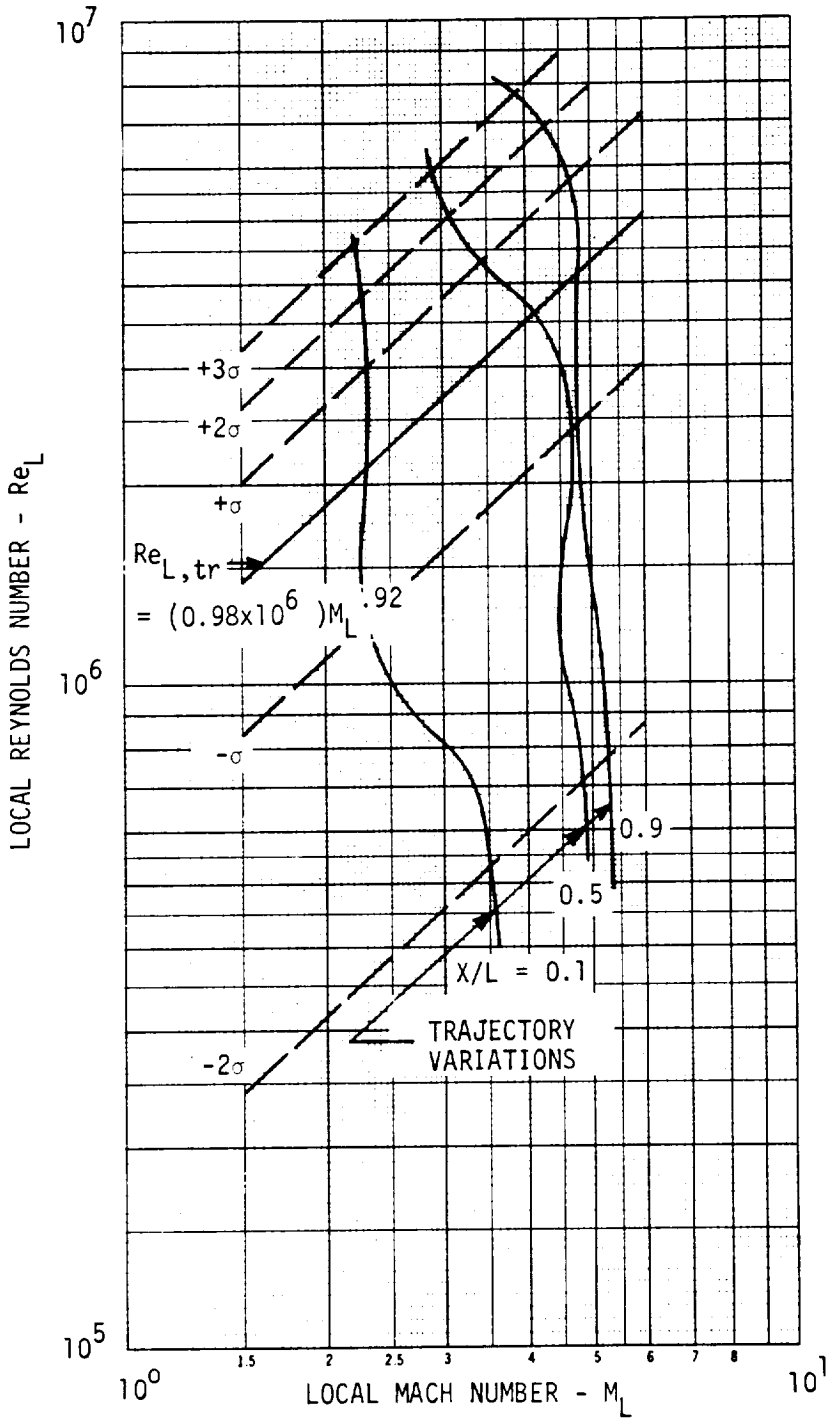

FIGURE 62

PREDICTIONS OF MOMENTUM THICKNESS REYNOLDS NUMBERS AT TRANSITION FOR ORBITER FLIGHT CONDITIONS

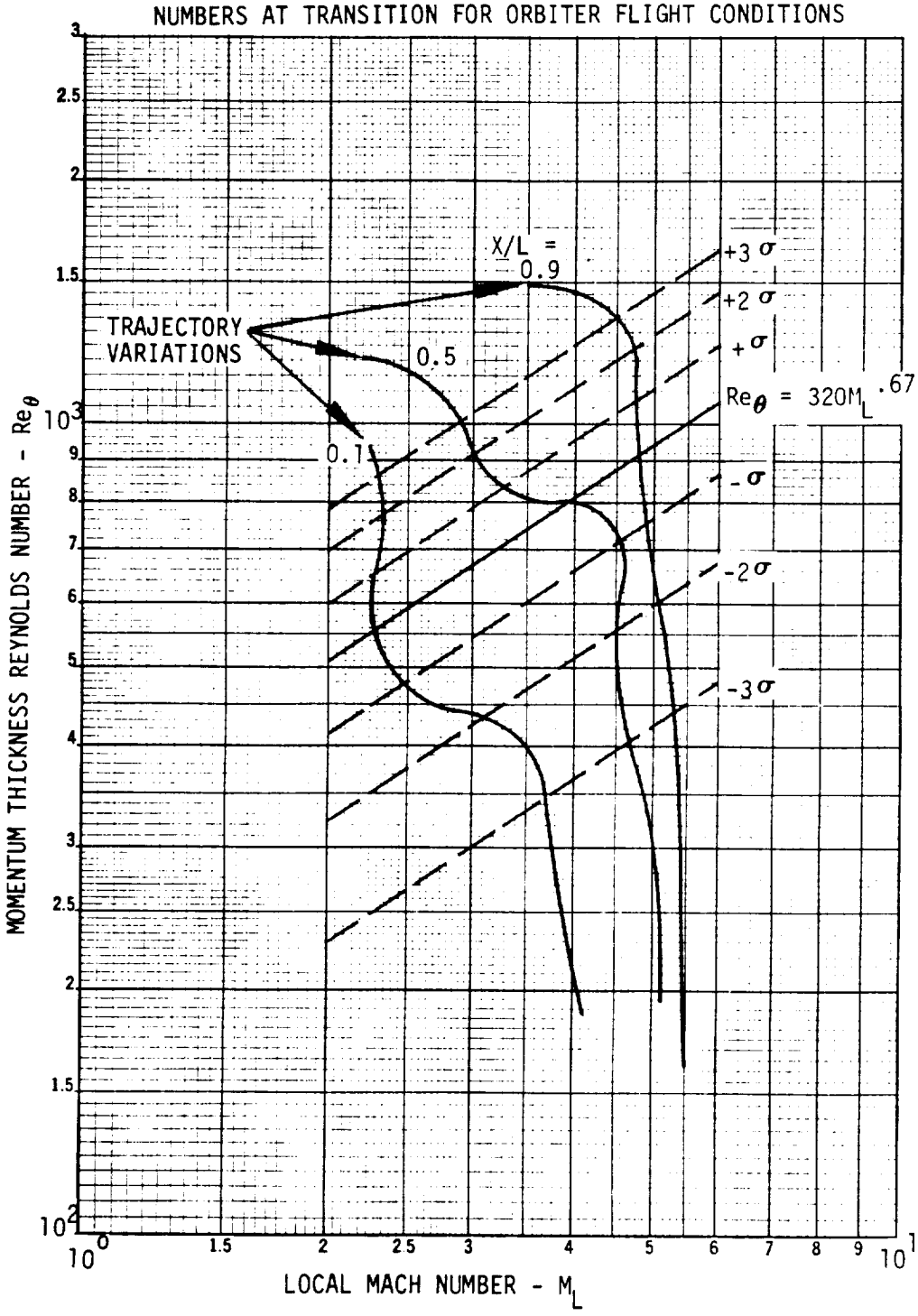

FIGURE 63

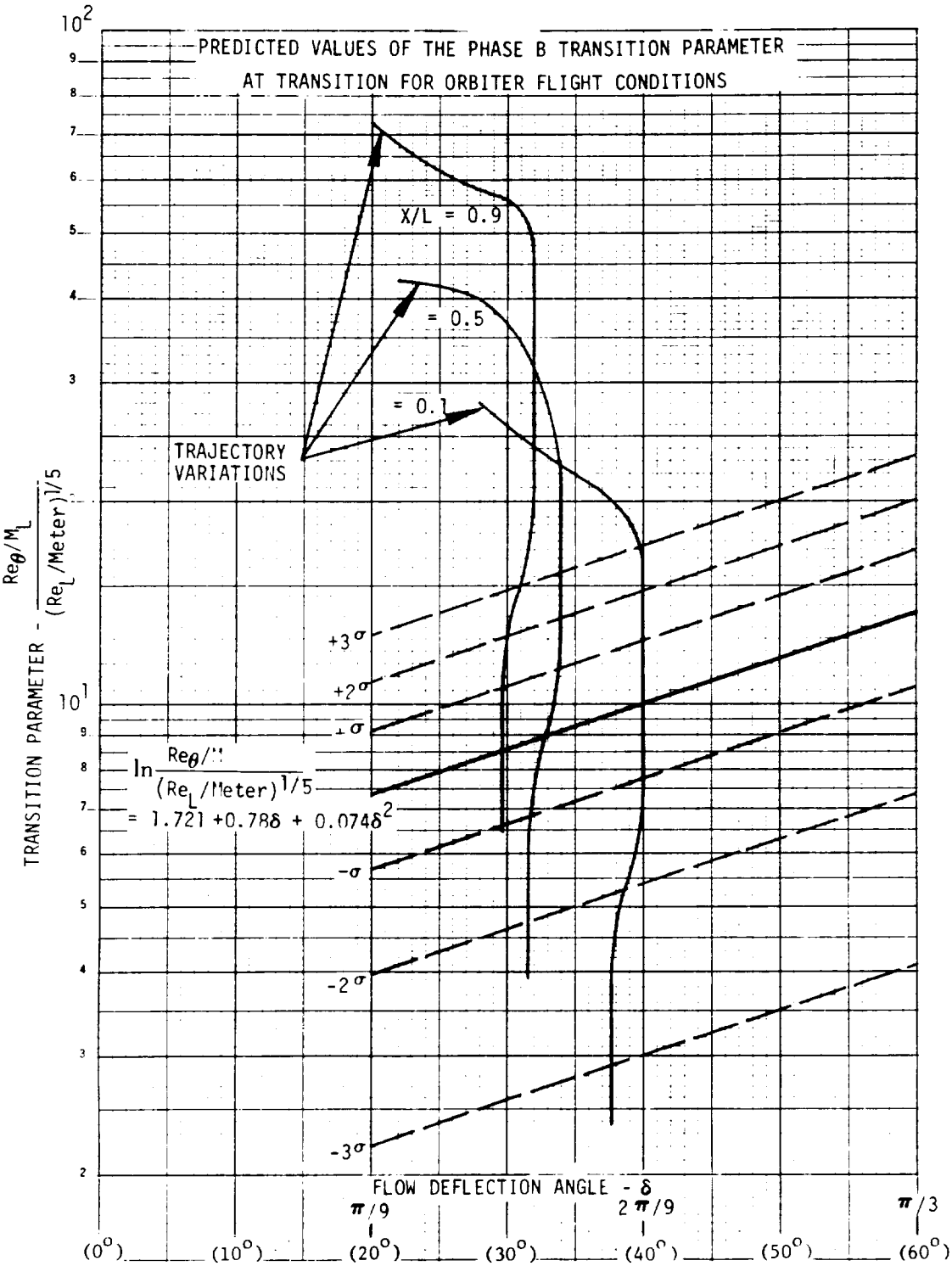
PREDICTED VALUES OF THE PHASE B TRANSITION PARAMETER
AT TRANSITION FOR ORBITER FLIGHT CONDITIONS
X/L = 0.9
= 0.5
= 0.1
TRAJECTORY VARIATIONS
+3σ
+2σ
+σ
-σ
-2σ
-3σ
$\ln \frac{Re_\theta/''}{(Re_L/Meter)^{1/5}} = 1.721 + 0.78\delta + 0.074\delta^2$
TRANSITION PARAMETER - $\frac{Re_\theta/M_L}{(Re_L/Meter)^{1/5}}$
10^2
10^1
FLOW DEFLECTION ANGLE - δ
π/9
2π/9
π/3
(0°) (10°) (20°) (30°) (40°) (50°) (60°)

of the trajectory variations of the transition parameters, the data correlations and lines corresponding to one through three standard deviations of the transition data about these fits. Transition is predicted to occur at the intersection of the trajectory and correlation curves.

A summary of transition altitudes for the better correlation attempts described in Section IV are contained in Figure 64. Altitudes corresponding to nominal and one standard deviation are listed for X/L = 0.5. Based on these results, the correlations which include the ratio of wall to local temperature and surface deflection angle have the smallest uncertainty in altitude. The nominal transition altitude is between 70 km (230,000 ft) and 72 km (235,000 ft) for these correlations. The altitude uncertainty corresponding to one standard deviation is less than 4.6 km (15,000 ft). The altitude uncertainty for the more commonly used correlation forms is approximately twice as great. Care should be used in generalizing these results since it is well known that extrapolation of ground test transition data to flight is still questionable. Therefore, it is recommended that uncertainties based on both optimistic and conservative transition be evaluated and compared.

3. Scale to Flight - As previously discussed, the question of scaling uncertainties measured in ground test to the flight situation is not completely resolved. It is recognized that the ground test data contain sources of error which are not present in flight. Accuracy analyses by tunnel operators usually indicate that these error sources are small (although there is some indication that data taken by the Shuttle contractors using Stycast models may contain significant errors). If the instrumentation-related errors are small compared with the total data scatter, it is likely that the major source of the scatter is the inability of theory to match the actual aerothermodynamic phenomena. The uncertainty thus produced may therefore propagate to the flight situation. This study was hampered by the limited quantity of data on similar configurations spanning large Mach number/Reynolds number ranges with wall cooling (e.g. T_w/T_{aw}) comparable with flight. As a result, conclusive proof that the wind tunnel derived uncertainties could be extrapolated to flight could not be derived. Therefore, the various approaches to deriving uncertainty factors were compared for various confidence levels (both for one-and two-sided normal distributions) of the data about representative theoretical approaches. An example which corresponds to peak turbulent heating for the orbiter centerline is shown in Figure 65. Nominal and off-nominal heating corresponding to one, two, and three standard deviations of

FIGURE 64
TRANSITION ALTITUDE UNCERTAINTIES

$X/L = 0.5$

EQUATION	TRANSITION ALTITUDE Km (KFT.)		
	$-\sigma$	Nominal	$+\sigma$
Local Reynolds Number			
$Re_{L,tr} = (0.984 \times 10^6) M_e^{0.923}$	67.4 (221)	58.7 (192.5)	55.2 (181)
$Re_{L,tr} = (2.305 \times 10^6) M_e^{1.05} (T_w/T_{T_\infty})^{1.04}$	76.7 (251.5)	74.0 (243)	71.8 (235.5)
$Re_{L,tr} = 6 \times 10^6 - (6.19 \times 10^6)\delta + (1.275 \times 10^6)\delta^2$	69.5 (228)	65.8 (216)	57.8 (189.5)
$Re_{L,tr} = -14.6 \times 10^6 + (2.63 \times 10^4)(T_w/T_e) + (1.32 \times 10^6)(T_w/T_e)^2 + (6.49 \times 10^7)\delta - (8.2 \times 10^7)\delta^2 + (3.2 \times 10^7)\delta^3$	71.6 (235)	70.1 (230)	67.7 (222)
Momentum Thickness Reynolds Number			
$\ln \frac{Re_\theta/M_e}{(Re_L/Meter)^{0.2}} = 1.721 + 0.7786\,\delta + 0.0743\,\delta^2$	83.5 (274)	77.7 (255)	74.2 (243.5)
$Re_\theta = 320\, M_e^{0.67}$	66.4 (218)	56.7 (186)	54.7 (179.5)
$Re_\theta = 470\, M_e^{0.73} (T_w/T_{T_\infty})^{0.47}$	74.2 (243.5)	71.9 (236)	70.3 (230.5)
$Re_\theta = 982\, M_e^{0.414} (T_w/T_{T_\infty})^{0.44} (\delta + 1)^{-1.028}$	74.0 (243)	71.9 (236)	70.3 (230.5)
$Re_\theta = -1051 + 4.15 \frac{T_w}{T_e} + 160.8 (\frac{T_w}{T_e})^2 + 6447\,\delta - 8537\,\delta^2 + 3420\,\delta^3$	73.3 (240.5)	71.6 (235)	70.1 (230)
$Re_\theta = 602 (T_w/T_e)^{0.66}$	Indeterm.	86.0 (282)	Indeterm.

FIGURE 65
MAXIMUM HEATING RATE VS STANDARD DEVIATIONS
MDAC ORBITER

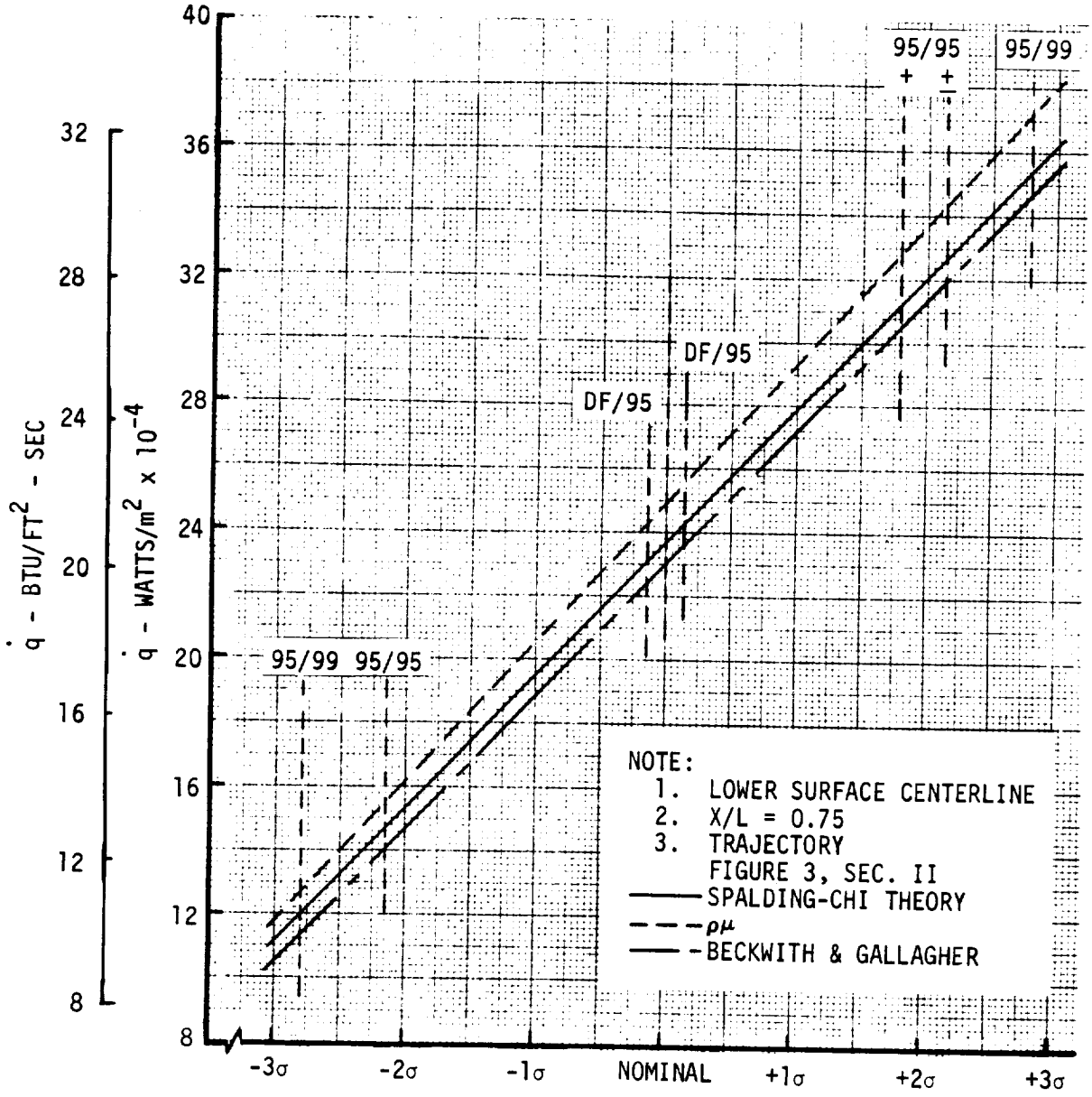

the data about each theory were made for the Spalding-Chi, Beckwith and Gallagher and $\rho\mu$ turbulent theories. It is important to note that differences exist even for the nominal case since the theories extrapolate differently to the flight conditions. This occurs even though the standard deviation of the data about best fits for each theory were essentially the same at the flight angle of attack. Comparison of the data with theory could not,therefore,be used to select the theory which best modeled the test data.

Included on the curve are the heating rate excursions related to various statistical approaches and confidence levels. These include 95-percent confidence limits for the mean (indicated in the figure as DF) and confidence limits with tolerance for two sided confidence levels for the data sample of 166 points. Because of the large sample size, the factor placed on the mean would be quite small and, if used as a design factor, would not even encompass the range of heating rates predicted in flight for nominal conditions by the three theories. In applying tolerance limits with confidence it is recognized that the standard deviation is not precisely known, and, therefore, it is necessary to express for a given confidence level the percentage of the data which will fall in the interval. The intervals for 95-percent confidence that 95 and 99-percent of the data will fall within the interval are also included in the figure. If the sample were infinite (the total population) the 95/95 location would be at 1.96 σ. Also included on the figure are the values for 95/95 corresponding to one-sided confidence limits; that is, values corresponding to a 95-percent confidence level that the peak values will not be exceeded.

It is interesting to note that the use of two standard deviations to represent a 95-percent confidence level, the approach used in the BGRV design and also applied by Scottaline in Reference 19 is midway between the 95/95 confidence limit with tolerance for one-sided and two-sided distributions.

In Figures 66 through 68,flight test data are compared with ground test results as a function of angle of attack. These results for a slender axisymmetric configuration indicate that the three-dimensional effects are well modeled by the laminar ground test data (Figure 66 and 67)and that the majority of the flight data are within two standard deviations of the ground test scatter. The turbulent data (Figure 68) are slightly lower than predicted by the ground test derived heating method (modified Spalding-Chi) and all measurements were lower than predictions based on two standard deviations of the ground test results.

FIGURE 66

FORWARD CONE FLIGHT DATA REFERENCED TO GROUND TEST CORRELATIONS

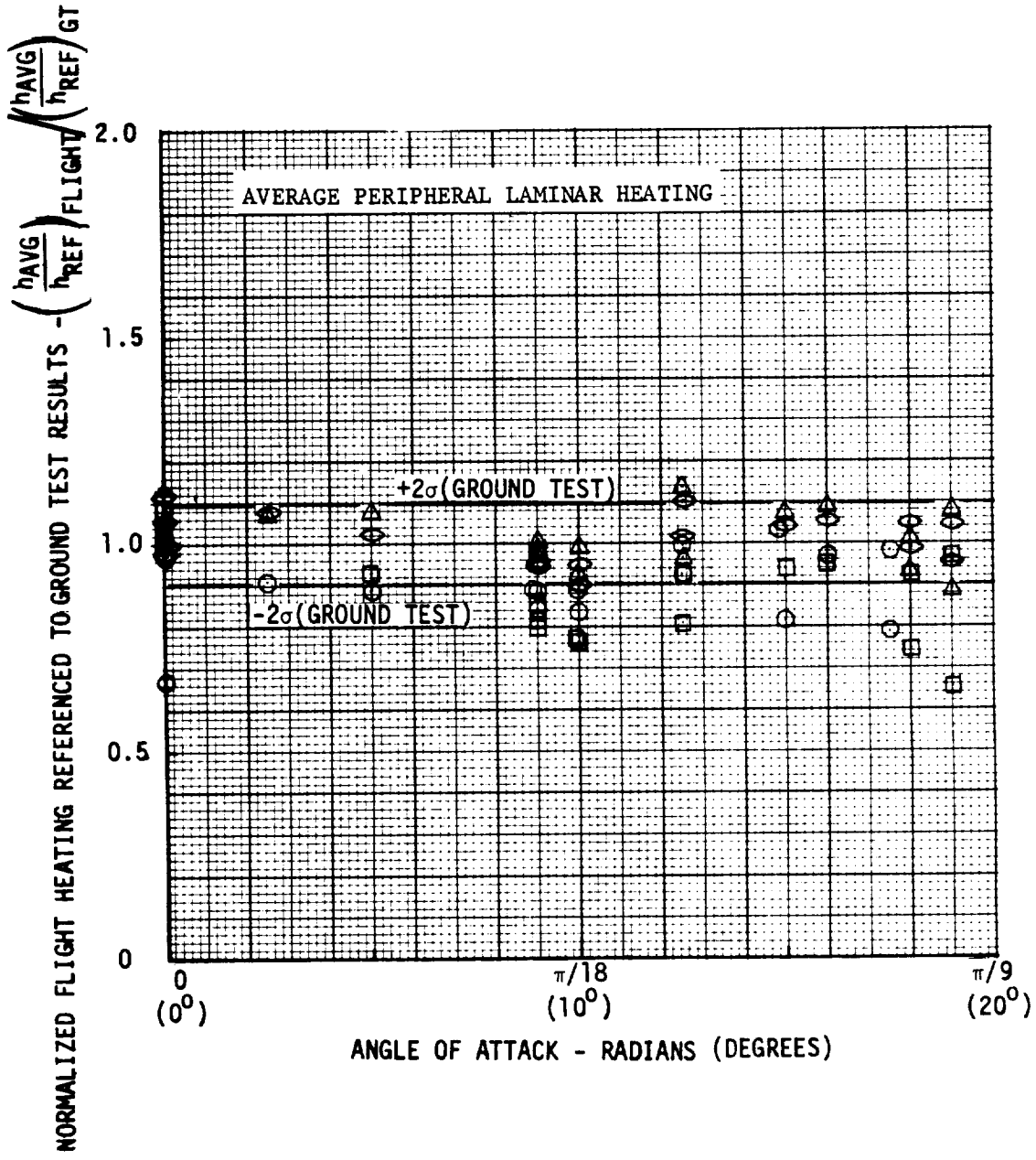

FIGURE 67

AFT CONE FLIGHT DATA REFERENCED TO GROUND TEST CORRELATIONS

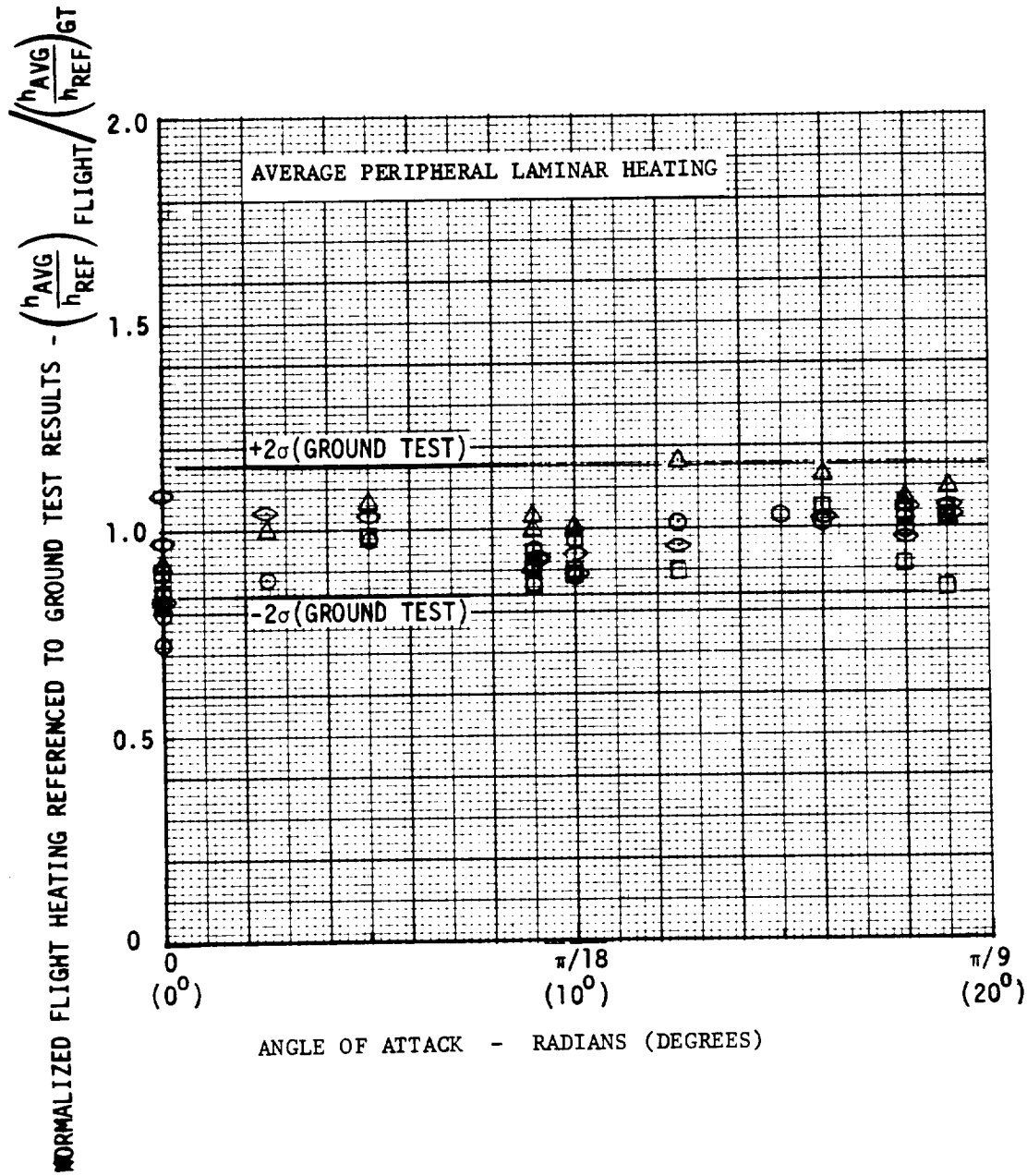

FIGURE 68

COMPARISON OF GROUND TEST AND FLIGHT TEST TURBULENT HEATING DATA DISPERSION

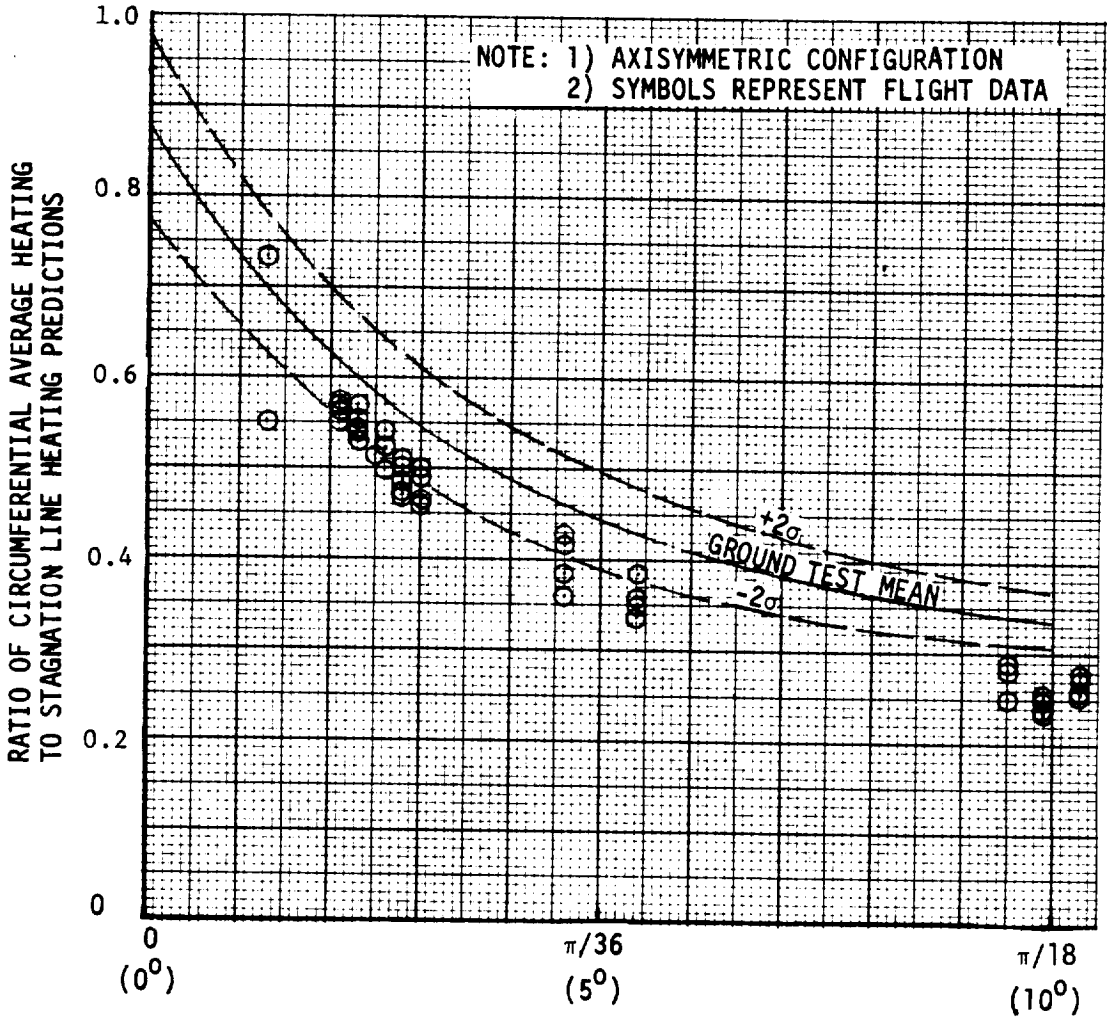

Because of limitations in the sample size and the large scatter present in the existing shuttle data, it does not appear justified to utilize highly sophisticated statistics to define confidence levels with tolerance since the difference in results from using the standard deviation as a measure of confidence is small. However, it is recommended that future evaluations of aerodynamic heating uncertainties for application to Phase C/D use the more sophisticated approach, one-sided tolerance limits with confidence.

VI THERMAL PROTECTION SYSTEM REQUIREMENTS

Thermal protection system weights were made for the Shuttle booster and orbiter using the data correlations derived in this study for nominal heating and for uncertainties corresponding to one, two, and three standard deviations of the data around the nominal value. The configurations consisted of the GD/C B-15B-2 booster and the MDC 050 B orbiter. These were selected because of the range and quality of the heating data available on these configurations. The trajectory for the booster consisted of a representative heat sink booster trajectory with a staging velocity of approximately 2.155 km/sec (7050 ft/sec). The orbiter trajectory was the MDC Phase B design baseline reentry trajectory for 2040 km (1100 nmi) lateral cross range. The TPS concept for the booster was aluminum heat sink, and, for the orbiter, was RSI attached through strain isolation foam to aluminum structure.

TPS requirements for the canards, control surfaces, and base region were not included in this study. Also, the effect of plume impingement heating to the booster upper surface by the orbiter engine was neglected.

Calculations were made for all laminar and all turbulent flow, as well as for both optimistic and conservative boundary layer transition criteria.

1. Booster TPS Requirements - A sketch of the booster and the locations for which TPS requirements were calculated is shown in Figure 69. The vehicle length was assumed to be 82 meters (269 feet). The surface areas corresponding to each of the fourteen regions for which the calculations were made are also included in the figure. It was assumed that the unit weight of the TPS was uniform for each region. The TPS concept for the booster was aluminum heat sink, that is, sufficient skin thickness was provided to limit the peak temperatures of the aluminum structure to 450°K (350°F). The LH_2 fuel and LOX tanks were assumed to be an integral part of the structure, and it was assumed that internal insulation was used to maintain preflight temperatures of the LH_2 tank above the LOX temperature 89°K (-300°F). This temperature was assumed to be the liftoff temperature in all tank areas. In the nontank areas the liftoff temperature was assumed to be 300°K (80°F). The thermal analysis model assumed one-dimensional heat flow through the skin with an adiabatic back surface. The analysis technique consisted of calculations of temperature histories of the aluminum for various

FIGURE 69

AREA BREAKDOWN FOR GD/C BOOSTER TPS CALCULATIONS

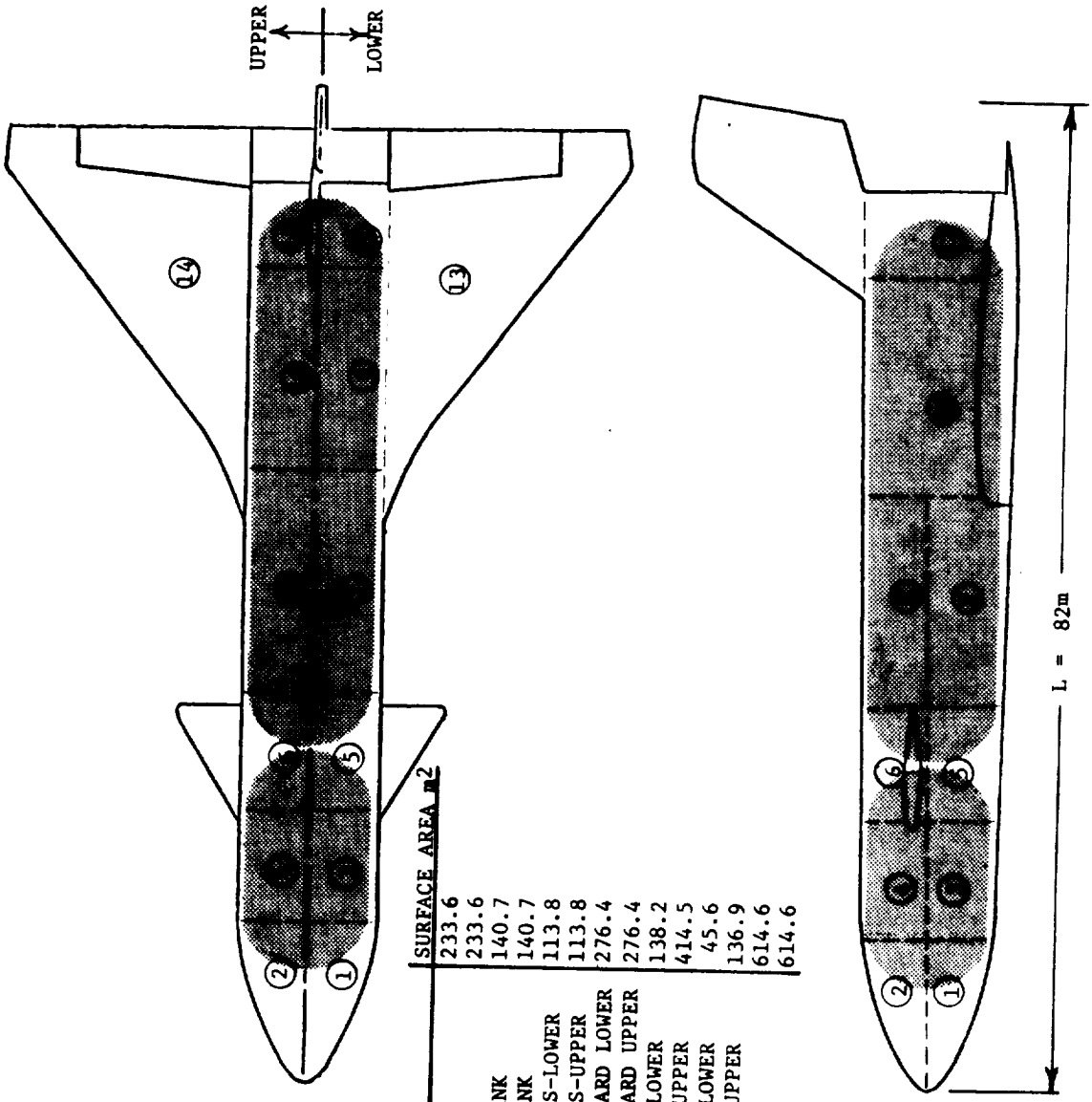

	LOCATION	SURFACE AREA m^2
1.	LOWER NOSE	233.6
2.	UPPER NOSE	233.6
3.	LOWER LOX TANK	140.7
4.	UPPER LOX TANK	140.7
5.	BETWEEN TANKS-LOWER	113.8
6.	BETWEEN TANKS-UPPER	113.8
7.	H_2 TANK-FORWARD LOWER	276.4
8.	H_2 TANK-FORWARD UPPER	276.4
9.	H_2 TANK-AFT LOWER	138.2
10.	H_2 TANK-AFT UPPER	414.5
11.	AFT H_2 TANK-LOWER	45.6
12.	AFT H_2 TANK-UPPER	136.9
13.	LOWER WING	614.6
14.	UPPER WING	614.6

skin thickness with interpolation of the results to determine the thickness which would achieve a peak temperature of 450°K (350°F).

The reference heat pulse for the booster is presented in Figure 70. The convective heating rates were computed for the stagnation point of a one foot diameter sphere using the method of Fay-Riddell for equilibrium air. A wall temperature of 311°K (100°F) was assumed for these calculations. The peak reference heating rate prior to separation of the booster and orbiter is approximately 4 x 10^4 watts/m^2 (3.5 BTU/ft^2 sec) and during entry 8 x 10^4 watts/m^2 (7.0 BTU/ft^2 sec). The small total heat load and the fact that the booster tank structure has a large potential for heat absorption, since it is initially at cryogenic temperatures make the use of heat sink TPS a logical choice for the booster. A skin thickness of 0.46 cm (0.18 in.) would be able to absorb this heat load to a 1-ft diameter nose. This is less than the structural requirements over much of the vehicle.

a. Heat Sink Requirements - The initial analyses were conducted to establish for the booster skin thicknesses to absorb the convective heat load independent of the structural requirements. The nominal heating rates were based on the correlations for the booster heating described in Section IV at the 14 locations shown in Figure 69. The total surface area for which thicknesses were determined was 3496 m^2 (37,607 ft^2). Figures 71 and 72 contain summarized unit weights and total heat sink weight in SI and engineering units respectively. For the nominal heat pulses the average unit weight of heat sink is 13.6 kg/m^2 (2.8 lb/ft^2) which is equivalent to an average skin thickness of 0.51 cm (0.20 in.). It should be noted that this is an average, just as the tabulated values are the average thicknesses in the region for which the calculations were made. These results correspond to the minimum weight heat sink TPS, since they do not account for structural requirements in the tank areas, which encounter critical loads during boost when temperatures are low.

Heat sink weights are also summarized for heating pulses which are 1, 2 and 3σ higher than nominal. These were obtained by applying the heating multipliers summarized in Figure 55 of Section V. As shown in Section V, these uncertainties correspond (approximately) to 68, 95 and 99.7-percent confidence levels. Using more refined statistical approaches would only slightly change the rather large uncertainties shown in the table. Therefore, more elaborate analysis techniques are not justified.

FIGURE 70

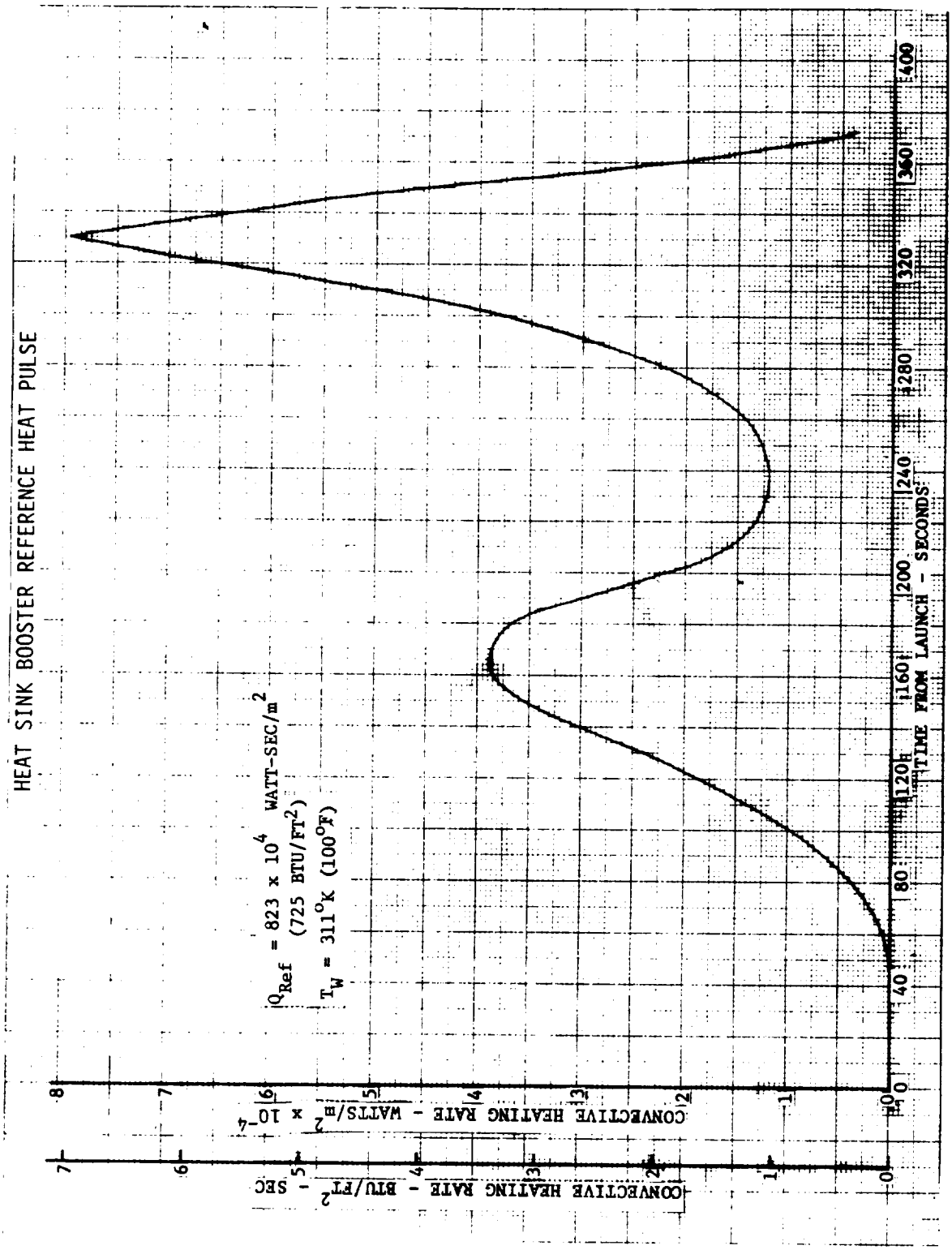
HEAT SINK BOOSTER REFERENCE HEAT PULSE
Q_{Ref} = 823 x 10^4 WATT-SEC/m^2 (725 BTU/FT^2)
T_W = 311°K (100°F)
CONVECTIVE HEATING RATE - BTU/FT^2 - SEC
CONVECTIVE HEATING RATE - WATTS/m^2 x 10^{-4}
TIME FROM LAUNCH - SECONDS
0 40 80 120 160 200 240 280 320 360 400

FIGURE 71
TPS WEIGHT BREAKDOWN
NOMINAL MDAC-E TRANSITION CRITERION
GD/C HEAT SINK BOOSTER
S.I. UNITS

VEHICLE LOCATION	AREA m^2	THERMAL PROTECTION SYSTEM WEIGHT							
		NOMINAL		1σ		2σ		3σ	
		Kg/m^2	Kg	Kg/m^2	Kg	Kg/m^2	Kg	Kg/m^2	Kg
NOSE									
LOWER	234	36.52	8,546	46.14	10,797	56.39	13,195	66.31	15,517
UPPER	234	8.25	1,931	12.109	2,834	15.87	3,714	19.433	4,547
BODY									
LOX TANK-LOWER	141	13.72	1,935	17.14	2,417	20.41	2,878	23.78	3,353
LOX TANK-UPPER	141	0.659	93	0.918	129	1.245	176	1.504	212
BETWEEN TANKS-	114	20.70	2,360	26.27	2,995	31.84	3,630	37.60	4,286
BETWEEN TANKS-UPPER	114	1.045	119	1.489	170	1.929	220	2.393	273
H_2 TANK									
FWD LOWER	276	13.33	3,679	16.60	4,582	19.87	5,484	23.19	6,400
FWD UPPER	276	1.191	329	1.621	447	2.002	553	2.441	674
AFT LOWER	138	19.73	2,723	24.51	3,382	29.05	4,009	33.74	4,656
AFT UPPER	415	1.191	494	1.621	673	2.002	838	2.441	1,013
AFT H_2 TANK									
LOWER	46	21.73	1,000	26.90	1,237	32.27	1,484	37.74	1,736
UPPER	137	3.320	455	4.931	676	6.592	903	8.447	1,157
WING									
LOWER	615	33.74	20,750	41.75	25,676	50.44	31,019	59.08	36,334
UPPER	615	1.030	633	1.533	943	2.358	1,450	3.970	2,442
TOTAL	3,496		45,047		56,958		69,553		82,600
RATIO TO NOMINAL	-		1.0		1.27		1.54		1.84

NOTE: σ BASED ON UNCERTAINTY IN HEATING RATES

FIGURE 72

TPS WEIGHT BREAKDOWN
NOMINAL MDAC-E TRANSITION CRITERION
GD/C HEAT SINK BOOSTER
ENGINEERING UNITS

VEHICLE LOCATION	AREA FT^2	THERMAL PROTECTION SYSTEM WEIGHT							
		NOMINAL		1σ		2σ		3σ	
		PSF	LB	PSF	LB	PSF	LB	PSF	LB
NOSE									
LOWER	2,515	7.48	18,803	9.45	23,773	11.55	29,053	13.58	34,166
UPPER	2,515	1.690	4,250	2.480	6,237	3.250	8,174	3.980	10,010
BODY									
LOX TANK-LOWER	1,515	2.81	4,260	3.51	5,311	4.18	6,33	4.87	7,383
LOX TANK-UPPER	1,515	0.135	205	0.188	285	0.255	386	0.308	467
BETWEEN TANKS-LOWER	1,225	4.24	5,191	5.38	6,586	6.52	7,984	7.70	9,438
BETWEEN TANKS-UPPER	1,225	0.214	262	0.305	374	0.395	484	0.490	600
H_2 TANK									
FWD LOWER	2,975	2.73	8,111	3.40	10,118	4.07	12,096	4.75	14,131
FWD UPPER	2,975	0.244	726	0.332	988	0.410	1,220	0.500	1,488
AFT LOWER	1,488	4.04	6,008	5.02	7,464	5.95	8,849	6.91	10,277
AFT UPPER	4,462	0.244	1,089	0.332	1,481	0.410	1,829	0.500	2,231
AFT H_2 TANK									
LOWER	491	4.45	2,183	5.51	2,706	6.61	3,246	7.73	3,797
UPPER	1,474	0.680	1,002	1.010	1,489	1.350	1,990	1.730	2,550
WING									
LOWER	6,616	6.91	45,693	8.55	56,566	10.33	68,320	12.10	80,074
UPPER	6,616	0.211	1,396	0.314	2,077	0.483	3,196	0.813	5,379
TOTAL	37,607		99,179		125,455		153,160		181,991
RATIO TO NOMINAL	-		1.0		1.27		1.54		1.84

NOTE: σ BASED ON UNCERTAINTY IN HEATING RATES

If thermal considerations alone are looked at, the uncertainty in heat sink weight is approximately 85 percent for a confidence level of 99.7 percent. A review of the results shows that the major weight increment is on the wing lower surface. This occurs because of the large area involved. The average upper surface unit weights are considerably less than those on the lower surface,and thus have a smaller impact on the heat sink requirements.

The above figures were based on boundary layer transition onset predictions using the MDAC-E developed transition criterion which was recommended by the Shuttle Aerothermodynamic Working Group as an interim criterion. Total vehicle heat sink weights were also made to assess the effect of heating uncertainties for assumed completely laminar and completely turbulent flow. Weight increments (from nominal) which resulted from these analyses are shown in Figure 73. These show that a weight reduction of 21,791 kg (48,041 lb) is possible if the flow were laminar and a weight increase of 4270 kg (9413 lb) if the vehicle were designed for turbulent flow. All weight increments are relative to the nominal weight based on the MDC Phase B transition criterion which is 45,047 kg (99,179 lb).

The effect of transition criterion on the TPS weight is shown in Figure 74. It is interesting to note that use of the optimistic fit to the Shuttle transition data, i.e., local Reynolds number versus local Mach number, has only a slight effect on the booster heat sink weight. The transition criterion used in this comparison is shown in Figures 61 and 63 of Section V. The uncertainties from these figures corresponding to the transition data scatter for 1, 2,and 3σ were used to evaluate the effect of transition uncertainty on the TPS weight. These results were combined statistically with the effect of uncertainty in heating rate. The combined uncertainties are summarized in Figure 75 from both the MDC and optimistic transition criteria. The combined weight uncertainty was obtained as the root sum square of the uncertainty due to heating rate prediction and boundary layer transition data scatter. That is,

$$\Delta W = \sqrt{(\Delta W_q)^2 + (\Delta W_T)^2}$$

where ΔW_T was obtained from Figure 74 and ΔW_q, from Figures 71 and 72 at corresponding values of σ. As shown in Figure 75, 34,981 kg (77,118 lb) would be required to assure a confidence level of approximately 99.7

FIGURE 73

TPS WEIGHT INCREMENTS DUE TO ALL LAMINAR AND ALL TURBULENT FLOW

GD/C BOOSTER LOWER SURFACE

ΔW IN KILOGRAMS

FLOW	NOMINAL	1σ	2σ	3σ
LAMINAR	-21,791	-18,262	-14,747	-10,548
TURBULENT	+ 4,270	+15,993	+29,511	+43,666

ΔW IN POUNDS

FLOW	NOMINAL	1σ	2σ	3σ
LAMINAR	-48,041	-40,261	-32,511	-23,253
TURBULENT	+ 9,413	+35,259	+65,059	+96,265

FIGURE 74

TPS WEIGHT INCREMENTS DUE TO UNCERTAINTY IN TRANSITION

GD/C BOOSTER LOWER SURFACE

ΔW IN KILOGRAMS

CRITERION	NOMINAL	1σ	2σ	3σ
MDAC	0	+ 930	+1674	+1859
OPTIMISTIC	-3533	- 744	+1227	+1859
MDAC-OPTIMISTIC	3533	1674	447	0

ΔW IN POUNDS

CRITERION	NOMINAL	1σ	2σ	3σ
MDAC	0	+2050	+3690	+4099
OPTIMISTIC	-7789	-1640	+2705	+4099
MDAC-OPTIMISTIC	7789	3690	985	0

FIGURE 75

TPS WEIGHT INCREMENTS DUE TO COMBINED UNCERTAINTIES IN HEATING RATE AND TRANSITION ONSET-GD/C BOOSTER LOWER SURFACE

ΔW IN KILOGRAMS

CRITERION	NOMINAL	1σ	2σ	3σ
MDAC	0	+10,242	+22,257	+34,981
OPTIMISTIC	-3,533	+6,203	+16,687	+24,379

ΔW IN POUNDS

CRITERION	NOMINAL	1σ	2σ	3σ
MDAC	0	+22,580	+49,068	+77,118
OPTIMISTIC	-7,789	+13,675	+36,788	+53,746

percent if the MDC transition criterion is used and 24,379 kg (53,746 lb) if a more optimistic transition criterion is utilized.

b. Combined Heat Sink and Structural Requirements - It should be recognized that the previous discussion concerned heat sink requirements only. Because the booster TPS is also structure, the values in Figures 71 and 72 must be adjusted to reflect structural requirements. This is done in Figures 76 and 77 for SI and engineering units, respectively.

Structural requirements for the LOX tank, internal tank region, and LH_2 tank were developed in Reference 20. Using the values reported in the above reference it was found that the LOX tank, internal tank, and LH_2 tank upper surfaces were sized by structural requirements. In addition, heat sink requirements were less than structural requirements for the nominal and 1σ heating on the lower surface of the LOX and LH_2 tanks. A portion of the wing upper surface was also sized by structural rather than heat sink requirements. Integrating these effects result in a considerably lower TPS uncertainty (in percent of dry weight) than if thermal considerations alone are included. The 84-percent uncertainty for a confidence level of 0.997 is reduced to approximately 55-percent of dry weight.

FIGURE 76

COMBINED STRUCTURAL AND HEAT SINK WEIGHT BREAKDOWN
NOMINAL MDAC-E TRANSITION CRITERION
GD/C HEAT SINK BOOSTER
S. I. UNITS

VEHICLE LOCATION	AREA m^2	THERMAL PROTECTION SYSTEM WEIGHT							
		NOMINAL		1σ*		2σ*		3σ*	
		Kg/m^2	Kg	Kg/m^2	Kg	Kg/m^2	Kg	Kg/m^2	Kg
NOSE									
LOWER	233.6	36.52	8,529	46.14	10,784	56.39	13,178	66.30	15,498
UPPER	233.6	8.25	1,928	12.11	2,829	15.87	3,708	19.43	4,540
BODY									
LOX TANK - LOWER	140.7	18.99**	2,673	18.99**	2,673	20.41	2,873	23.78	3,349
LOX TANK - UPPER	140.7	18.99**	2,673	18.99**	2,673	18.99	2,673	18.99	2,673
BETWEEN TANKS - LOWER	113.8	20.70	2,355	26.27	2,987	31.83	3,621	37.59	4,281
BETWEEN TANKS - UPPER	113.8	17.09**	1,945	17.09**	1,945	17.09**	1,945	17.09**	1,945
H_2 TANK									
FWD LOWER	276.4	16.60**	4,588	16.60	4,588	19.87	5,487	23.19	6,410
FWD UPPER	276.4	16.60**	4,588	16.60**	4,588	16.60**	4,588	16.60**	4,588
AFT LOWER	138.2	19.72	2,725	24.51	3,386	29.05	4,014	33.74	4,662
AFT UPPER	414.5	16.60	6,882	16.60**	6,882	16.60**	6,882	16.60**	6,882
AFT H_2 TANK									
LOWER	45.6	21.73	990	26.90	1,227	32.27	1,472	37.74	1,722
UPPER	136.9	3.32	455	4.93	675	6.59	903	8.45	1,157
WING									
LOWER	614.6	33.74	20,726	41.74	25,658	50.44	30,990	59.08	36,322
UPPER	614.6	3.01	1,852	3.37**	2,071	4.01**	2,464	5.22**	3,211
TOTAL	3493.4		62,909		72,966		84,798		97,240
RATIO TO NOMINAL BOOSTER DRY WEIGHT	-		1.0		1.16		1.35		1.55

* σ BASED ON UNCERTAINTY IN HEATING RATES
** STRUCTURAL REQUIREMENT INCLUDED

FIGURE 77

COMBINED STRUCTURAL AND HEAT SINK WEIGHT BREAKDOWN
NOMINAL MDAC-E TRANSITION CRITERION
GD/C HEAT SINK BOOSTER
ENGINEERING UNITS

VEHICLE LOCATION	AREA FT^2	THERMAL PROTECTION SYSTEM WEIGHT							
		NOMINAL		1σ*		2σ*		3σ*	
		PSF	LB	PSF	LB	PSF	LB	PSF	LB
NOSE									
LOWER	2,515	7.48	18,803	9.45	23,773	11.55	29,053	13.58	34,166
UPPER	2,515	1.69	4,250	2.48	6,237	3.25	8,174	3.98	10,010
BODY									
LOX TANK-LOWER	1,515	3.89**	5,893	3.89**	5,893	4.18	6.333	4.87	7,383
LOX TANK-UPPER	1,515	3.89**	5,893	3.89**	5,893	3.89	5,893	3.89	5,893
BETWEEN TANKS-LOWER	1,225	4.24	5,191	5.38	6,586	6.52	7,984	7.70	9,438
BETWEEN TANKS-UPPER	1,225	3.5**	4,288	3.50**	4,288	3.50**	4,288	3.50**	4,288
H_2 TANK									
FWD LOWER	2,975	3.40**	10,115	3.40	10,115	4.07	12,096	4.75	14,131
FWD UPPER	2,975	3.40**	10,115	3.40**	10,115	3.40**	10,115	3.40**	10,115
AFT LOWER	1,488	4.04	6,008	5.02	7,464	5.95	8,849	6.91	10,277
AFT UPPER	4,462	3.40*	15,171	3.40**	15,171	3.40**	15,171	3.40**	15,171
AFT H_2 TANK									
LOWER	491	4.45	2,183	5.51	2,706	6.61	3,246	7.73	3,797
UPPER	1,474	0.68	1,002	1.01	1,489	1.35	1,990	1.73	2,550
WING									
LOWER	6,616	6.91	45,693	8.55	56,566	10.33	68,320	12.10	80,074
UPPER	6,616	0.617	4,082	0.69**	4,565	0.821**	5,432	1.07**	7,079
TOTAL	37,607		138,687		160,861		186,944		214,372
RATIO TO NOMINAL BOOSTER DRY WEIGHT	-		1.0		1.16		1.35		1.55

* σ BASED ON UNCERTAINTY IN HEATING RATES
** STRUCTURAL REQUIREMENT INCLUDED

2. Orbiter TPS Requirements - A sketch of the orbiter configuration used to define the TPS requirements is shown in Figure 78. This configuration was selected since it was a configuration for which a large amount of test data were available and represented a viable design for the fully reusable shuttle system. The MDC Phase B studies had baselined a metallic TPS for this configuration. More recent NASA decisions have led to selection of a reusable surface insulation (RSI) as the shuttle baseline TPS. Since the TPS weight sensitivities would be different for a metallic than for an RSI system, an RSI thermal protection system was studied to allow more direct application of these results to the current Shuttle orbiter. A sketch of the TPS installation is shown in Figure 79. Mullite RSI is attached through a foam layer to the aluminum structure. The use of mullite provides reuse capability to 1530°K (2300°F) and overshoot capability to approximately 1860°K (2900°F). The foam layer is applied to isolate the RSI from the structural bending loads carried by the aluminum structure, thereby preventing potential damage to the RSI by structural buckling. The sizing of the RSI thickness and foam had two temperature constraints: an RSI-to-foam-bondline temperature limit of 590°K (600°F) and a peak aluminum structural temperature of 450°K (350°F). Because of handling and fabrication limits the minimum thickness of RSI which can be applied is 0.635 cm (0.25 in.). The weights presented herein include the weight of RSI, its silicone waterproof coating, strain isolation foam, and adhesives required to bond the elements of the thermal protection system together. An aluminum thickness of 0.15 cm (0.06 in.) was assumed in these analyses.

The RSI was sized for reentry only, since the small boost phase heat pulse will not produce critical bondline or structural temperatures and this heat will be dissipated during orbit for the majority of Shuttle orbiter missions. The possible exceptions to this case are abort or once-around missions. However, even for these remote situations, the boost phase is not likely to have a major effect on the sensitivities derived from this study for the reentry heat pulse. The initial temperature of the TPS component was assumed to be 311°K (100°F), a value consistent with normal vehicle attitude and orbital thermal control and orbit inclination.

Typical reentry heat pulses are included in Figure 80 for a lower surface centerline location at 10 percent of the vehicle length. The three heat pulses correspond to all laminar, to all turbulent, and to assumed transition onset based on the MDC Phase B transition criterion (Figure 47, Section IV). For the transitional heat pulse, fully developed turbulent flow was assumed to occur when

FIGURE 78

AREA BREAKDOWN FOR ORBITER TPS CALCULATIONS

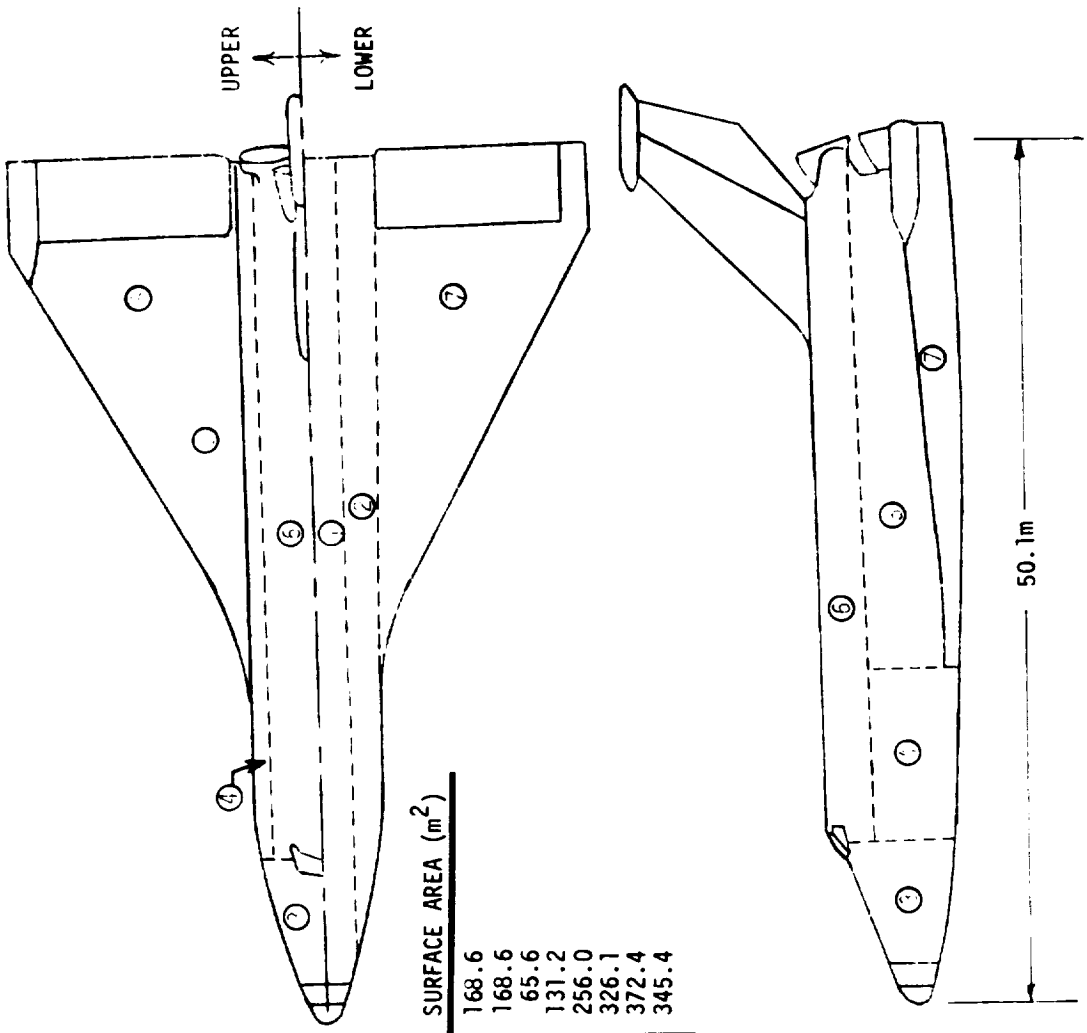

LOCATION	SURFACE AREA (m^2)
1. LOWER SURFACE-INBOARD	168.6
2. LOWER SURFACE-OUTBOARD	168.6
3. NOSE	65.6
4. FOWARD SIDE BODY	131.2
5. AFT SIDE BODY	256.0
6. UPPER SURFACE	326.1
7. WING LOWER SURFACE	372.4
8. WING UPPER SURFACE	345.4

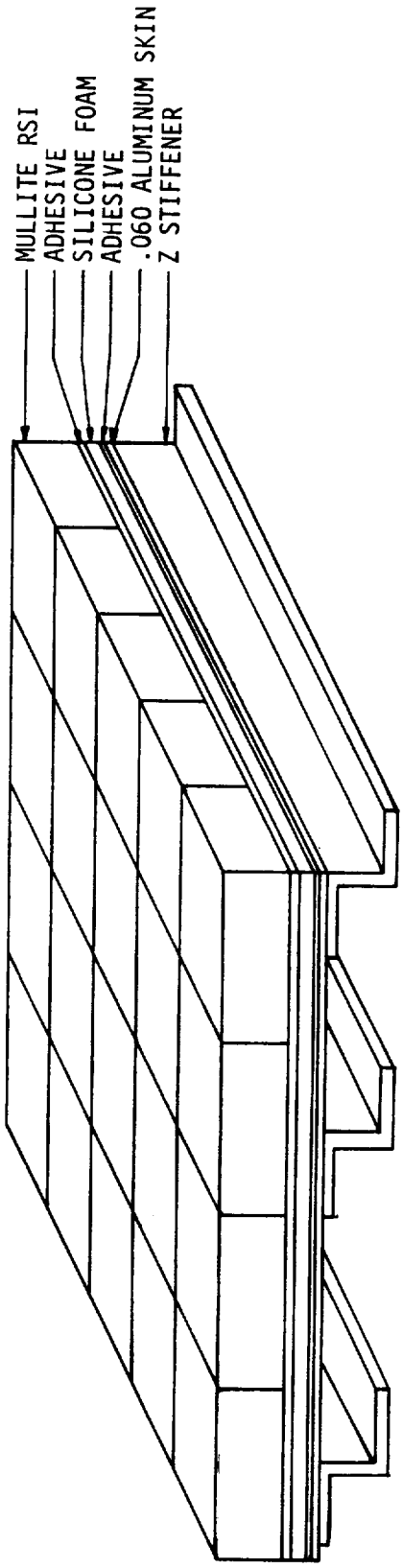

FIGURE 79
ORBITER TPS ARRANGEMENT

FIGURE 80
REENTRY HEAT PULSE
MDAC DELTA WING ORBITER LOWER SURFACE CENTERLINE
X/L = 0.10

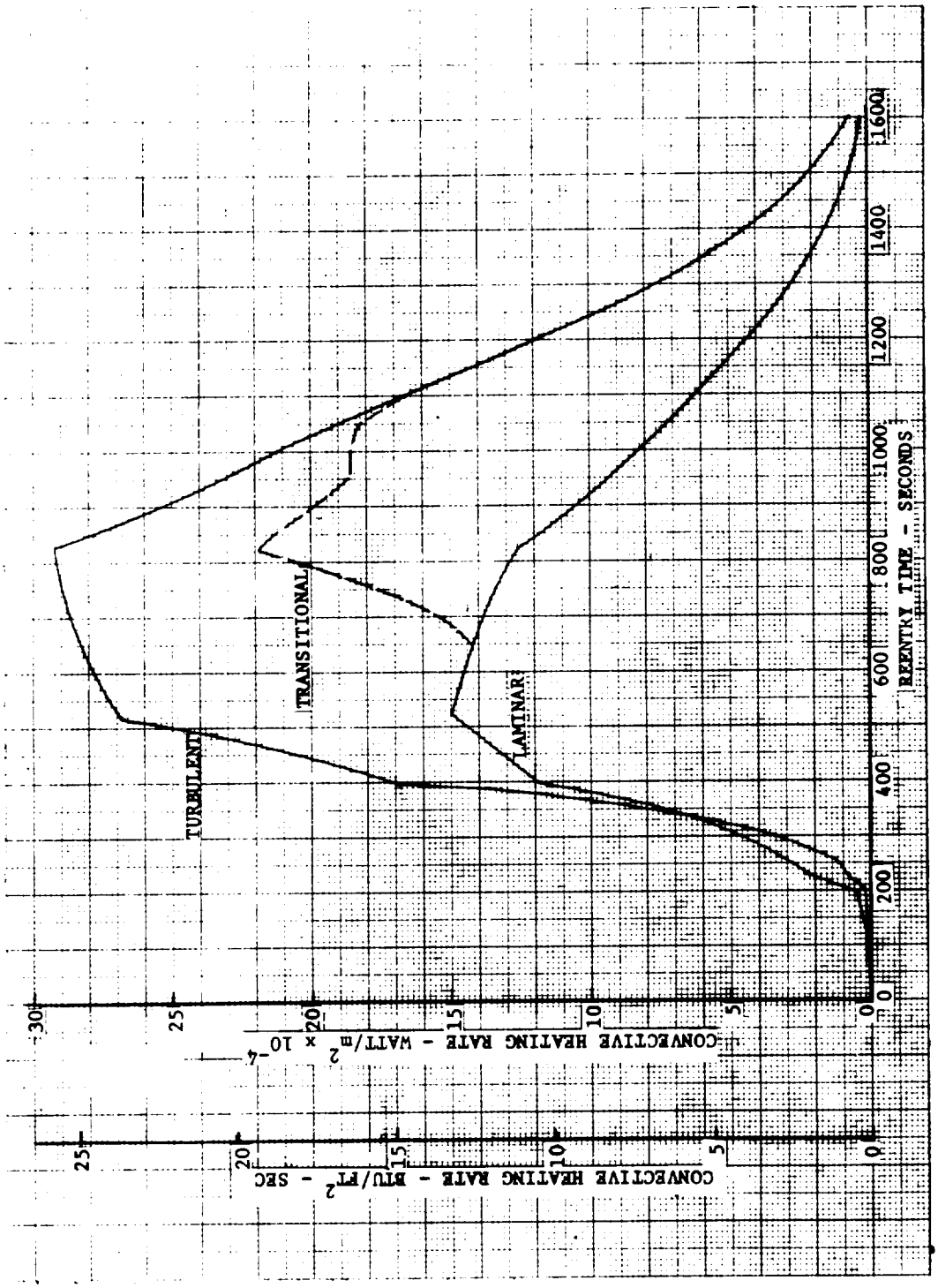

transition onset was predicted at X/L = 0.05. That is, the extent of transitional flow was equal to the length of the vehicle for which the flow was laminar. The reentry time from 122 km (400,000 ft) is approximately 1500 seconds for this 2040 km (1100 nmi) cross range trajectory. The heating rate histories were computed using the correlations developed for the orbiter in Section IV. For the lower surface centerline these consisted of heating rates computed using the Eckert Flat Plate Reference Enthalpy Method with local flow conditions based on equivalent cone flow. The analyses were made for real air in thermodynamic equilibrium. Correlation factors, Figure 34 of Section IV, were applied to these calculations as a function of angle of attack to account for the three dimensional characteristics of the flow. For turbulent flow a similar approach was utilized. The heating was computed using the Spalding-Chi correlation with a Reynolds analogy factor corresponding to $(P_r)^{-2/3}$. Factors developed from the test data correlations to account for three-dimensional flow field effects were also applied to these heating rates. The correlation curve used for the lower surface centerline is also included in Figure 34 of Section IV.

TPS requirements were determined from correlations of TPS unit weight as a function of integrated heat load. The average unit weight and total TPS weight are summarized in Figures 81 and 82 for SI and engineering units, respectively. The weight breakdown is summarized for the eight sections into which the vehicle was divided. The nominal heat pulses and heat pulses corresponding to heating multipliers derived from Figure 56 of Section V for 1,2, and 3σ uncertainties were used to define these TPS requirements. The MDC transition criteria was used in these analyses. The results show that the orbiter TPS weight is much less sensitive to the aerodynamic heating uncertainties than booster TPS weights due to the fact that the majority of the aerodynamic heating is reradiated to space. As the heating rate is increased, a greater fraction of the total heat is reradiated. Thus, the percent which is conducted to the structure is reduced. A 3σ design would require a 15-percent weight increase. The greatest weight penalty associated with the heating uncertainties is on the wing lower surfaces, primarily because of the large area involved. The locations having the largest uncertainties in heating are regions for which the nominal heating is quite low; it was found that only slight increases above minimum RSI thickness were required for the 3σ case.

Figure 83 summarizes the weight increments (from the nominal in Figures 81 and 82) if laminar or turbulent flow is assumed for the entire

FIGURE 81
TPS WEIGHT BREAKDOWN
NOMINAL MDAC-E TRANSITION CRITERION
MDAC DWO
S.I. UNITS

VEHICLE LOCATION	AREA m^2	THERMAL PROTECTION SYSTEM WEIGHT							
		NOMINAL		1σ		2σ		3σ	
		Kg/m^2	Kg	Kg/m^2	Kg	Kg/m^2	Kg	Kg/m^2	Kg
NOSE	65.6	5.71	375	6.15	403	6.54	429	6.93	455
LOWER SURFACE-INBOARD	168.6	12.01	2,025	12.79	2,156	13.67	2,305	14.31	2,413
OUTBOARD	168.6	11.52	1,942	12.30	2,074	14.06	2,371	14.99	2,527
FORWARD SIDE	131.2	4.64	609	5.08	666	5.49	720	5.86	769
AFT SIDE	256.0	4.45	1,139	4.45	1,139	4.79	1,226	5.03	1,288
UPPER SURFACE	326.1	4.45	1,451	4.45	1,451	4.45	1,451	4.52	1,474
WING LOWER SURFACE	372.4	12.26	4,566	13.04	4,856	14.36	5,348	15.09	5,620
WING UPPER SURFACE	345.4	4.45	1,537	4.45	1,537	4.45	1,537	4.45	1,537
TOTAL UNCERTAINTY STUDY	1833.9		13,644		14,282		15,387		16,083
REMAINING SURFACES	332.9		3,128		3,128		3,128		3,128
TOTAL	2166.8		16,772		17,410		18,515		19,211
RATIO TO NOMINAL	-		1.00		1.04		1.10		1.15

NOTE: σ BASED ON UNCERTAINTY IN HEATING RATES
NOMINAL TRANSITION CRITERION

FIGURE 82
TPS WEIGHT BREAKDOWN
NOMINAL MDAC-E TRANSITION CRITERION
MDAC DWO
ENGINEERING UNITS

VEHICLE LOCATION	AREA FT^2	THERMAL PROTECTION SYSTEM WEIGHT							
		NOMINAL		1σ		2σ		3σ	
		PSF	LB	PSF	LB	PSF	LB	PSF	LB
NOSE	706	1.17	826	1.26	890	1.34	946	1.42	1,003
LOWER SURFACE-INBOARD	1,851	2.46	4,553	2.62	4,850	2.80	5,183	2.93	5,423
OUTBOARD	1,851	2.36	4,368	2.52	4,665	2.88	5,331	3.07	5,683
FORWARD SIDE	1,412	0.950	1,341	1.04	1,468	1.125	1,589	1.20	1,694
AFT SIDE	2,756	0.911	2,511	0.911	2,511	0.98	2,701	1.03	2,839
UPPER SURFACE	3,510	0.911	3,198	0.911	3,198	0.911	3,198	0.925	3,247
WING LOWER SURFACE	4,009	2.51	10,063	2.67	10,704	2.94	11,786	3.09	12,388
WING UPPER SURFACE	3,718	0.911	3,387	0.911	3,387	0.911	3,387	0.911	3,387
TOTAL UNCERTAINTY STUDY	19,813		30,247		31,673		34,121		35,664
REMAINING SURFACES	3,583		6,895		6,895		6,895		6,895
TOTAL	23,396		37,142		38,568		41,016		42,559
RATIO TO NOMINAL	-		1.00		1.04		1.10		1.15

NOTE: σ BASED ON UNCERTAINTY IN HEATING RATES
NOMINAL TRANSITION CRITERION

FIGURE 83

TPS WEIGHT INCREMENTS DUE TO

ALL LAMINAR AND ALL TURBULENT FLOW

MDAC DWO LOWER SURFACE

ΔW IN KILOGRAMS

FLOW	NOMINAL	1σ	2σ	3σ
LAMINAR	-2586	-1996	-1325	- 738
TURBULENT	+ 158	+ 901	+1504	+2046

ΔW IN POUNDS

FLOW	NOMINAL	1σ	2σ	3σ
LAMINAR	-5700	-4400	-2920	-1627
TURBULENT	+ 349	+1987	+3316	+4510

flight. The small increment for the nominal turbulent case results from the fact that the lower surface of the orbiter is essentially designed by fully turbulent flow if the MDC Phase B transition criterion is used. This figure shows that a significant weight reduction is possible if the flow remains laminar in flight. Assessment of the effect of the transition criterion and its uncertainty was made and is summarized in Figure 84. This figure shows that the use of an optimistic transition criterion can reduce nominal TPS requirement by approximately 2240 kg (5000 lb). However, if the effect of scatter of the data about the best fit to the transition data is included, the difference in TPS weight becomes insignificant. This is shown graphically in Figure 85, in which the unit weight of the TPS is shown for the best correlation fits and uncertainties associated with 1, 2, and 3σ of the transition data about the best fits. At this location, which corresponds to an X/L of 0.5, the maximum difference (conservative to optimistic) in unit weight is reduced from 3.4 kg/m^2 (0.7 lb/ft^2) for the nominal values to 0.39 kg/m^2 (0.08 lb/ft^2) for a 3σ deviation in transition onset.

The combined effect of heating prediction and transition onset uncertainties are compared in Figure 86 for the MDC and optimistic transition criteria. These were combined using the root sum square technique discussed above. This figure shows that the 3σ design would be 2050 kg (4510 lb) heavier than the nominal using the MDC criterion and that the 3σ design would actually be 91 kg (200 lb) lighter than the nominal based on the MDC transition criterion. This shows that the selection of the transition criterion to apply to the orbiter has a major influence on TPS weight, a situation which was not critical for the booster. The use of the optimistic criterion would result in a 3σ design approximately 13 percent lighter than would be predicted using the MDC criterion.

The above weight studies and tradeoffs were made under the implicit assumption that 1σ corresponded to a 68-percent confidence limit that the heating would not be exceeded in flight. As discussed in Section V, this use of the standard deviation to define confidence limits is not precise. Therefore, the more sophisticated approach which develops confidence limits with tolerance has been used to estimate the effects of heating uncertainties on orbiter TPS weight. These results are summarized in the detailed weight breakdown of Figures 87 and 88 for SI and engineering units respectively. To achieve a 95-percent confidence level that 95-percent of the data in flight will not exceed the design requirements (95/95) a 13-percent increase in TPS weight is required. By comparison with the results in

FIGURE 84

TPS WEIGHT INCREMENTS DUE TO UNCERTAINTY IN TRANSITION
MDAC DWO LOWER SURFACE

ΔW IN KILOGRAMS

CRITERION/UNCERTAINTY	NOMINAL	1σ	2σ	3σ
MDAC	0	+ 158	+158	+158
OPTIMISTIC	-2236	-1361	-662	-209
MDAC-OPTIMISTIC	2236	1519	820	367

ΔW IN POUNDS

CRITERION/UNCERTAINTY	NOMINAL	1σ	2σ	3σ
MDAC	0	+ 349	+ 349	+349
OPTIMISTIC	-4930	-3000	-1460	-460
MDAC-OPTIMISTIC	4930	3349	1809	809

FIGURE 85

EFFECT OF TRANSITION UNCERTAINTY
ON TPS UNIT WEIGHT
MDAC DELTA WING ORBITER
X/L = 0.5

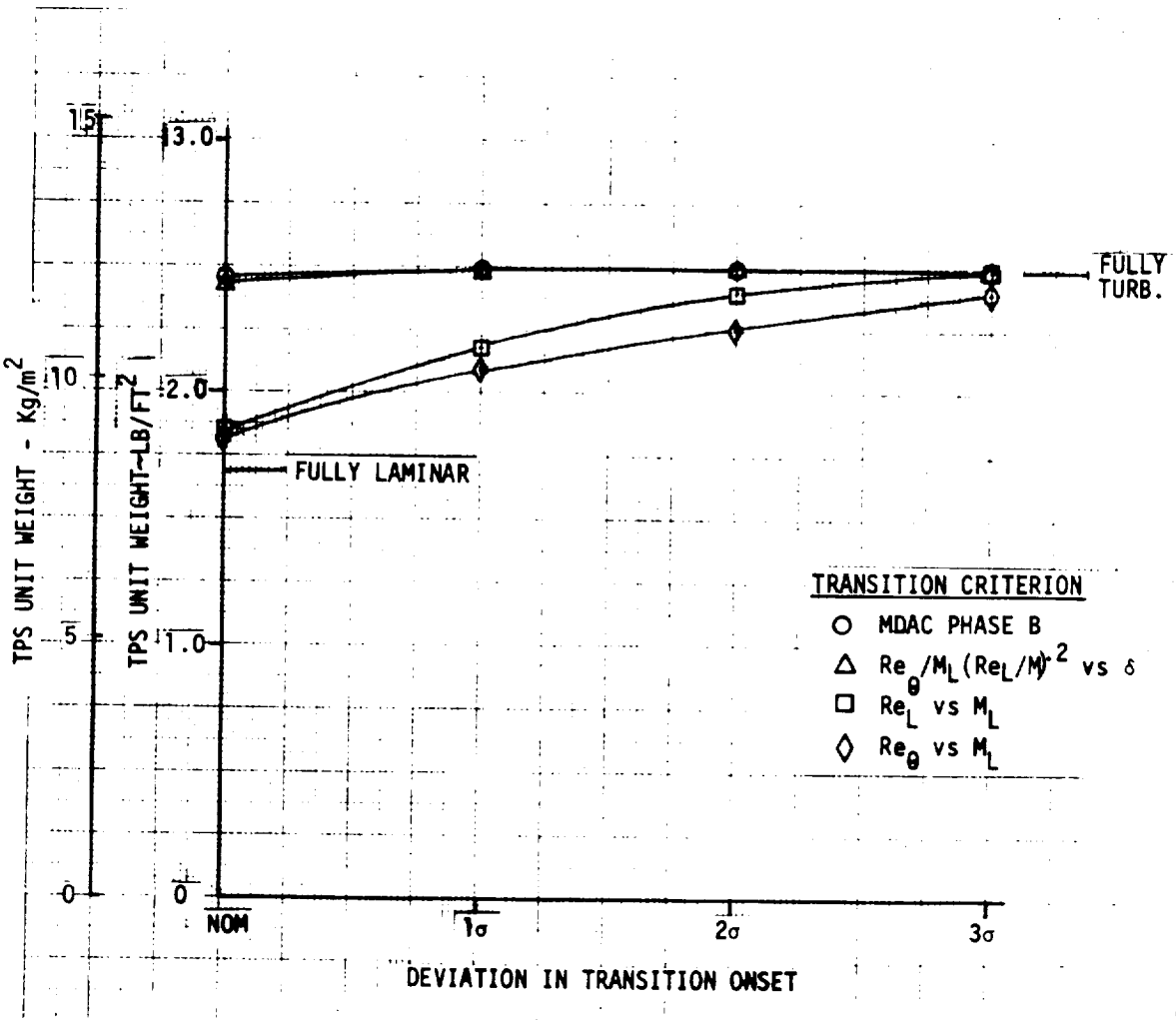

FIGURE 86

TPS WEIGHT INCREMENTS DUE TO COMBINED
UNCERTAINTIES IN HEATING RATE AND TRANSITION ONSET
MDAC DWO LOWER SURFACE

ΔW IN KILOGRAMS

CRITERION/UNCERTAINTY	NOMINAL	1σ	2σ	3σ
MDAC	0	+ 582	+1504	+2046
OPTIMISTIC	-2236	-1359	- 617	- 91

ΔW IN POUNDS

CRITERION/UNCERTAINTY	NOMINAL	1σ	2σ	3σ
MDAC	0	+1283	+3316	+4510
OPTIMISTIC	-4930	-2995	-1360	- 200

FIGURE 87

TPS WEIGHT BREAKDOWN
NOMINAL MDAC-E TRANSITION CRITERION
MDAC DWO
S.I. UNITS

VEHICLE LOCATION	AREA m^2	THERMAL PROTECTION SYSTEM WEIGHT							
		NOMINAL		95/95		95/99		99/99	
		Kg/m^2	Kg	Kg/m^2	Kg	Kg/m^2	Kg	Kg/m^2	Kg
NOSE	65.6	5.71	375	6.74	442	6.93	455	7.03	461
LOWER SURFACE-INBOARD	168.6	12.01	2,025	13.77	2,322	14.06	2,371	14.11	2,379
OUTBOARD	168.6	11.52	1,942	14.70	2,478	15.09	2,544	15.38	2,593
FORWARD SIDE	131.2	4.64	609	5.81	762	5.86	769	5.96	782
AFT SIDE	256.0	4.45	1,139	4.98	1,272	5.03	1,288	5.13	1,313
UPPER SURFACE	326.1	4.45	1,451	4.56	1,487	4.60	1,500	4.66	1,520
WING LOWER SURFACE	372.4	12.26	4,566	14.79	5,508	15.19	5,657	15.43	5,746
WING UPPER SURFACE	345.4	4.45	1,537	4.45	1,537	4.45	1,537	4.45	1,537
TOTAL UNCERTAINTY STUDY	1833.9		13,644		15,808		16,121		16,331
REMAINING SURFACES	332.9		3,128		3,128		3,128		3,128
TOTAL	2166.8		16,772		18,936		19,249		19,459
RATIO TO NOMINAL	-		1.00		1.13		1.15		1.16

FIGURE 88
TPS WEIGHT BREAKDOWN
NOMINAL MDAC-E TRANSITION CRITERION
MDAC DWO

ENGINEERING UNITS

VEHICLE LOCATION	AREA FT^2	THERMAL PROTECTION SYSTEM WEIGHT							
		NOMINAL		95/95		95/99		99/99	
		PSF	LB	PSF	LB	PSF	LB	PSF	LB
NOSE	706	1.17	826	1.38	973	1.42	1,000	1.44	1,015
LOWER SURFACE-INBOARD	1,851	2.46	4,553	2.82	5,220	2.88	5,330	2.89	5,350
OUTBOARD	1,851	2.36	4,368	3.01	5,575	3.09	5,725	3.15	5,825
FORWARD SIDE	1,412	0.950	1,341	1.19	1,675	1.20	1,700	1.22	1,725
AFT SIDE	2,756	0.911	2,511	1.02	2,800	1.03	2,850	1.05	2,900
UPPER SURFACE	3,510	0.911	3,198	0.933	3,275	.943	3,310	.954	3,350
WING LOWER SURFACE	4,009	2.51	10,063	3.03	12,135	3.11	12,450	3.16	12,650
WING UPPER SURFACE	3,718	0.911	3,387	0.911	3,387	0.911	3,387	0.911	3,387
TOTAL UNCERTAINTY STUDY	19,813		30,247		35,040		35,752		36,202
REMAINING SURFACES	3,583		6,895		6,895		6,895		6,895
TOTAL	23,396		37,142		41,935		42,647		43,097
RATIO TO NOMINAL	-		1.00		1.13		1.15		1.16

Figure 81, a corresponding 2σ design would require a 10-percent increase in weight. Thus, the use of more rigorous statistics results in slightly higher heating multipliers than derived from direct use of values at 1,2,and 3σ.

Since the upper surface of the wing encounters low heating and the TPS is sized entirely by the minimum RSI thickness, a study was made to evaluate the use of thickened aluminum or titanium heat sinks. Unit weights of these heat sink concepts are compared with the RSI TPS as a function of trajectory heat load in Figure 89. This curve shows that a 1σ design is possible with no weight penalty for the aluminum heat sink concept,and a 2σ design if titanium is used. However, the RSI concept provides the lightest weight if it is necessary to design for a 3σ heat pulse.

FIGURE 89

MDAC DELTA WING ORBITER
UPPER WING HEAT SINK TPS REQUIREMENTS

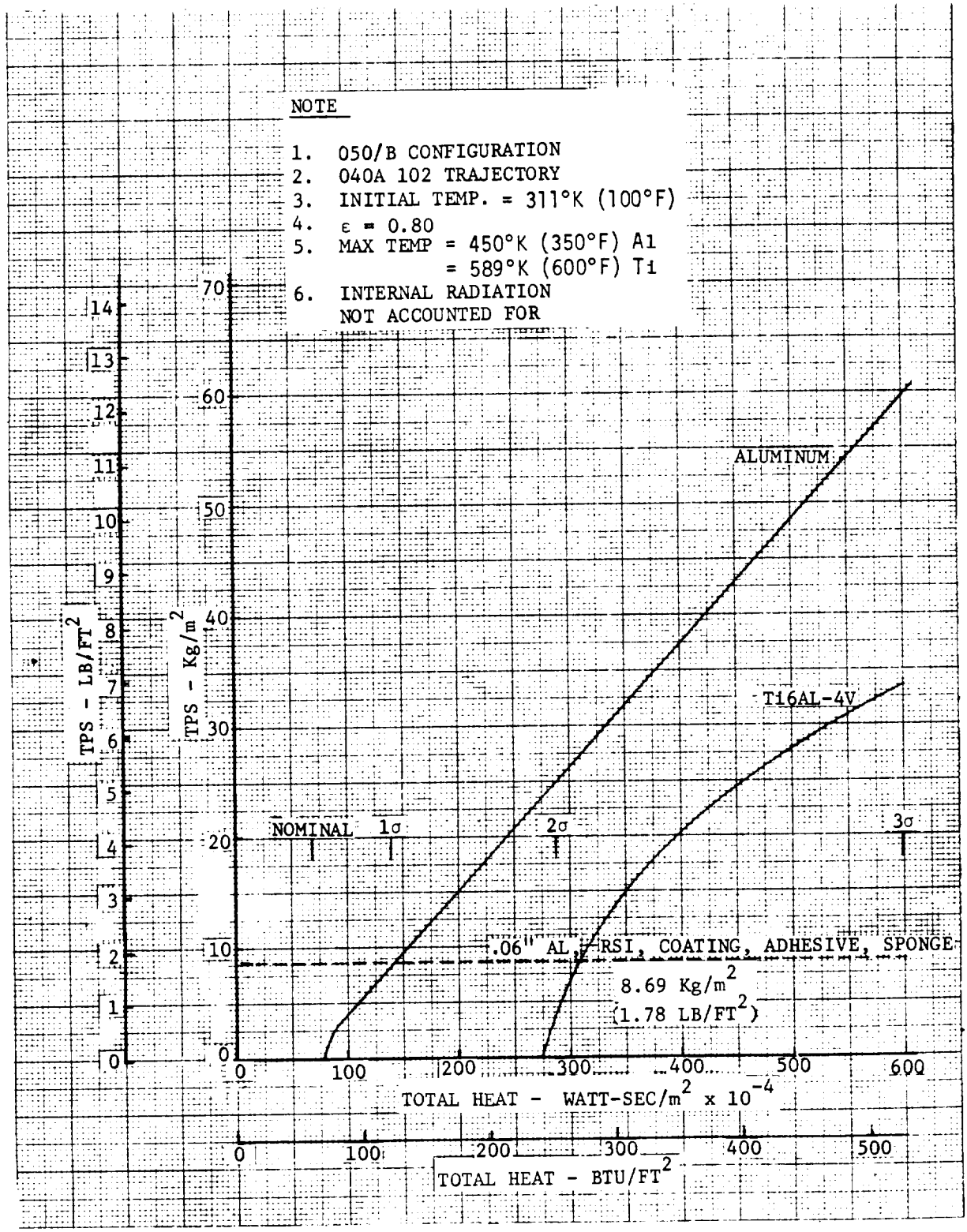

VII CONCLUSIONS AND RECOMMENDATIONS

This study has provided an assessment of the effect of aerodynamic heating uncertainties on Space Shuttle TPS weights, thereby identifying the prediction methods for which improvement is most important. These include windward turbulent heating for the booster and orbiter and development of more reliable boundary layer transition criteria for the orbiter. Mated interference heating was found to be less critical than initially suspected because of the low staging velocity of the heat sink booster and apparent Mach number dependence of the interference heating. Uncertainties in the heating to upper surface shielded regions at reentry angles of attack were quite large. However, for the vehicle and TPS concepts studied in this program, the heat sink or RSI thickness in shielded regions was essentially sized by structural or manufacturing limitations. These uncertainties could, on the other hand, be critical for other configurations or TPS concepts.

The heat sink booster was found to be much more sensitive to aerodynamic heating uncertainties and a high confidence (3σ) design would be approximately 55-percent heavier (in skin and structure weight) than required if nominal heating is assumed. The equivalent penalty in TPS for the orbiter would be approximately 15-percent. In addition to the above general conclusions, a number of specific observations can be made:

1. The Shuttle heating data base is reasonable for the current state of Shuttle development. However, this study was hampered by certain limitations in this data base. For example, it was difficult to separate the effect of geometric and environmental variables on the heating uncertainties, since few configurations were tested over a wide range of Mach and Reynolds numbers. In particular, the variations in tunnel conditions prevented the selection of a theory which best matched the data even though differences in scale to flight would result for each theory. In addition, the emphasis on paint data made the data reduction and evaluation process difficult and increased the derived uncertainties. Care was taken to minimize these effects, but the reported uncertainties do contain some.

2. Mated interference heating uncertainties, though large, were not a major contributor to the weight uncertainties because of the low staging velocities and correspondingly low interference heating multipliers predicted by the correlation used in this study. Alternate correlation approaches, in terms of Reynolds number or both Mach number and Reynolds number, could affect this conclusion. These

were not tried because of the limited amount of low Mach number data on the mated configurations.

3. The statistical approach to evaluating data scatter and applying the results to flight were reviewed. A more sophisticated approach (than simply relying on the standard deviation of the data sample) to establish confidence levels was developed. This approach provides confidence that a percentage of the data population will be less than the design value with some confidence level. This approach is valid if it is assumed that the factors affecting ground test scatter will also occur and are scalable to flight. It is known that this is not a "universal truth", since a portion of the ground test scatter may be due to data fits or instrumentation error. However, if the major portion of the scatter is due to improper modeling of the data by theory, such scaling is possible. Unfortunately, because of insufficient flight test data, statistics cannot be employed to validate whether ground test data and their uncertainties scale to flight. However, comparisons of the scatter in BGRV flight data with ground test data and predictions provide some assurance that the approach is reasonable.

4. The uncertainty in predicting lee side heating using simple correlating approaches was found to be quite large at the reentry angles of attack. Simple correlation in terms of h/h_{ref} produced a scatter of approximately an order of magnitude. More careful screening of the data or improved correlation should reduce this uncertainty. Further development of lee side methodology is certainly needed, even though these uncertainties were not found to be critical for the fully reusable Shuttle concept. Should it be desired to fly at lower angles of attack during reentry, the heating level would increase and large uncertainties could penalize the design. For that matter, if the orbiter TPS concept were changed to heat sink or heat shield on shielded areas, large weight penalties would be required to design for these uncertainties. It should be noted that the low tunnel heating rates measured in these areas make the data sensitive to instrumentation errors. More data are necessary to reduce the shielded region uncertainties, but it may be necessary to improve tunnel instrumentation if reliable data are to be obtained.

5. The boundary layer transition criterion was found to be a significant contributor to the TPS weight uncertainty for the orbiter. This uncertainty will probably not be greatly reduced through additional ground tests. However, additional ground testing can provide an understanding of the sensitivity of

transition to configuration variables, e.g., nose geometry, lower surface curvature. It should also be noted that the better correlating approaches used a configuration related parameter, Re_θ. The cooling parameter which was found to improve the correlation was the ratio of wall to edge temperature rather than wall to recovery temperature. For this correlation, transition on the orbiter was predicted at 72 km (235,000 ft), whereas, the MDC Phase B criterion predicted transition at 78 km (255,000 ft) and correlation of the data in terms of local Reynolds number at 58.5 km (192,500 ft).

6. Except at angles of attack near zero, the use of normal shock entropy to predict local flow conditions provided no improvement in the data correlation. The edge properties used in this study were analytically derived for cones having equivalent deflection angles to the local surface angles. These were computed only for those cases where the data were compared with a theoretical two-dimensional prediction method. For data correlated to Fay-Riddell stagnation point theory, such assumptions are not necessary. Since the Shuttle configurations are quite complex, it is probable that the data scatter could have been reduced if the boundary layer edge properties had been better defined. This is particularly true for the turbulent data which is more sensitive to local Reynolds number than for the laminar case.

7. Many data points were not evaluated in this study either for lack of resources or unavailability of the data in time for use. The tests have been cataloged and are reposing in SADSAC. It would seem desirable to develop automated processing techniques which would allow correlation of these results without the time consuming reading of isotherms or hand conversion of coefficients to appropriate equivalent theoretical local flow conditions. Also, the data in SADSAC should be screened for errors, and invalid or inaccurate data removed.

8. It is recommended that particular care be taken in Phase C/D that (1) a statistically meaningful data base be obtained, (2) instrumentation errors be assessed, and (3) best methods for scaling to flight be developed on the basis of the match of the test data to theory.

VIII LIST OF SYMBOLS

Symbol	Definition
C	Model Wing Local Chord Length
H(T), H(.9TO), h	Heat Transfer Coefficient
K	Multiple of the standard deviation corresponding to various proportions included within the tolerance range
L	Model reference length (body axial length)
m	Meter
M	Mach number
N	Normal distribution
n	Sample size
P	Pressure
$\dot{q}$	Heating rate
Re	Reynolds Number
Re_∞/L	Free-stream Unit Reynolds Number
Re_θ	Momentum Thickness Reynolds Number
s	Sample standard deviation
S	Model Wing Exposed Semi-span Length
SI	Standard International
T	Temperature
V	Velocity
w	TPS weight
X	Axial distance
$\bar{x}$	Sample mean
Y	Wing outboard distance from root
α	Angle of attack
δ	Local Flow Deflection Angle
θ_s	Shock angle

Symbol	Definition
Λ	Leading edge sweep angle
μ	Population mean
ϕ	Peripheral angle
χ^2	Chi-square distribution
σ	Population standard deviation
$\hat{\sigma}$	Unbiased estimate of the population standard deviation
t	Time, student's t distribution
Δ	Increment in parameter prefixed
Subscripts	
B	Booster alone
B+O	Booster mated with orbiter
$\mathfrak{L}$	Lower surface centerline value
e	Edge conditions
L	Local conditions
tr	Transition location
ϕ	Local peripheral value
∞	Free stream
s	Stagnation point
Ref	Reference value of h or $\dot{q}$ for a unit (R=1') sphere scaled to model size.
w	Wall condition

IX REFERENCES

1. "A Minature Version of the JA70 Aerodynamic Heating Computer Program, H800 (MINIVER)", MDC Report No. G0462, D. Hender, 1 June 1970, revised January 1972.
2. "Data Report, AFFDL Temperature Sensitive Heat Transfer Test on an 80° Delta Wing",Report MDC E0276, J. W. Stultz and A. L. Fehrman, 28 December 1970.
3. "Reentry Heat Transfer to a Delta-Wing Space Shuttle Booster at High Angles of Attack", GDC Report FZA-452, R. O. Doughty, O. R. Brock and R. C. Erickson, 25 March 1971.
4. "Convair Straight-Wing (B-8B) and Delta Wing (B-9J) Boosters, Aerodynamic Heat Transfer to the Space Shuttle Booster Surfaces at Hypersonic Speeds", SADSAC Report DMS-DR-1020, October 1970.
5. "Convair Straight-Wing (B-8B) and Delta-Wing (B-9J) Booster, Aerodynamic Heat Transfer to the Space Shuttle Booster Surfaces at Hypersonic Speeds", SADSAC Report DMS-DR-1024, October 1970.
6. "Heat Transfer Rate Measurements on Convair Booster (B-15B-2) and North American Rockwell Orbiter (161B) at Nominal Mach Number of 8", J. D. Warmbrod, W. R. Martindale, R. K. Matthews, SADSAC Report DMS-DR-1177, November 1971.
7. "Aerodynamic Heating of a Space Shuttle Delta-Wing Booster at M = 7.4", C. E. DeRose, W. K. Lockman, A. Roberge, N. Nicodemus, NASA TMX-62,058 (DMS-DR-1179), September 1971.
8. Data Analysis Report, Interference Heating/CAL Test Program of MDC Delta Wing Orbiter/Booster, B. M. Levine, McDonnell Douglas Astronautics Company Design Note, to be published.
9. Investigation of Configuration Effects on Entry Heat Transfer Distributions and Definition of Interference Heating Areas on Space Shuttle Orbiter Configurations, SADSAC Report DMS-DR-1056, January 1970.
10. Thermal Mapping Investigation - MDC/MMC Phase B Space Shuttle Vehicles, SADSAC Report DMS-DR-1036, Vols. I & II, November 1970.
11. Mathematical Methods for Computers, John Wiley and Sons, Inc., New York, 1960, pp. 191-203, A. Ralston and H. S. Wilf.
12. "Suggested Refinement for Calculation of Cross-flow Corrections", MDAC-East Informal Memo, L. C. Baranowski, 29 July 1970.

13. Thermal Environment/Gasdynamics Heating, Report MDC E0400, McDonnell Douglas Corporation, 30 June 1971.

14. "Correlation of Flight Boundary Layer Transition", AFFDL-TR-71-36, D. H. Stuerke, R. V. Masek , D. L. Mattox , and L. Mockapetris , May 1971 (Secret).

15. "Hypersonic Simulation for Lifting Body Transition Studies", Proceedings of the Boundary Layer Transition Workshop held 3-5 November 1971, Volume III, S. R. Pate , and J. C. Adams , W. D. McCauley, ed., Aerospace Report No. TOR-0172 (S2B16-16)-5, Aerospace Corporation, San Bernardino, California, 20 December 1971.

16. "Influence of Cross-flow on Windward Centerline Heating", McDonnell Douglas Corporation Report MDC E0535, L. C. Baranowski , McDonnell Douglas Corporation, St. Louis, Missouri,23 December 1971.

17. Handbook of Probability and Statistics with Tables, Second Edition, R. S. Burington and D. C. May, Jr., McGraw-Hill Book Co., New York, 1970.

18. Techniques of Statistical Analysis, McGraw Hill Book Co., New York, 1947, edited by M. W. Hastay, G. C. Eisenhart, and W. A. Walies.

19. "Determination of Aerothermodynamic Environment Uncertainties with Application to Space Shuttle Vehicles", C. A. Scottoline, NASA TMX-2507, Space Shuttle Aerothermodynamics Technology Conference, Vol. II, Heating, February 1972.

20. "Study of Structural Active Cooling and Heat Sink Systems for Space Shuttle", Final Report, MDC Report E0638, 30 June 1972.